USGS
science for a changing world

World-Wide Standardized Seismograph Network: A Data Users Guide

By Jon Peterson and Charles R. Hutt

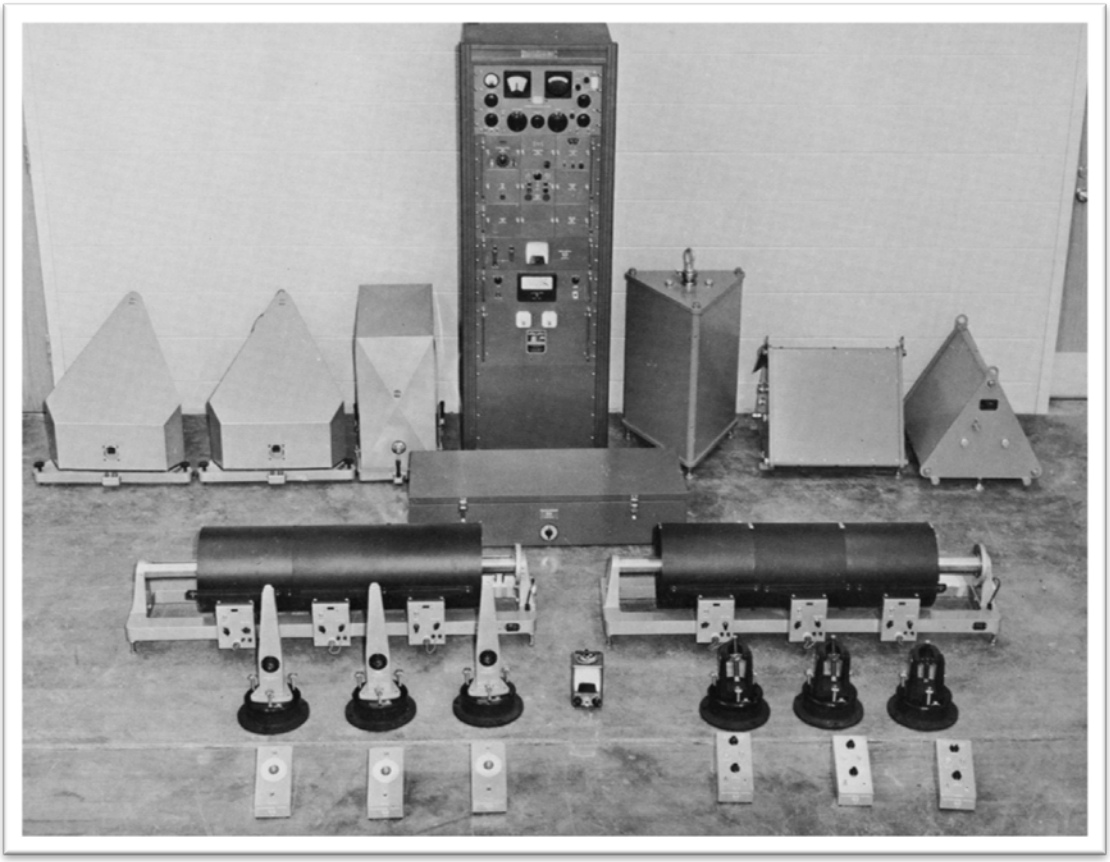

Open-File Report 2014–1218

U.S. Department of the Interior
U.S. Geological Survey

U.S. Department of the Interior
SALLY JEWELL, Secretary

U.S. Geological Survey
Suzette M. Kimball, Acting Director

U.S. Geological Survey, Reston, Virginia: 2014

Suggested citation:
Peterson, Jon, and Hutt, C.R., 2014, World-Wide Standardized Seismograph Network—A data users guide: U.S. Geological Survey Open-File Report 2014–1218, 74 p., *http://dx.doi.org/10.3133/ofr20141218.*

ISSN 2331-1258 (online)

Foreword

A good case can be made that the World-Wide Standardized Seismograph Network (WWSSN) was the first community instrument that enabled Global Seismology to become a quantitative, predictive science. Seismograms from WWSSN stations in the western United States figured very prominently in my first experience with seismological research as a new graduate student. Many of those images are personal icons of how body and surface waves from large earthquakes should be viewed. Normally we worked with large, expanded copies of seismograms from microfiche, but occasionally we would get one-to-one photographic copies of the originals by requesting data from operators of the seismic stations after an important earthquake.The WWSSN data were "gold" to our group of waveform modelers because the data came from seismic instruments that were accurately timed and had a standard, calibrated instrument response. For the first time, the variation of waveform amplitude, shape, and timing could be compared over a region or over the entire Earth to infer characteristics of the source and propagation medium using quantitative seismology.

Data from the WWSSN played a pivotal role in developing the paradigm of Plate Tectonics in the 1960s. Reliable P- and S-wave travel times could be picked to locate many hundreds of earthquakes at teleseismic distances, and good first motions could be used to infer fault plane solutions that illuminated the stress condition and geometry of Earth's plates. In the process of using this exquisite analog data set, it became clear that further advances in quantitative analysis of seismograms required digital data, culminating in the digital global seismic networks that we have today.

By modern digital standards, the WWSSN was a very low dynamic range system. As Jon Peterson and Bob Hutt point out in this report, to have an analog WWSSN system equivalent to today's recorders would require a photographic recording drum 17 kilometers (km) wide with a distance between the galvanometer and drum of 54 km! Even so, there were plenty of "sweet spot" distances where earthquakes of all sizes could be adequately observed.

Today there is an incredible wealth of digital seismic observations from the entire planet, so one could wonder what use analog data play in modern seismic problems. The answer is simple. Seismology is a very young scientific field and the historical data set is a precious commodity for learning about the past. Earthquake hazard evaluations depend on analysis of source parameters from historical earthquakes. The analog data may be the only data available from past earthquakes in areas where the built environment was previously undeveloped. New phenomena found after the analog era, such as "slow" earthquakes, non-volcanic tremor, or episodic slip in subduction zones might benefit from a look at the historical WWSSN data to review any relationship of these signals with the occurrence of previous great earthquakes. Future discoveries of new signals may be recorded in the analog WWSSN archives.

As anyone who has fielded a seismic experiment knows, it is very difficult to collect good data and a tragedy when the data are lost either though instrument malfunction or collection errors. The WWSSN was a grand experiment that generated an unprecedented collection of high quality, continuous data from approximately 100 stations around the world. This alone makes it one of seismology's best success stories. Waveform studies using these data have pushed the field forward on all fronts and have motivated most, if not all, present day large-scale seismic experiments and networks. The data are important for both historical and scientific reasons.

Chuck Langston
March 28, 2014

Preface

This report was originally drafted in the late 1970s. It was not published at the time, probably because the authors had become too distracted by new digital recording technology, new sensor systems, and new networks. We hope that this belated effort will still be of benefit to those who may have occasion to use WWSSN data and that this report will fill a gap in the historical record of the first truly global seismograph network.

Credit for resurrection of the report goes to William H.K. Lee. Willie Lee has taken a prominent role in the rescue and preservation of seismic data, including the WWSSN data.[1] A few years ago, he came upon a copy of this document's early draft and urged that it be published. This report is the result of that suggestion.

Some changes have been made to the original draft report. A tutorial has been added as an introduction to the derivation of the WWSSN transfer function in Appendix A1. The original report included only the design transfer function. Now that we have online access to recorded calibration data, we were able to produce a more useful transfer function based on the averaging of recorded calibration data, and we have included a method for data users to derive transfer functions specific to any of the seismograph components.

We would like to acknowledge and thank James W. Dewey, Charles A. Langston, William H.K. Lee, and Adam T. Ringler for reviewing the report and providing suggestions that have made the report more accurate and readable. In addition, we would like to thank Chuck Langston for providing the Foreword to this report summarizing the impact of the WWSSN on seismology and suggesting where the data might continue to be useful.

Reaching further back in time, we would like to acknowledge the accomplishments of the WWSSN installation teams. The installers (as they were called) were mostly geophysicists recruited from oil exploration crews hard hit by a slump in the oil industry. At the peak, there were 15 two-man installation teams working somewhere between northern Greenland and the South Pole. On each team, one team member was a Coast and Geodetic Survey employee and one was contracted from Texas Instruments. The first WWSSN system was installed at Albuquerque in 1961, and 12 more were installed by the end of that year. Fifty-two systems were installed in 1962, a truly remarkable accomplishment; 24 more were installed in 1963, 14 in 1964, 9 in 1965, 1 in 1966, and 4 in 1967. When not installing new systems, the teams were performing maintenance and training and installing modifications at existing stations. It was an adventurous life for some. Others met their wives-to-be in such far-flung places as Samoa, Thailand, and Finland. Installer tales are endless, but they all survived unscathed, give or take a few cases of malaria. The work of the installers would not have been possible without the indispensable support of the host station personnel who dealt with complex logistical and technical issues and whose hospitality was always well appreciated. The installation of the WWSSN was a job well done by all those involved.

[1] See Lee and Benson (2008).

Contents

Figures

Tables

Conversion Factors

SI to Inch/Pound

Multiply	By	To obtain
	Length	
centimeter (cm)	0.3937	inch (in.)
meter (m)	3.281	foot (ft)
kilometer (km)	0.6214	mile (mi)
meter (m)	1.094	yard (yd)
	Area	
square kilometer (km^2)	247.1	acre
square meter (m^2)	10.76	square foot (ft^2)
square kilometer (km^2)	0.3861	square mile (mi^2)
	Volume	
liter (L)	33.82	ounce, fluid (fl. oz)
	Mass	
gram (g)	0.03527	ounce, avoirdupois (oz)

World-Wide Standardized Seismograph Network: A Data Users Guide

By Jon Peterson and Charles R. Hutt

1. Background

Our primary source for the early history of the World-Wide Standardized Seismograph Network (WWSSN) is an article by Oliver and Murphy (1971). Their article includes the rationale for creation of the network, station siting, recording bands and instrumentation, and concludes with a review of preliminary results using network data. The following paragraphs include a summary of some topics discussed in their article.

Seismologists had long recognized the need for a global network of accurately calibrated and accurately timed seismographs in the years before the World-Wide Standardized Seismographic Network was installed. The opportunity to fill that need came as a result of nuclear test ban discussions held in 1958. A panel on seismic improvement, chaired by Dr. Lloyd Berkner, was formed in the United States to consider research needs for improving the national capability in the detection and discrimination of underground nuclear explosions.[2] The panel's report formed the basis of Project Vela Uniform, a program of fundamental and applied research managed by the Defense Advanced Research Projects Agency (DARPA). One of the panel recommendations was for the installation of standardized seismographs, with accurate clocks, at 100 to 200 existing seismograph stations. The new network was not intended for the surveillance of nuclear tests; its role was to produce the data needed for fundamental research in seismology. The recommendation of the project was adopted and implemented as the World-Wide Standardized Seismograph Network. The WWSSN was a technological milestone in seismology, producing abundant high quality data for research. The precedent-setting program also created a global network infrastructure, including the data-exchange procedures and station technical capabilities needed to support the establishment of the more advanced networks in operation today.

The task of deploying and operating the WWSSN was assigned by DARPA to the U.S. Coast and Geodetic Survey (C&GS), the principal federal agency engaged in seismological operations at that time. Leonard M. Murphy, Chief of the Seismology Branch in the C&GS, was the program manager during the planning and installation of the WWSSN. Following a suggestion of the Berkner Panel, the National Academy of Sciences/National Research Council established a Committee on Seismological Stations in 1960 to provide guidance in planning the new network. The Committee, chaired by Dr. James T. Wilson, issued a report in June 1960 that provided several broad recommendations on station siting and data management, as well as equipment specifications. Based largely on the Committee's recommendations, the C&GS published performance specifications and issued a request for proposals in November 1960, and

[2] For more information on the Berkner Panel and related activities, please refer to Bolt (1971) and Romney (2009).

by the end of the year responses had been received from several organizations. A contract for development and production of the WWSSN systems was awarded to the Geotechnical Corporation of Garland, Texas, in early 1961, and the first system was installed at the C&GS Albuquerque Seismological Laboratory (ASL) in October 1961.

Most organizations outside of the United States with an active interest in seismology were offered WWSSN systems. Of those that accepted, about half were universities and the others were government agencies. Organizations in Soviet-bloc countries did not participate, nor did China, France, or French-speaking countries in Africa. Organizations in Canada did not participate but provided seismograms from a new national network in Canada for copying and distribution along with the WWSSN seismograms. The organizations that did participate were asked to provide the vault facilities and to operate the equipment and send the seismograms to the C&GS for copying. New vaults were constructed at 53 stations, some with grants from the C&GS. Training was provided by the installation teams. In some countries, the WWSSN provided the first opportunity to establish programs in seismology and participate in international data exchange. Geotech delivered 127 WWSSN systems; 121 were installed, 1 was given to the USSR, and the others were used for training and maintenance. For more information on the creation of the WWSSN, see Kisslinger and Howell (2003).

Concurrent with the installation of the network, facilities were established to copy and distribute the data. In 1961, the C&GS awarded a contract to the Itek Corporation for development of a panoramic microfilm seismogram reproduction system capable of reducing original seismograms to 70 millimeter (mm) film chips at the rate of 240,000 per year. The system also included an archival facility and equipment for copying the seismograms onto a variety of film media, including 70 mm chips and rolls and 35 mm rolls. The WWSSN Data Center began operation in Washington, D.C., in 1962, was moved to Asheville, North Carolina, in 1966, and was moved again in 1975 to Boulder, Colorado.

The WWSSN was essentially complete by the end of 1967. A number of field modifications had been made to improve system performance, an operation and training center had been established at the Albuquerque Seismological Laboratory, and routine maintenance visits were being made to the stations. Data Center operations were initially hampered by technical problems and serious interruptions were caused by the moves, but during its peak year, 300,708 seismograms were copied and a total of 3,342,174 copies of seismograms were distributed to data users.

Fiscal year 1967 (July 1966–June 1967) was the last year that the WWSSN was funded by DARPA. Plans had been made to transfer funding responsibilities from the Defense Department to the Commerce Department, but an impasse developed in Congress over the transfer, and the WWSSN program was left unfunded. The Environmental Science Services Administration (ESSA), the administrative home of the C&GS, diverted enough funds annually to cover the cost of operating supplies for the domestic stations (it had been prohibited from funding the foreign stations) and the National Science Foundation (NSF) agreed to cover the cost of supplies for the foreign stations. Most of these expenses related to the purchase and shipment of photographic supplies. The ASL was able to continue limited repair of equipment, but routine maintenance visits and training programs were suspended. In 1973, the seismology program, including ASL and the WWSSN, was transferred from the National Oceanic and Atmospheric Administration (NOAA), a successor to ESSA, to the U.S. Geological Survey (USGS). The Data Center operations remained with NOAA. On several occasions, the USGS attempted to obtain permanent funding for the network but was unsuccessful. The WWSSN continued in operation at

a reduced level of support until 1996 when network support was officially terminated by the USGS. By this time, some of the stations had closed and many had been upgraded with new digital-recording equipment.

The copying of seismograms onto high-resolution 70-mm and 35-mm film continued at the NOAA Data Center until 1978. From that point until the network was closed in 1996, the seismograms were copied onto lower-resolution microfiche. The master 70-mm chip file is believed to hold approximately 4,000,000 seismograms recorded between 1961 and 1978, including about 450,000 Canadian records. There is one nearly complete set of 70-mm film chips at the Albuquerque Seismological Laboratory. Other currently less-accessible sets of WWSSN seismogram copies include 70-mm film chips stored at Columbia University and 35-mm roll films stored at the Earthquake Research Institute in Japan and at USGS offices in Menlo Park, California (Calif.). The USGS set of 35-mm rolls is now stored at ASL.

Since 2000, efforts have been made at ASL to digitally scan the 70-mm chips to digital files (.tif or .jpeg) so that they can be made freely available to the data-user community. It has been a slow process because of uncertain funding. The scanned images available to date are less than 5 percent of the total number of WWSSN seismograms. They include many nuclear tests performed by the United States and the former USSR, large earthquakes, all six components from a few selected high-quality WWSSN stations, and the long-period vertical component of a larger subset of WWSSN stations. Some of the scans are available from the IRIS DMC at *http://www.iris.edu/spud/filmchip*. Most of the scans done to date have not yet been transferred to the IRIS DMC due to formatting and documentation required by the DMC. However, all of the scans done to date are available from ASL. Some examples and a short description of the scanning effort can be found at *http://earthquake.usgs.gov/regional/asl/data/wwssnhist.php*. This website will be updated with information on WWSSN data availability.

The purpose of this report, which is based on an unpublished draft prepared in the 1970s, is to provide seismologists with the information they may need to use the WWSSN data set as it becomes available in a more easily accessible and convenient format on the Internet. The report includes a description of the WWSSN network, station facilities, operations and instrumentation, a derivation of the instrument transfer functions, tables of transfer functions, a description of calibration techniques, and a description of a method used to determine important instrument constants using recorded calibration data.

2. WWSSN Network Configuration and Station Information

In July 1978, the WWSSN consisted of 115 stations, several of which were inactive (see fig. 2.1). A total of 127 stations had been installed and placed in operation. Some of the stations were closed and the equipment reinstalled at new sites. A list of the WWSSN stations that have been in operation, with locations, component magnifications, and operating dates, is given in table 2.1.

Detailed descriptions of the individual WWSSN stations are contained in the *Handbook: World-Wide Standardized Seismograph Network*, published by the University of Michigan (1964). The handbook contains information derived from station-installation reports giving station environment, geology, topography, vault construction, and other factors that might affect the recorded data. It was revised on several occasions, the last revision being in July 1966. The handbook is available on the website *http://www.iris.edu/seismo/info/stations/*. Information about the stations installed after 1966 is contained in unpublished installation reports on file at the Albuquerque Seismological Laboratory.

Figure 2.1 Map of the World-Wide Standardized Seismograph Network stations.

Table 2.1. List of all World-Wide Standardized Seismograph Network Stations installed. (SP,short period; LP, long-period)

WWSSN Station list								
Code	Station	Coordinates		Elevation (meters)	Magnification*		Open	Closed
		Latitude (deg) (min) (sec)	Longitude		SP	LP		
AAE	Addis Ababa, Ethiopia	09 01 45.0 N	38 45 56.0 E	2,442	25,000	1,500	5/62	
AAM	Ann Arbor, Michigan	42 17 59.0 N	83 39 22.0 W	249	12,500	1,500	10/62	
ADE	Adelaide, Australia	34 58 01.0 S	138 4232.0 E	655	25,000	750	4/62	
AFI	Afiamalu, Samoa Islands	13 54 33.6 S	171 46 38.1 W	706	12,500	750	9/62	
AKU	Akureyri, Iceland	65 41 12.0 N	18 06 24.0 W	24	12,500	375	7/64	
ALQ	Albuquerque, New Mexico	34 56 33.0 N	106 27 27.0 W	1,849	200,000	3,000	10/61	
ANP	Anpu, Taiwan	25 11 00.0 N	121 31 00.0 E	827	6,250	750	3/63	
ANT	Antofagasta, Chile	23 42 18.0 S	70 24 55.0 W	80	50,000	3,000	12/62	
AQU	L'Aquila, Italy	42 2114.0 N	13 24 11.0 E	720	25,000	3,000	4/62	
ARE	Arequipa, Peru	16 27 43.5 S	71 29 28.6 W	2,452	50,000	1,500	1/62	
ATL	Atlanta, Georgia	33 26 00.0 N	84 20 15.0 W	272	50,000	3,000	6/63	
ATH	Athens, Greece	37 58 20.0 N	23 43 00.0 E	95	12,500	1,500	3/62	
BAG	Baguio City, Philippines	16 24 39.0 N	120 34 47.0 E	1,507	25,000	3,000	3/62	
BDF	Brasilia, Brazil	15 30 49.8 S	47 54 12.0 W	1,260	100,000	1,500	9/73	
BEC	Bermuda	32 22 46.0 N	64 40 52.0 W	41	25,000	1,500	12/61	
BHP	Balboa Heights, Panama	8 57 39.0 N	79 33 29.0 W	36	12,500	750	12/61	2/77
BKS	Berkeley, California	37 52 36.0 N	122 14 06.0 W	276	25,000	3,000	5/62	
BLA	Blacksburg, Virginia	37 12 40.7 N	80 25 15.6 W	634	100,000	1,500	8/62	
BOG	Bogota, Columbia	4 37 23.0 N	74 03 54.0 W	2,658	12,500	3,000	4/62	
BOZ	Bozeman, Montana	45 36 00.0 N	111 38 00.0 W	1,575	200,000	3,000	8/63	11/77
BUL	Bulawayo, Zimbabwe	20 08 36.0 S	28 36 48.0 E	1,341	100,000	750	1/63	
CAR	Caracas, Venezuela	10 30 24.0 N	66 55 39.5 W	1,035	25,000	3,000	4/62	
CCG	Camp Century, Greenland	77 10 00.0 N	61 08 00.0 W	1,920	100,000	1,500	12/62	2/63
CHG	Chiengmai, Thailand	18 47 24.0 N	98 58 37.0 E	416	200,000	3,000	3/63	
CMC	Coppermine, Canada	67 50 00.0 N	115 05 00.0 W	31	200,000	3,000	4/63	3/69
COL	College Outpost, Alaska	64 54 00.0 N	147 47 36.0 W	320	100,000	1,500	1/64	
COP	Copenhagen, Denmark	55 41 00.0 N	12 26 00.0 E	13	12,500	750	1/62	
COR	Corvallis, Oregon	44 35 08.6 N	123 18 11.5 W	121	25,000	1,500	7/62	
CTA	Charters Towers, Australia	20 05 18.0 S	146 15 16.0 E	357	100,000	3,000	2/63	
DAG	Danmarkshavn, Greenland	76 46 12.0 N	18 46 12.0 W	0	50,000	750	9/72	
DAL	Dallas, Texas	32 50 46.0 N	96 47 02.0 W	187	25,000	1,500	11/61	
DAV	Davao, Philippines	7 05 16.0 N	125 34 29.0 E	85	6,250	3,000	9/64	
DUG	Dugway, Utah	40 11 42.0 N	122 48 48.0 W	1,477	400,000	3,000	5/62	
EIL	Eilat, Israel	29 33 00.0 N	34 57 00.0 E	200	200,000	750	1/69	
EPT	El Paso, Texas	31 46 18.0 N	106 30 21.0 W	1,186	100,000	1,500	6/77	
ESK	Eskdalemuir, Scotland	55 19 00.0 N	03 12 18.0 W	242	12,500	750	4/64	
FLO	Florissant, Missouri	38 48 06.0 N	90 22 12.0 W	160	50,000	3,000	8/61	8/71
FVM	French Village, Missouri	37 59 02.4 N	90 25 33.6 W	310	50,000	1,500	10/74	
GDH	Godhavn, Greenland	60 15 00.0 N	53 32 00.0 W	23	25,000	1,500	11/62	

*Magnifications may vary seasonally; they are listed on the seismogram.

**Only shows stations that closed before 1978 when the copying to 70 millimeter film chips ended.

Table 2.1. List of all World-Wide Standardized Seismograph Network Stations installed. (SP,short period; LP, long-period)—Continued

WWSSN Station list								
Code	Station	Coordinates		Elevation (meters)	Magnification*		Open	Closed
		Latitude (deg) (min) (sec)	Longitude		SP	LP		
GEO	Georgetown, D.C.	38 54 00.0 N	77 04 00.0 W	29	25,000	750	11/61	
GIE	Galapagos Islands	00 44 00.0 S	90 18 00.0 W	30	12,500	750	5/64	
GOL	Golden, Colorado	39 42 01.0 N	105 22 16.0 W	2,359	400,000	1,500	12/61	
GRM	Grahamstown, South Africa	33 18 48.0 S	26 34 24.0 E	610	25,000	1,500	11/67	
GSC	Goldstone, California	35 18 06.0 N	116 48 16.6 W	990	100,000	1,500	2/63	
GUA	Guam, Mariana Islands	13 32 18.0 N	144 54 42.0 E	230	6,250	750	4/63	
HKC	Hong Kong, China	22 18 12.8 N	114 10 18.8 E	27	12,500	750	5/63	
HLW	Helwan, Egyt	29 51 30.0 N	31 20 30.0 E	116	50,000	3,000	5/62	
HNR	Honiara, Solomon Islands	9 25 55.9 S	159 56 49.6 E	72	12,500	1,500	2/62	
HOW	Howrah, India	22 25 00.0 N	88 18 33.0 E	3	1,600	1,500	11/63	12/68
IST	Istanbul, Turkey	41 02 44.0 N	28 59 45.0 E	50	25,000	1,500	1/62	
JCT	Junction City, Texas	30 28 46.0 N	99 48 98.9 W	591	100,000	1,500	3/65	
JER	Jerusalem, Israel	31 46 19.0 N	35 11 50.0 E	770	50,000	3,000	8/64	
KBL	Kabul, Afghanistan	34 32 27.0 N	69 02 35.4 E	1,920	400,000	6,000	6/68	
KBS	Kingsbay, Spitsbergen	78 55 03.0 N	11 55 26.0 E	46	25,000	1,500	10/67	
KEV	Kevo, Finland	69 45 19.0 N	27 00 24.0 E	80	25,000	1,500	9/62	
KIP	Kipapa, Hawaii	21 25 24.0 N	158 00 54.0 W	70	12,500	750	12/62	
KOD	Kodaikanal, India	10 14 00.0 N	77 28 00.0 E	2,345	50,000	1,500	11/64	
KON	Kongsberg, Norway	59 38 56.7 N	9 35 53.6 E	216	50,000	1,500	5/62	
KRK	Kirkenes, Norway	69 43 27.0 N	30 03 45.0 E	25	25,000	1,500	5/62	5/69
KTG	Kap Tobin, Greenland	70 25 00.0 N	21 59 00.0 W	6	25,000	750	8/63	
LAH	Lahore, Pakistan	31 33 00.0 N	74 20 00.0 E	210	3,125	750	8/62	12/68
LEM	Lembang, Indonesia	6 50 00.0 S	107 37 00.0 E	1,252	25,000	750	10/64	
LON	Longmire, Washington	46 45 00.0N	121 48 36.0 W	854	100,000	1,500	8/62	
LOR	Lormes, France	47 16 06.0 N	3 51 32.0 E	520	100,000	3,000	3/66	
LPA	La Plata, Argentina	34 54 32.0 S	57 55 55.0 W	14	3,125	750	2/62	
LPB	La Paz, Bolivia	16 31 57.6 S	68 05 54.1 W	3,292	50,000	1,500	3/62	
LPS	La Palma, El Salvador	14 17 32.0 N	89 09 43.0 W	1,000	50,000	1,500	7/62	
LUB	Lubbock, Texas	33 35 00.0 N	101 52 00.0 W	979	25,000	1,500	12/61	
MAL	Malaga, Spain	36 43 39.0 N	4 24 40.0 W	60	25,000	1,500	3/62	
MAN	Manila, Philippines	14 39 43.2 N	121 04 36.7 E	70	6,250	1,500	6/62	
MAT	Matsushiro, Japan	36 32 30.0 N	138 12 32.0 E	422	100,000	3,000	8/65	
MDS	Madison, Wisconsin	43 22 29.0 N	89 45 36.0 W	278	100,000	1,500	11/61	
MHI	Mashhad, Iran	36 18 00.0 N	59 29 40.2 E	1,100	25,000	750	10/75	
MNN	Minneapolis, Minnesota	44 54 52.0 N	93 14 17.7 W	224	50,000	3,000	7/62	4/65
MSH	Mashhad, Iran	36 18 40.0 N	59 35 16.0 E	987	12,500	1,500	9/65	9/75
MSO	Missoula, Montana	46 49 45.0 N	113 56 26.0 W	1,264	100,000	1,500	9/73	
MUN	Mundaring, Australia	31 58 42.0 S	116 12 30.0 E	253	25,000	750	5/62	
NAI	Nairobi, Kenya	1 16 26.6 S	36 48 13.2 E	1,692	50,000	1,500	6/63	
NAT	Natal, Brazil	5 07 00.0 S	35 02 00.0 W	10	25,000	1,500	6/65	
NDI	New Delhi, India	28 41 00.0 N	77 13 00.0 E	207	50,000	1,500	4/63	
NHA	Nhatrang, Viet Nam	12 12 36.0 N	109 12 42.0 E	5	25,000	1,500	5/62	
NIL	Nilore, Pakistan	33 39 00.0 N	73 15 06.0 E	536	100,000	1,500	7/69	
NNA	Nana, Peru	11 59 15.2 S	76 50 31.7 W	575	50,000	3,000	6/62	
NOR	Nord, Greenland	81 36 00.0 N	16 41 00.0 W	36	50,000	750	10/63	4/72

*Magnifications may vary seasonally; actual magnifications are listed on the seismogram.

**Only shows stations that closed before 1978 when the copying to 70 millimeter film chips ended.

Table 2.1. List of all World-Wide Standardized Seismograph Network Stations installed. (SP,short period; LP, long-period)—Continued

WWSSN Station list								
Code	Station	Coordinates			Magnification*		Open	Closed
		Latitude (deg) (min) (sec)	Longitude	Elevation (meters)	SP	LP		
NUR	Nurmijarvi, Finland	60 30 32.4 N	24 39 05.1 E	102	25,000	1,500	7/62	
OGD	Ogdensburg, New Jersey	41 05 15.0 N	74 35 45.0 W	–367	50,000	3,000	9/61	
OXF	Oxford, Mississippi	34 30 42.5 N	89 24 33.0 W	101	50,000	3,000	9/63	
PDA	Ponta Delgada, Azores	37 44 48.0 N	25 39 48.0 W	35	6,250	750	2/62	
PEL	Peldehue, Chile	33 08 37.0 S	70 41 07.0 W	690	50,000	1,500	3/64	
PLM	Palomar, California	33 21 12.4 N	116 51 42.1 W	1,692	50,000	750	11/61	1/63
PMG	Port Moresby, Papua	9 24 33.0 S	147 09 14.0 E	67	25,000	1,500	6/62	
POO	Poona, India	18 32 00.0 N	75 51 00.0 E	560	50,000	1,500	10/64	
PRE	Pretoria, South Africa	25 45 12.0 S	28 11 24.0 E	1,333	50,000	1,500	9/62	
PTO	Porto, Portugal	41 08 19.0 N	8 36 08.0 W	88	25,000	1,500	3/63	
QUE	Quetta, Pakistan	30 11 18.0 N	66 57 00.0 E	1,721	200,000	1,500	7/62	
QUI	Quito, Ecuador	00 12 00.5 S	78 30 01.8 W	2,837	3,125	3,000	2/63	5/76
RAB	Rabaul, New Britain	04 11 28.6 S	152 19 11.4 E	184	12,500	750	2/62	
RAR	Rarotonga, Cook Islands	21 12 45.0 S	159 46 24.0 W	28	6,250	375	5/65	
RCD	Rapid City, South Dakota	44 04 30.0 N	103 12 30.0 W	995	25,000	1,500	12/61	12/74
RIV	Riverview, Australia	33 49 45.7 S	151 09 30.0 E	25	12,500	750	1/63	
SBA	Scott Base, Antarctica	77 51 01.0 S	166 45 22.0 E	38	50,000	750	2/63	
SCP	State College, Pennsylvania	40 47 42.0 N	77 51 54.0 W	352	50,000	1,500	12/61	
SDB	Sa Da Bandeira, Angola	14 55 33.0 S	13 34 19.0 E	1,781	100,000	1,500	10/64	2/75
SEO	Seoul, South Korea	37 34 00.0 N	126 58 00.0 E	86	12,500	375	3/63	
SHA	Spring Hill, Alabama	30 41 39.7 N	88 08 34.1 W	61	6,250	1,500	3/62	
SHI	Shiraz, Iran	29 38 17.9 N	52 31 11.8 E	1,596	50,000	1,500	5/63	
SHK	Shiraki, Japan	34 31 56.0 N	132 40 39.0 E	285	12,500	1,500	12/65	
SHL	Shillong, India	25 34 00.0 N	91 53 00.0 E	1,600	200,000	3,000	4/63	
SJG	San Juan, Puerto Rico	18 06 42.0 N	66 09 00.0 W	457	50,000	750	10/64	
SNA	Sanae, Antarctica	70 18 54.0 S	02 19 30.0 W	57	50,000	NR	2/64	
SNG	Songkhla, Thailand	07 10 24.0 N	100 37 12.0 E	4	25,000	1,500	11/65	
SOM	Sombrero, Chile	52 46 51.0 S	69 14 32.0 W	73	6,250	375	10/64	
SPA	South Pole, Antarctica	90 00 00.0 S	00 00 00.0	2,927	100,000	750	2/63	
STU	Stuttgart, Germany	48 46 19.0 N	09 11 42.0 E	360	25,000	750	1/62	
TAB	Tabriz, Iran	38 04 03.0 N	46 19 36.0 E	1,430	6,250	1,500	8/65	
TAU	Tasmania University, Tasmania	47 54 35.7 S	147 19 13..5 E	132	25,000	750	5/62	
TOL	Toledo, Spain	39 52 53.0 N	04 02 55.0 W	480	25,000	1,500	3/62	
TPM	Tepoztlan, Mexico	18 59 00.0 N	99 03 42.0 W	1,500				Inactive
TRI	Trieste, Italy	45 42 32.0 N	13 45 51.0 E	126	50,000	3,000	7/63	
TRN	Trinidad	10 38 56.1 N	61 24 10.0 W	24	25,000	1,500	1/62	
TUC	Tucson, Arizona	32 18 35.0 N	110 46 56.0 W	985	200,000	1,500	12/62	
UME	Umeä, Sweden	63 48 54.0 N	20 14 12.0 E	16	50,000	5,500	1/62	
UNM	Mexico City, Mexico	19 19 44.4 N	99 10 41.1 W	2,257	6,250	1,500	6/67	10/70
VAL	Valentia, Ireland	51 56 22.0 N	10 14 39.0 W	14	25,000	1,500	10/62	
WEL	Wellington, New Zealand	41 17 10.0 S	174 46 06.0 E	122	6,250	750	4/62	
WES	Weston, Massachusetts	42 23 04.9 N	71 19 19.5 W	60	50,000	3,000	10/61	
WIN	Windhoek, Namibia	22 34 00.0 S	17 06 00.0 E	1,728	50,000	1,500	12/62	

* Magnifications may vary seasonally; actual magnifications are listed on seismograms.
** Only shows stations that closed before 1978 when the copying to 70 millimeter film chips ended.

3. WWSSN Instrumentation

The WWSSN system design was based on specifications developed in 1960 by the Coast and Geodetic Survey with advice from a panel of seismologists assembled by the National Academy of Sciences. An initial contract for the manufacture and assembly of 125 WWSSN systems was awarded to the Geotechnical Corporation of Garland, Texas. The most detailed description of the WWSSN system is provided in the *Operation and Maintenance Manual, World-Wide Seismograph System, Model 10700* (Geotechnical Corp., 1962). A few hard copies are on hand at ASL.

The WWSSN system consisted of three short-period seismographs, three long-period seismographs, a timing and power console, and various support equipment. Major components of the system are shown in figure 3.1 and a block diagram of the system is shown in figure 3.2.

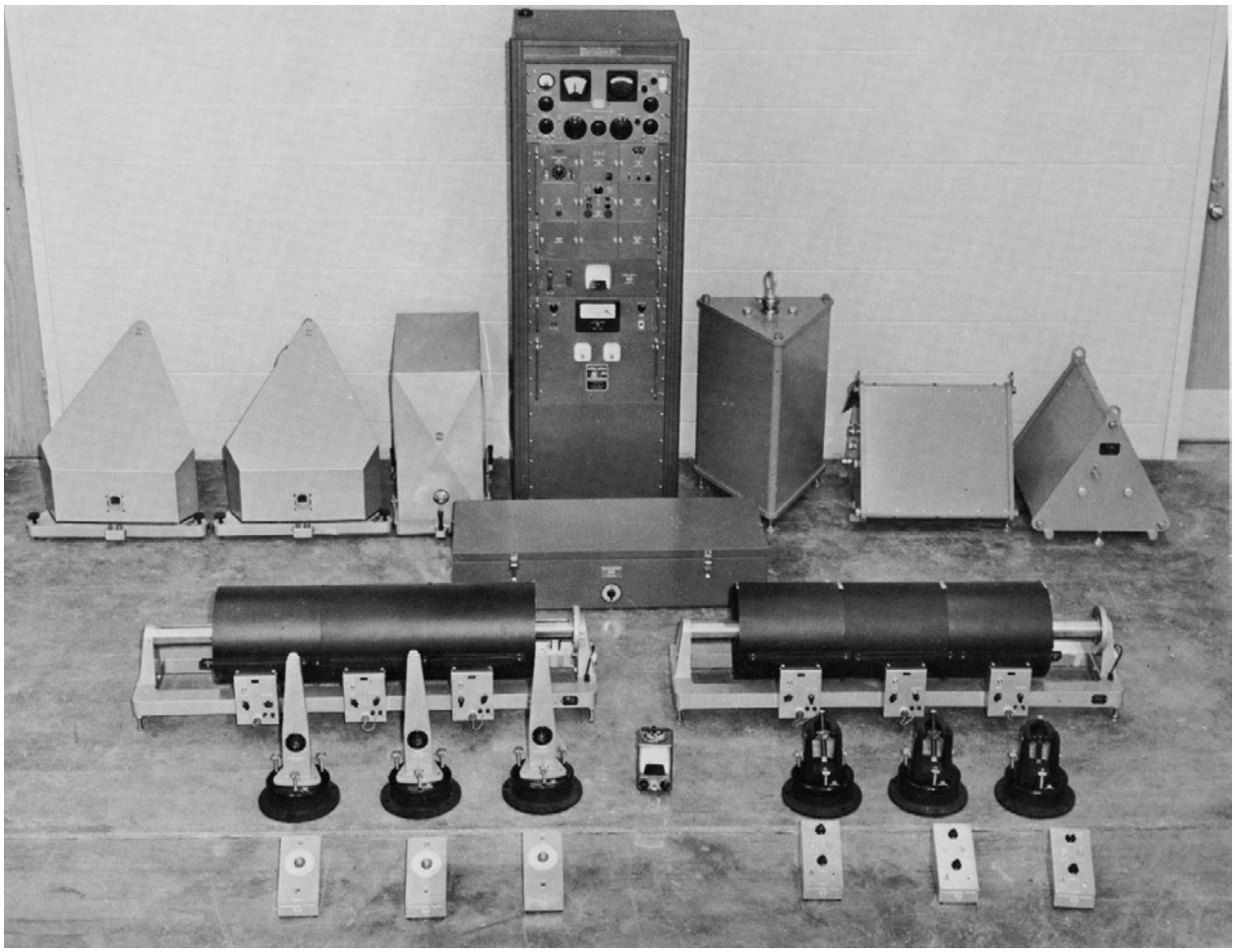

Figure 3.1 Components of the World-Wide Standardized Seismograph Network system. Long-period seismometers are shown in the upper left, galvanometers and recorders in the lower left. Short-period seismometers are shown in upper right, galvanometers and recorder in lower right. The electronics console contains timing system, controls, and power supply.

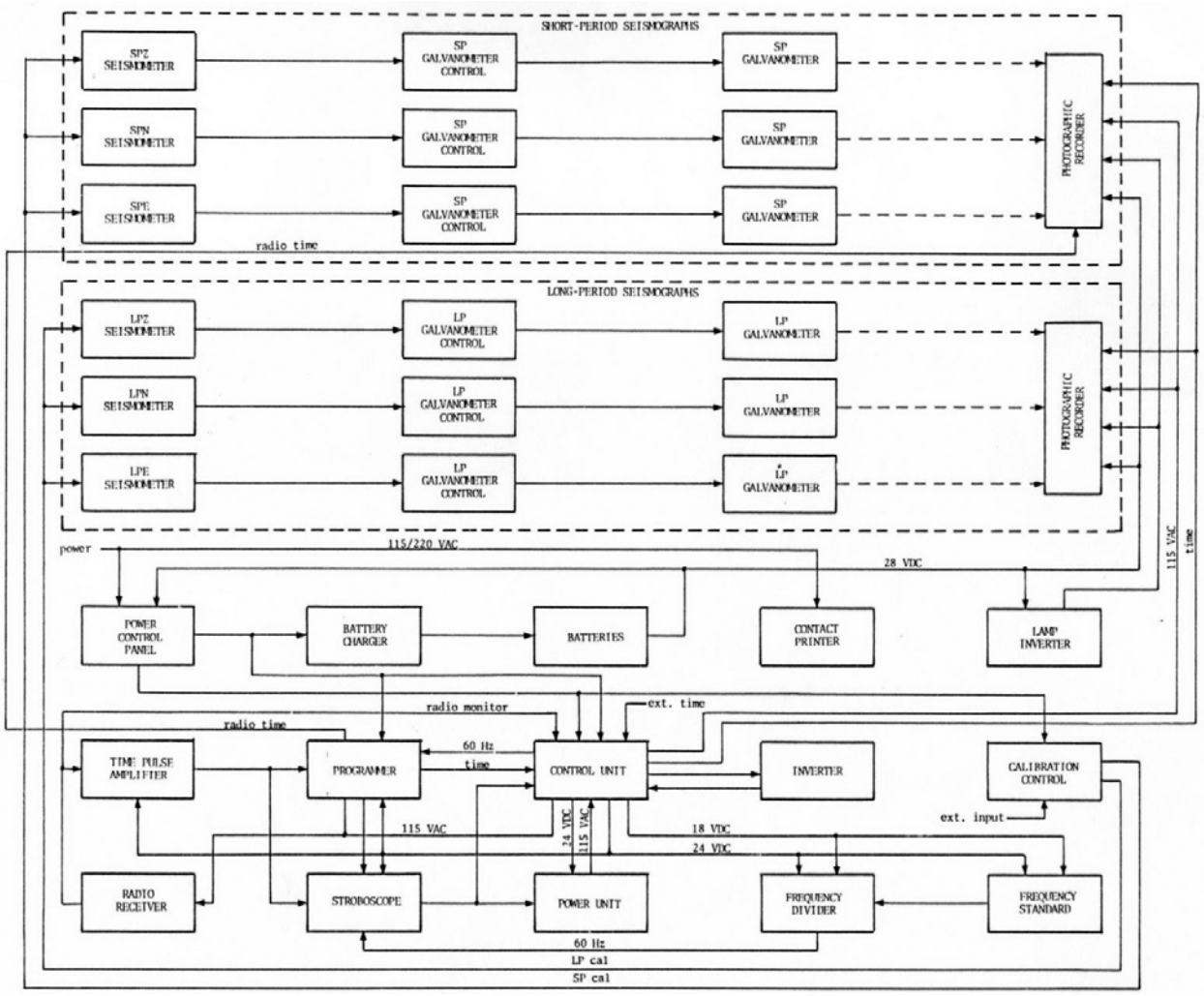

Figure 3.2 Block diagram of World-Wide Standardized Seismograph Network system.

The short- and long-period seismographs were oriented along the vertical, north-south and east-west axes. A seismograph component consisted of a seismometer, a galvanometer control unit, a galvanometer, and a photographic drum recorder. The short-period, Benioff-type variable-reluctance seismometers were operated at a period of 1 second (s). Originally, the Sprengnether (Press-Ewing type) long-period seismometers were operated at a period of 30 s; the period was reduced to 15 s in the mid-1960s to improve stability.

The galvanometers, driven by signals generated in the seismometers, were recorded optically on the drum recorders. The short-period galvanometers had an air-damped period of 0.75 s, and the long-period galvanometers were operated with an air-damped period of 100 s.

The galvanometer control units were located in the circuits between the seismometers and galvanometers. They contained step and trim attenuators that permitted adjustment of seismograph magnification as well as function switches used to test the free period and damping of the instruments. The short-period control boxes also provided seismometer damping control. The long-period control boxes did not provide control of seismometer damping. The magnification of the short-period seismographs could be adjusted in 6 decibel (dB) steps between 3,125 and 400,000; the magnification of the long-period seismographs could be adjusted in 6 dB steps from 375 to 6,000. The peak

magnification of the long-period seismographs with 30-s seismometers was 3,000. Normally, the three seismograph components of each period range were operated at the same magnification.

The photographic recorders were placed with the galvanometers and control units in a darkroom. Light from a small lamp mounted in the recorder was reflected from the galvanometer mirror and focused sharply on photographic paper wrapped on the recorder drum. The light beam could be deflected slightly by an electromagnetic device to produce time marks that appeared on the recordings. The recorder drums were rotated and translated by synchronous motors.

4. WWSSN Station Facilities

Facilities for housing the WWSSN systems varied widely among the stations in the network. Many of the seismographs were installed in special vaults, some in mines or tunnels, and some in the basements of buildings. At a typical setup designed specifically for the WWSSN system, the equipment was installed in a walk-in vault constructed just below ground level (see fig. 4.1). The seismometers were located in a separate light-tight room on piers attached to rock. For convenience, the recorders and galvanometers also were set on piers, although these usually were constructed of cement blocks and attached to the floor. The timing and power console was located in an adjoining room, often the entryway, and a darkroom was required for developing the seismograms. Heating and air conditioning were avoided in the seismometer vault, if possible, although dehumidifiers frequently were used.

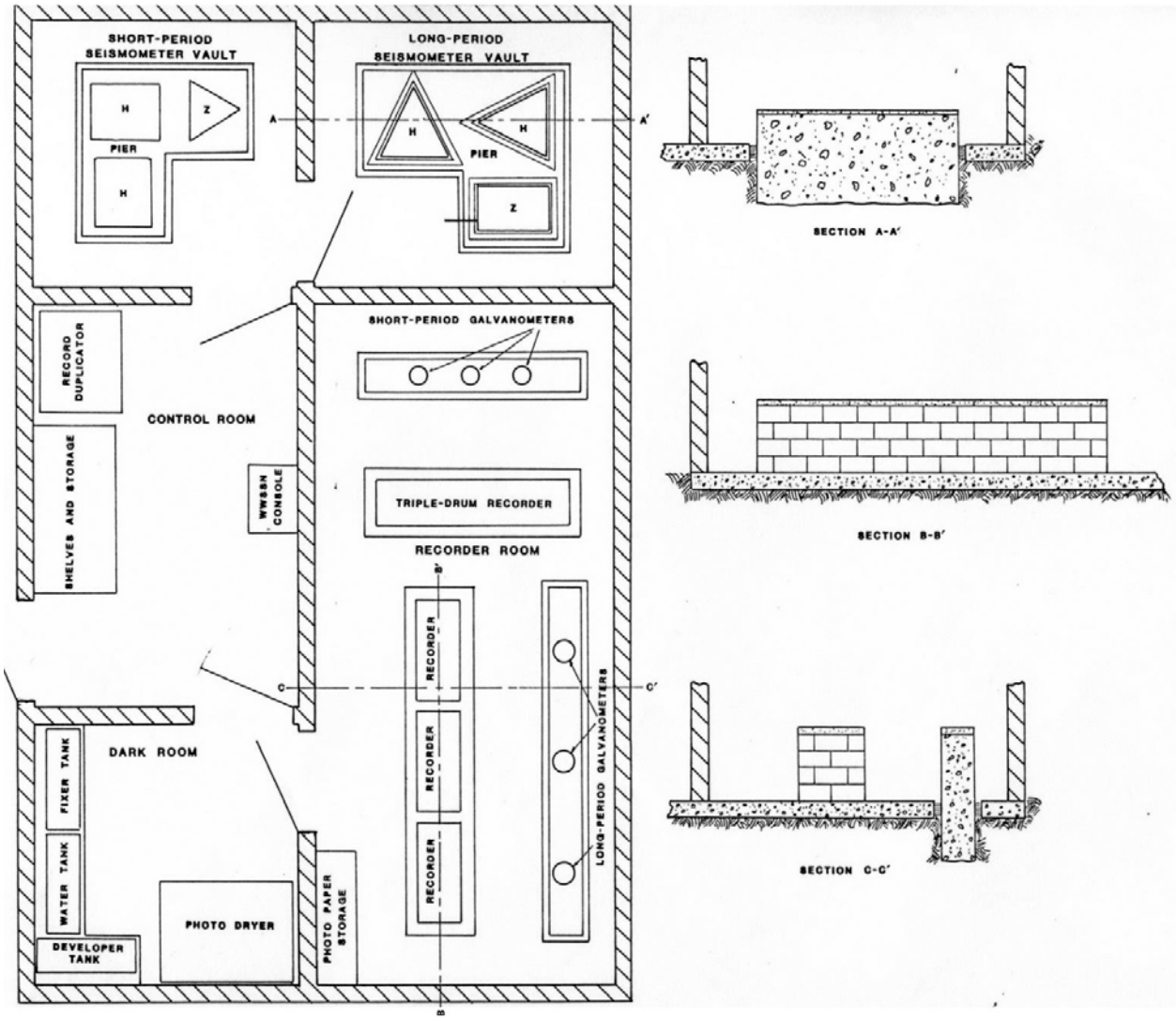

Figure 4.1 Typical World-Wide Standardized Seismograph Network Vault

5. WWSSN Operating Procedures

Once a day, usually in the early morning local time, records were changed on the photographic recorders; this was a process that generally took 10 to 15 minutes (min). After the record change, the station operator would apply a calibration pulse to the seismometers. The timing system was checked against radio-transmitted time signals and any error was noted and adjusted to zero. A record was kept of the daily timing error and when it reached 50 milliseconds or more an adjustment was made to the frequency of the crystal oscillator.

Two types of logs were maintained at the stations, an operational log and a maintenance log. The operational log was a daily record of time corrections, crystal settings, calibration currents, and seismograph attenuator settings. The maintenance log was a record of service performed by the station operator when malfunctions occurred. The logs were sent in periodically with the seismograms.

Most of the WWSSN stations sent in their seismograms to the Data Center for copying at regular intervals ranging from a few weeks to a month or more. A few stations used the copier provided to

duplicate the seismograms before sending them. After the seismograms had been microfilmed at the Data Center, they were returned to the stations.

Originally, it was planned that each station would be serviced annually by technicians based at ASL. During a maintenance visit, the equipment was serviced and the seismographs were completely recalibrated; these tasks required one or two weeks to complete. Maintenance reports and calibration test data were kept on file at the Albuquerque Seismological Laboratory. The visits were curtailed in 1969 and very few stations were visited between 1969 and 1978.

6. WWSSN Seismogram Format

The WWSSN seismograms were recorded on photographic paper that is approximately 0.91 meters (m) by 0.30 m in size. The helical trace is divided into 15-min segments on the short-period seismograms and into 30-min or 1-hour segments on the long-period seismograms. An upward deflection on the seismogram was intended to correspond to vertical, north, or east ground motion, depending on the component. Data users should be aware that there were a few instances where polarities were reversed inadvertently. A typical short-period seismogram is shown in figure 6.1 and a typical long-period seismogram is shown in figure 6.2.

The time mark format was the same on the short- and long-period records. Minute marks were recorded as upward deflections lasting 2 s. Hour marks are 5 s in length. The onset of the deflection corresponds to the beginning of each minute, and time should be measured from that point. Hour marks at 0000, 0600, 1200 and 1800 hours Greenwich Mean Time (GMT) were indicated by no deflection of the trace. Time marks on the short-period seismograms should line up as straight vertical lines; the time marks are angled slightly on the long-period seismograms. If the time marks do not form a straight line, this indicates that the recorders were not being driven by the precision 60 hertz (Hz) power source from the power and timing console. This does not affect the accuracy of the time marks.

The drum rotation rate was 60 mm per minute for the short-period recorders and 15 or 30 mm per minute for the long-period recorders. Spacing between the minute marks on the seismograms may not be precisely 60 mm, 30 mm or 15 mm because of slight deformations that occurred during the development and drying of the records. Translation rates were set at 2.5 mm per revolution for the short-period recorders and 10 mm or 5 mm per revolution for the long-period recorders.

Radio time signals were recorded automatically on the short-period north-component (SPN) records for 5-min intervals beginning at 0000, 0600, 1200 and 1800 hours GMT. The radio time was recorded as a series of pulses corresponding to seconds and may be used to verify timing accuracy. In the WWV station code used, the 59th second of each minute was skipped. The quality of the radio signals varied geographically and over the course of the day; often only one of the daily recorded transmissions was usable for checking the time.

The calibration pulses on the seismograms were applied manually shortly after the new records were placed on the recorders. The short-period seismometers were pulsed several times in succession, and the long-period seismometers were pulsed once.

As the seismograms were recorded, they were encoded with the station code and component by an activated plate fixed to the edge of the recorder drum. The stamp at the lower left corner of the seismogram was applied after the record had been developed, and the information was written in the stamped area by the station operator. All times reference GMT. If the time correction listed is positive (+30 milliseconds [ms], for example), the value in milliseconds should be added to the clock time measured from the time marks. Calibration currents are listed in units of milliamperes; G is the value of the calibrator electrodynamic constant and is listed in units of newtons per ampere.

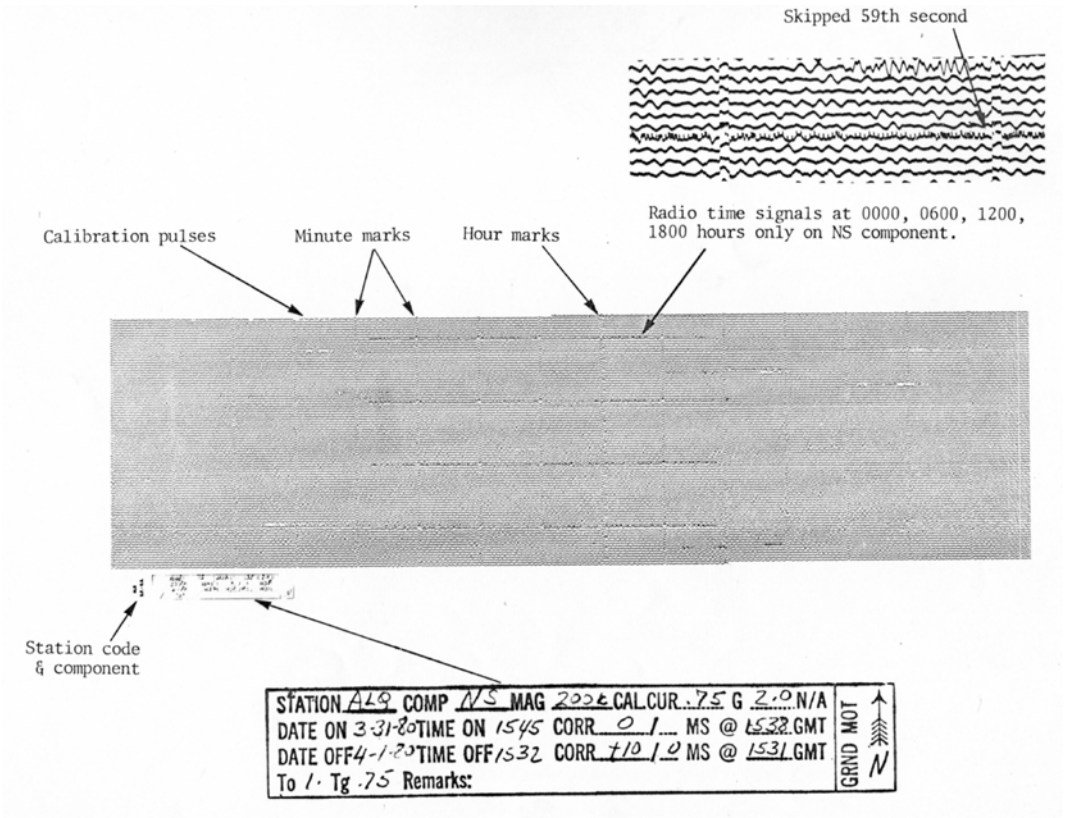

Figure 6.1 Typical World-Wide Standardized Seismograph Network short period seismogram.

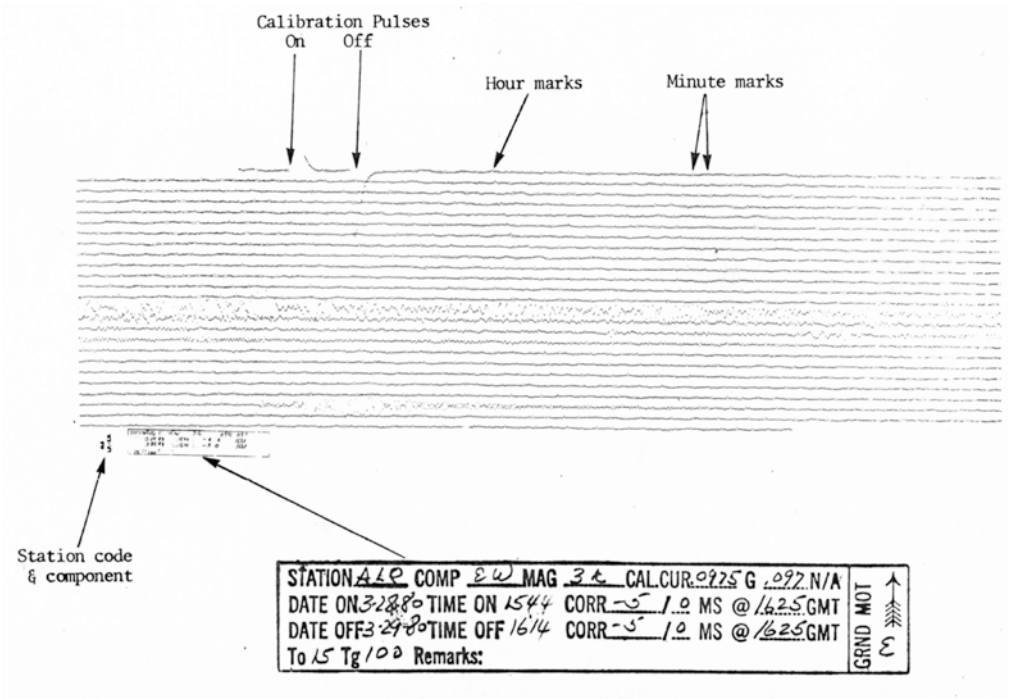

Figure 6.2 Typical World-Wide Standardized Seismograph Network long-period seismogram.

7. WWSSN Seismogram Noise Characteristics

The location of the seismometer vault had much to do with the noise that was observed on the short-period seismograms. Where possible, the vault was isolated from cultural activities (such as cities, roads, railroads, and dams) that are known to generate short-period noise. Nevertheless, there were few high magnification stations in the network that did not show some evidence of cultural noise during daytime hours. At most WWSSN stations, the operating magnification was limited by the level of natural microseisms. The observed periods of the recorded microseisms ranged from about 1 s for island sites to 8 or 9 s for interior continental sites. Often, the level of microseismic activity is seasonal and the magnifications at some stations were adjusted accordingly.

The seismometer vault itself had much to do with the noise that was observed in the long-period seismograms. The long-period seismographs were very sensitive to their environment, especially changes in air pressure and temperature. Pressure variation affected the vertical component seismometer by modulating the buoyant force of the atmosphere on the pendulum. This resulted in a sinusoidal-like noise on the vertical-component seismograms, generally having a period of 50 s or longer (see fig. 7.1*A*). Pressure changes with this characteristic were usually associated with windy conditions. Similar noise recorded on the horizontal long-period components is believed to have been caused by tilting during passage of wind-generated pressure cells, as described by Sorrels (1971). Temperature variations in the vault would affect the long-period seismographs in several interesting ways. They could have caused abrupt, slight deformation of the seismometer spring or hinges that produced pulses on the records (see fig. 7.1*B*). As shown in the figure, the pulses would often have one polarity as the temperature was rising during the day and the opposite polarity as the temperature was falling at night. Thermal differentials within the seismometer case could generate convection currents that resulted in long-period sinusoidal-like noise on the seismograms (see fig. 7.1*C*). This type of noise was reduced when small heaters were placed in the top of the seismometer case to stratify the air within the case. Temperature differentials could also produce thermoelectric currents in seismograph circuits (usually the control box) which would cause the traces to wander on the seismogram (see fig. 7.1*D*). The WWSSN seismometers were not well protected from thermal variations, so the magnitude of temperature-related noise depended largely on vault conditions. High humidity is another vault condition that adversely affected the seismographs, sometimes causing changes in sensitivity or response characteristics as a result of corrosion or leakage.

Most of the WWSSN long-period seismograms show some evidence of environmental noise, but at the majority of stations, the magnification was limited by microseisms in the 6–8-s period band. Except during rare periods of microseismic storms, earth noise at periods longer than 10 s could not be visually resolved on the WWSSN long-period seismograms.

By today's standard, the dynamic range of the WWSSN recording system was very limited. The zero-to-peak dynamic range of a drum recorder is about 44 dB if the smallest observable signal is 1 mm and the signal is centered on the record. For large events, the peaks and troughs of the signal were literally off the seismograms and recorded on adjacent recorders. By contrast, the dynamic range of 24-bit recorders used in modern seismographs is about 138 dB. A drum recorder with 138 dB of dynamic range would have to be nearly 17,000 m wide with a distance between the galvanometer and recorder of about 54,000 m.

A

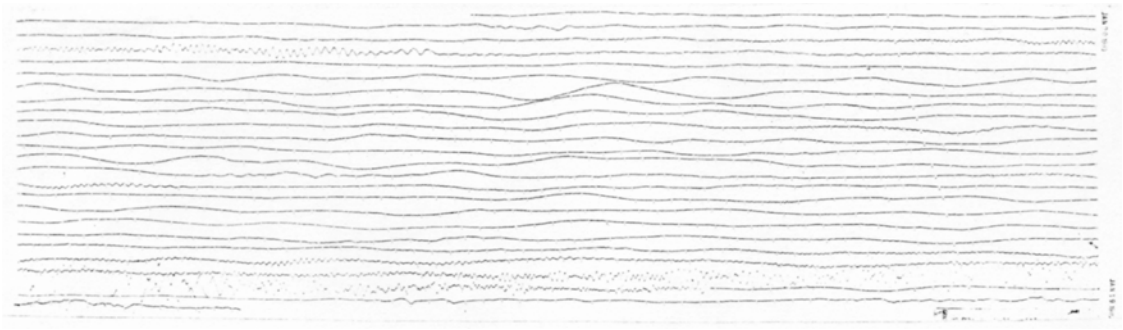

B

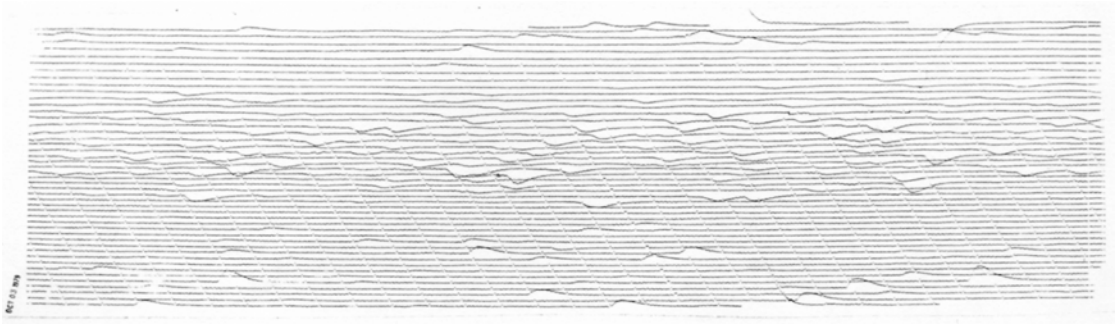

C

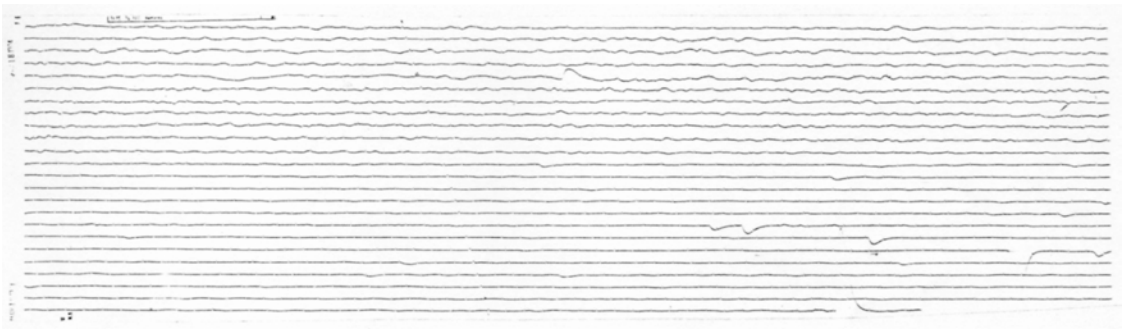

D

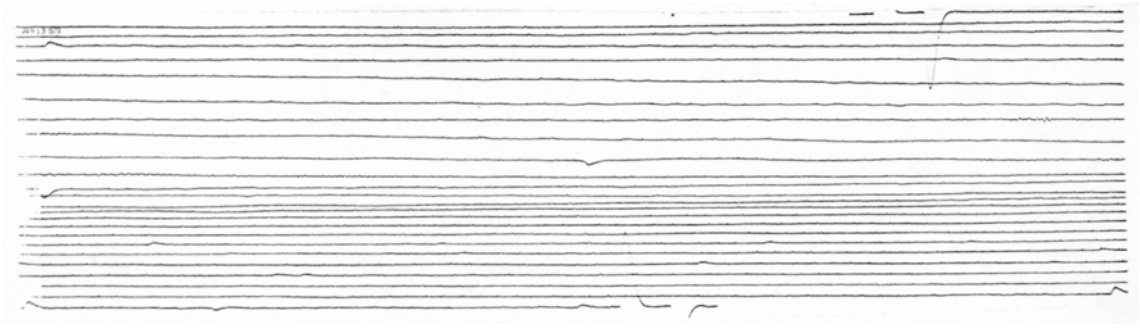

Figure 7.1 Types of noise on some World-Wide Standardized Seismograph Network Seismograms. *A,* Sinusoidal noise with a period of approximately 50 seconds or longer believed to be caused by pressure variations within the vault. *B,* Seismometer pulsing possibly caused by deformation of the seismometer spring or hinges due to temperature variations. *C*, Long-period sinusoidal noise possibly caused by convection currents. *D*, Wandering traces believed to be caused by thermal differentials.

8. WWSSN System Transfer Functions

8.1 Introduction

A seismograph transfer function describes the linear transformation of a signal between the input to the system—usually earth motion—and the output of the system—usually a pen, a light beam, a voltage, or a stream of digital bits. The transfer function provides the information needed to remove the instrument response and recover information in units of earth motion. In the past, theoretical seismograph response functions were computed to generate magnification and phase curves, especially before the advent of shaking tables and electrodynamic calibration devices, and they were (and still are) useful in the design and testing of seismographs. In the case of the WWSSN data, transfer functions could play a more important role in signal analysis if WWSSN waveforms were made available in a digital format.

The derivation of a generalized transfer function for the WWSSN seismographs is provided in Appendix A1. The equation below (eq. 8.1) is the same as the Laplace subsidiary system equation derived in Appendix A1 (eq. A1.53).

$$\frac{R(s)}{F(s)} = \frac{\dfrac{-2r_o\kappa_1 G_s G_g s}{MR_{11}K_g}}{\left(\left(s^2 + 2\lambda_{so}\omega_s s + \omega_s^2\right)(\alpha s + 1) + \dfrac{G_s^2 s}{MR_{11}}\right)\left(s^2 + 2\lambda_{go}\omega_g s + \omega_g^2 + \dfrac{G_g^2 s}{K_g R_{22}(\alpha s+1)} + \dfrac{\alpha G_g^2 s^2}{K_g\left(R_2+R_g+R_3\right)(\alpha s+1)}\right) - \dfrac{G_s^2 G_g^2 \kappa_1^{\,2} s^2}{MK_g R_{11}^2(\alpha s+1)}} \tag{8.1}$$

where

$R(s)$	is optical recording (meters)
$F(s)$	is force due to earth motion or calibration (newtons)
r_0	is distance from galvanometer to recorder (1 meter)
κ_1	is forward current gain in coupling circuit (unitless)
G_s	is electrodynamic constant of seismometer coil (volt-seconds/meter for the short-period seismometer and volt-seconds/radian for the long-period seismometer.)
G_g	is electrodynamic constant of galvanometer coil (newton-meters/ampere)
M	is inertial mass of seismometer (kilograms)
K_g	is moment of inertia about galvanometer suspension (kilogram-meter2)
R_{11}	is total resistance in seismometer circuit (ohms)
R_{22}	is total resistance in galvanometer circuit (ohms)
λ_{so}	is seismometer air damping ratio
ω_s	is seismometer natural angular frequency (radians/second)
λ_{go}	is galvanometer natural angular frequency (radians/second)
α	is ratio of seismometer inductance to total resistance in seismometer circuit
R_g	is resistance of galvanometer coil (ohms)
R_2	is coupling circuit resistance (ohms) (see fig A1.5)
R_3	is coupling circuit resistance (ohms) (see fig A1.5)

Although equation 8.1 describes a translational-type seismometer, it serves as well for a rotational (pendulum-type) seismometer by replacing the seismometer mass, M, in the equation with the seismometer moment of inertia, K_s. We will also define a sensitivity constant, S_c, as follows:

$$S_c = \frac{2r_o\kappa_1 G_s G_g}{MR_{11}K_g} \tag{8.2}$$

for the short-period seismograph, and

$$S_c = \frac{2r_o\kappa_1 G_s G_g}{K_s R_{11} K_g} \tag{8.3}$$

for the long-period seismograph. Equations 8.1 through 8.3 were used to compute the numerical transfer function poles and zeros that are presented in the following sections.

8.2 WWSSN Short-Period Transfer Functions

At the station, the first step in setting the short-period seismograph magnification was to adjust the calibrator electrodynamic constant, G_c, to a value of 2.0 newton/ampere (N/A) using a weight lift test, such as described in Section 9.1 and Appendix A1. Then κ_1 and R_{11} were adjusted using the short-period (SP) Galvanometer Control Box to set the operating magnification of the seismographs to one of the standard values depending on background noise. This was done by adjusting the attenuators on the control box so that a prescribed calibration current would produce a specified peak deflection on the seismogram, then adjusting a variable resistor in the control box to set the seismometer damping to a prescribed value. These calibration procedures are described in more detail in section 9.2.

The numerical transfer functions were derived in much the same way. The instrument constants listed in table 8.1 were substituted in equation 8.1 together with trial values of κ_1 and R_{11}. The values for κ_1 and R_{11} were then adjusted as necessary until the peak step response amplitude and overshoot ratio computed for the trial transfer function were in agreement with the values specified for the system. When the final transfer function was obtained, the sensitivity constant, S_c, and the magnification at the reference period were computed from the transfer function.

Table 8.1. World-Wide Standardized Seismograph Network short-period seismograph instrument parameters.

Parameter	Value	Units	Source[1]
M	107.5	kilograms	s
R_s	64.3	ohms	m
L_s	6.66	henries	m
G_s	360	volt-seconds/meter	m
G_c	2.0	newtons/ampere	a
ω_s	6.283	radians/second	a
λ_{so}	0.0088		m
R_c	293	ohms	m
K_g	1.7×10^{-10}	kilogram-meters^2	m
R_g	77.3	ohms	m
G_g	6.68×10^{-4}	newton-meters/ampere	m
ω_g	8.378	radians/second	m
λ_{go}	0.02		m
R_{11}	adjustable	ohms	a
R_{22}	158	ohms	m
κ_1	adjustable		a
r_o	1.0	meters	a

[1]s – manufacturer's specification
m – measured directly or computed from measured data
a – adjusted to specified value

Ideally, a single transfer function would adequately describe the short-period seismograph in any of its magnification configurations. For standard magnification settings of 50,000 and less, the dynamic response functions varied less than 2 percent in amplitude and 1° in phase, so the seismograph is adequately described in those cases by a single set of poles and zeros. However, at magnifications above 50,000, seismometer-galvanometer coupling caused a non-linear increase in seismograph sensitivity as the gain was increased. The most significant difference occurred at the highest magnification setting. Seismometer coil inductance affected both the sensitivity of the seismograph and the shape of the frequency response by producing the effect of a single-pole low-pass filter with a corner frequency at approximately 4.5 Hz depending on the value of R_{11}. As R_{11} changed when adjustments were made to the damping control, both the static sensitivity and dynamic characteristics of the seismograph were affected. Fortuitously, the effects on sensitivity of coupling and inductance offset one another at the higher magnification settings, so the calibration of the short-period seismographs was not significantly affected.

Transfer functions obtained for the WWSSN short-period seismograph are listed in table 8.2a and table 8.2b. Note that the transfer functions are presented as a table of complex poles and zeros where $j = \sqrt{-1}$ (see Appendix A1for further details). Also listed are adjusted values of κ_1, R_{11} and S_c, computed values for the peak step response amplitude and overshoot ratio and the computed seismograph magnification at a period of 1 s. The step response and amplitude response used in setting the values of κ_1 and S_c for a standard magnification of 50,000 are shown graphically in figure 8.1. Amplitude response curves computed from the transfer functions are presented in figure 8.2. A single phase response curve, computed at a magnification of 50,000, is shown in figure 8.3.

Table 8.2a. World-Wide Standardized Seismograph Network short-period transfer functions for earth displacement.

	Standard Magnifications		
	6,250	12,500	25,000
Poles	–3.962 ± j6.178	–3.973 ± j6.179	–3.973 ± j6.181
Poles	–7.193	–7.176	–7.109
Poles	–9.759	–9.790	–9.911
Poles	–21.432	–21.332	–21.239
Zeros	0	0	0
κ_1 (adjusted)	0.00731	0.01478	0.02955
R_{11} (adjusted)	194.8	194.4	194.2
Sc (computed)	28886	58405	116771
Computed peak step response amplitude (44 mm nominal)	34.0	44.0	44.0
Computed overshoot ratio (1/17 nominal)	1/17.0	1/17.0	1/17.0
Computed magnification at 1 second period	6002	12141	24286

Table 8.2b. World-Wide Standardized Seismograph Network short-period transfer functions for earth displacement.

	Standard Magnifications			
	50,000	100,000	200,000	400,000
Poles	–3.955 ± j6.187	–3.881 ± j6.212	–3.653 ± j6.298	–3.043 ± j6.533
Poles	–6.887	–6.313	–16.008 ± j4.949	–15.047 ± j11.404
Poles	–10.359	–11.980	–5.261	–3.847
Poles	–20.969	–19.781		
Zeros	0	0	0	0
κ_1 (adjusted)	0.0590	0.1175	0.2295	0.4225
R_{11} (adjusted)	193.9	192.9	188.2	171.2
Sc (computed)	233147	464318	906901	1669568
Computed peak step response amplitude (44 mm nominal)	44.0	44.0	44.0	44.0
Computed overshoot ratio (1/17 nominal)	1/17.0	1/17.0	1/17.0	1/17.0
Computed magnification at 1 second period	48582	97492	196301	407054

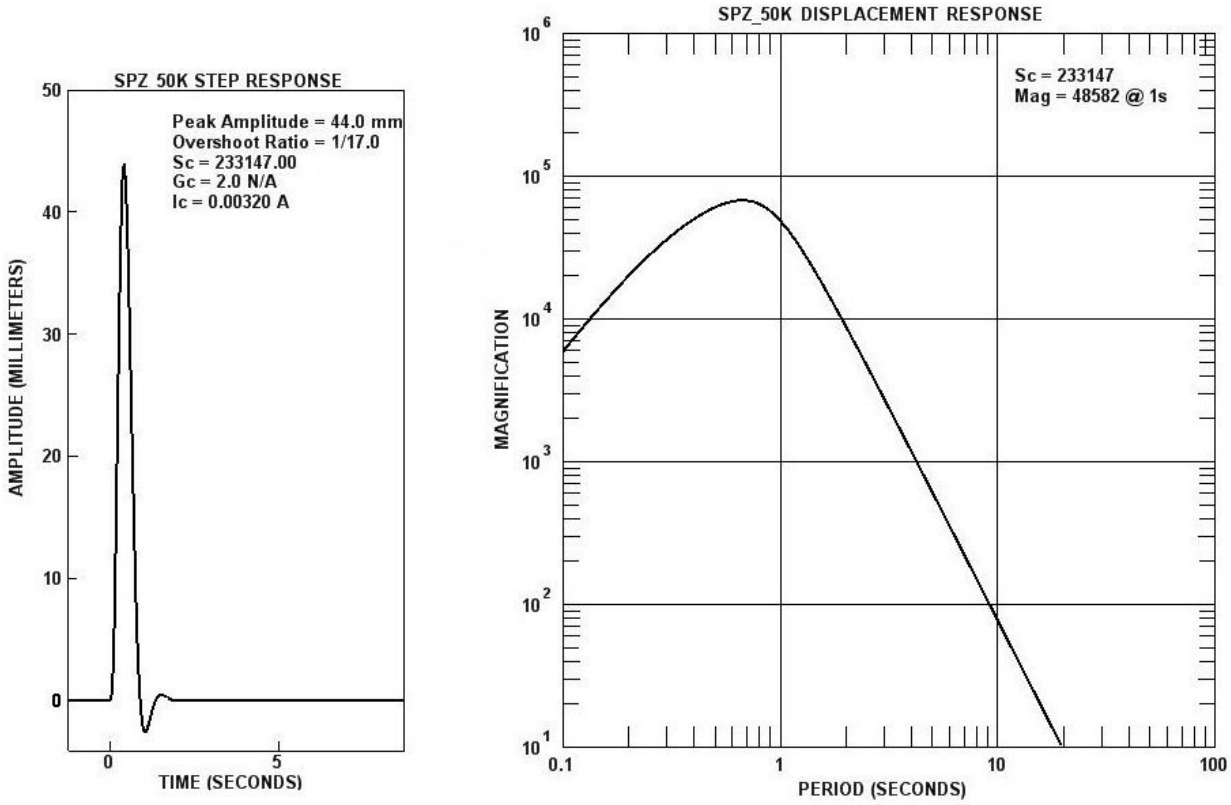

Figure 8.1 Computed step response used to set parameters for SP 50K transfer function and the amplitude response computed from the transfer function.

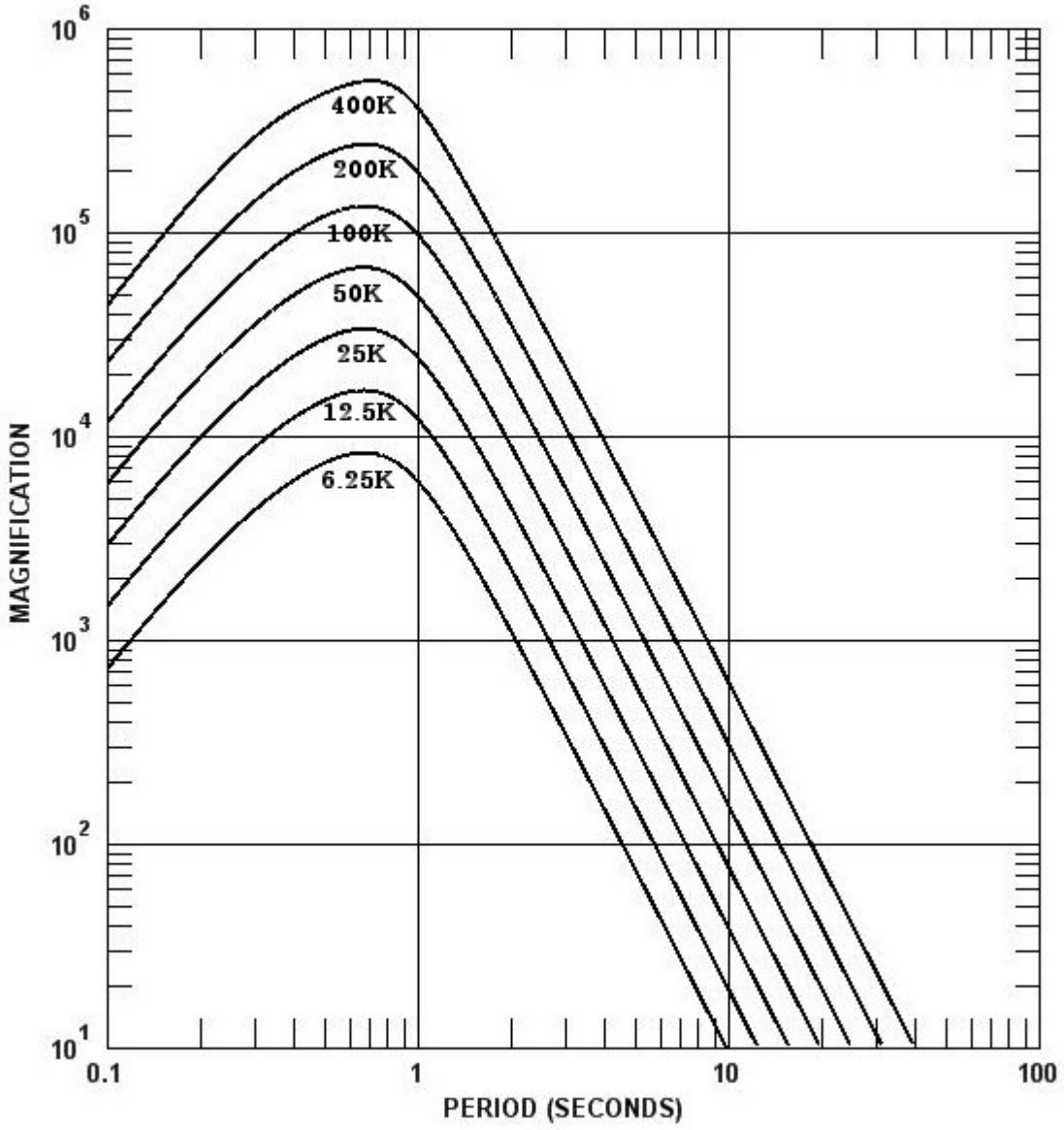

Figure 8.2. Computed magnification curves for the World-Wide Standardized Seismograph Network short-period system where K represents 1,000.

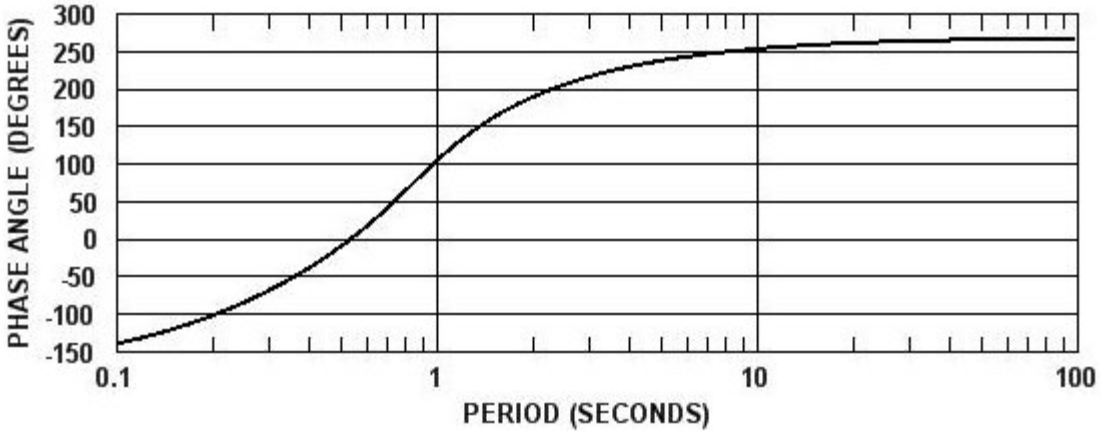

Figure 8.3 Computed phase response for the World-Wide Standardized Seismograph Network short-period system at a magnification of 50,000 at 1.0 second.

8.3 WWSSN Long-Period Transfer Functions

The transfer functions for the WWSSN long-period seismographs can be derived for any set of instrument parameters using the generalized system equation for a rotational seismograph. Computation is simplified in this case because inductive effects at periods longer than one second are negligible and α, the ratio of inductance to total circuit resistance, may be set to zero.

Values for the long-period instrument parameters are listed in table 8.3. The seismometer physical constants and electrodynamic constants of the signal coils were taken from Nuttli and McEvilly (1961). Other constants were measured or adjusted as indicated in the table. The seismometer and galvanometer coil resistances, R_s and R_g , nominally 500 ohms, varied among the instruments and were not recorded. The values given in the table are averages of a few measurements that were made during testing. Both R_{11} and R_{22} varied as the attenuators on the galvanometer control boxes were adjusted to set the magnification. The values shown are the average of measurements taken from four control boxes at the 12 dB setting while using the seismometer and galvanometer resistances shown in table 8.3. The values of R_{11} and R_{22} varied less than 1.5 percent from the average over the range of dB settings. The seismometer calibrator electrodynamic constant, G^*, was not adjustable and varied from instrument to instrument. Values measured during installation or maintenance were noted on the seismograms. The G^* values listed in Table 8.3 are averages taken from 32 vertical and 66 horizontal seismometers. Seismometer air damping also varied from the average value listed, by as much as ±20 percent in some cases, but this had only a small effect (less than 1 percent) on total damping.

Three important parameters of the seismograph were adjusted at the station during installation and follow-up maintenance visits. These were the seismometer and galvanometer periods and the galvanometer damping. Seismometer damping was not adjustable. The periods of the seismometers and galvanometers were set by making tilt adjustments to the instrument baseplates and observing and timing the air damped oscillations. These were subject to measurement error and possibly drift, especially for the 100-s galvanometer and the 30-s seismometer, both of which were operating near their maximum practicable period.

Table 8.3. World-Wide Standardized Seismograph Network long-period seismograph instrument parameters.

Parameter	Value		Units	Source[1]
	Vertical	Horizontal		
M	11.2	10.7	kilograms	s
K_s	1.229	1.322	kilogram-meters^2	s
r_{co}	0.3564	0.3576	meters	s
r_{cm}	0.3078	0.3454	meters	s
r_c	0.3480	0.3556	meters	s
R_s	480	480	ohms	m
L_s	1.16	1.16	henries	m
G_s	31.0	31.6	volt/radian/second	s
G^* (mean)	0.1036	0.09621	newtons/ampere	m
ω_s (15-100)	0.4189	0.4189	radians	a
ω_s (30-100)	0.2094	0.2101	radians	a
λ_{so} (15-100)	0.00972	0.0389		m
λ_{so} (30-100)	0.0286	0.0808		m
K_g	9.25×10^{-8}		kilogram/meters^2	s
R_g	490		ohms	m
G_g	3.088×10^{-3}		newton-meters/ampere	s
ω_g	0.06405		radians	a
λ_{go}	0.194			m
r_o	1.0		meters	a
R_{11}	989		ohms	m
R_{22}	986		ohms	m

[1]s – manufacturer's specification
m – measured directly or computed from measured data
a – adjusted to specified value

The long-period galvanometers were equipped with screw-driven magnetic shunts that could be used to change the value of G_g in order to compensate for variations in the factory setting of G_g and in R_{22} or R_g. A galvanometer test unit was provided that would drive the galvanometer with a step of current whose response could be timed and measured in the vault to set the damping to critical. However, the measurements were imprecise and uniformity was difficult to achieve, so the final settings for galvanometer damping varied from instrument to instrument. This variation had an effect on the transfer functions and the magnification setting.

The *design* transfer functions described below in table 8.4 are derived from the parametric values just as they are given in table 8.3. The vertical-component *design* transfer function for a magnification setting of 1,500 is believed to be a close approximation to the factory configuration used to derive the long-period amplitude and phase response curves and the calibration data that are provided in the manual. However, few of the long-period seismographs in the network were operated in conformance with the design specifications over the operating life of the WWSSN.

Because of the variability of physical constants for the individual components in the network, the long-period transfer functions suggested for use in place of the *design* transfer functions are based on averages, and they will be designated as *typical* transfer functions. They were derived from the system equation using the parametric values listed in table 8.3 for the nonadjustable constants and estimated from step response measurements in the case of the adjustable periods and damping. The

method used to estimate instrument period and damping from step response data is described in Appendix A2 and can be used by data users to generate transfer functions specific to individual seismograph components.

As previously noted, there were two operating configurations for long-period seismographs: an early configuration with a 30-s period seismometer followed by a more stable configuration with the seismometer operated at a 15-s period. The changes began at the stations in 1962 and were completed in 1965. The operating seismometer period is noted on the component seismogram. Separate transfer functions are derived for the two configurations. The transfer functions are derived from the system equation using appropriately chosen values for the constants. Magnification is computed from trial transfer functions while adjusting the forward current gain, κ_1, until the desired magnification at the seismometer period is achieved. Amplitude, phase, group delay, and step-response files are then derived from the final transfer function. A step response is generated by convolving the transfer function with a rectangular step input. The peak amplitudes of the computed step responses are used to derive calibration constants that can then be used to determine the magnification of components at operating stations.

The *typical* transfer functions serve better than the *design* transfer functions as general descriptions of the WWSSN long-period seismographs, and they are suggested for that purpose. However, user-generated transfer functions based on the analyses of component step responses would be preferable, especially for studies involving waveform analysis.

8.3.1 WWSSN Seismograph System *Design* Transfer Functions

Although the *design* transfer functions are not suggested for general use, they will be used in the following sections for purposes of comparison. The *design* transfer functions, computed using the parameters as they are listed in table 8.3, are provided in table 8.4 for a magnification of 1,500. This is believed to be the magnification setting of the instruments used in early calibration testing.

Table 8.4. World-Wide Standardized Seismograph Network long-period seismograph *design* transfer functions.

***DESIGN* TRANSFER FUNCTIONS FOR MAGNIFICATION OF 1500**				
	LP30		**LP15**	
	Vertical	**Horizontal**	**Vertical**	**Horizontal**
Poles	–0.07048+ j0.03112	–0.07085+j0.03037	–0.39710+j0.10490	–0.39610+j0.11110
Poles	–0.07048–j0.03112	–0.07085–j0.03037	–0.39710–j0.10490	–0.39610–j0.11110
Poles	–0.04038	–0.04095	–0.05223	–0.05241
Poles	–0.75067	–0.74445	–0.08168	–0.08116
Zeros	0.0	0.0	0.0	0.0
T_s	30.0	29.9	15.0	15.0
λ_s	1.916	1.898	0.953	0.951
T_g	98.1	98.1	98.1	98.1
G_g	0.003088	0.003088	0.003088	0.003088
λ_g	1.010	1.010	1.010	1.010
σ^2	0.03918	0.03650	0.03461	0.03233
κ_1	0.22220	0.21755	0.20836	0.20456
S_c	378.38	351.06	354.81	330.1

Graphical comparisons of the two seismometer configurations are shown in figure 8.4 for amplitude, in figure 8.5 for phase and in figure 8.6 for the step responses.

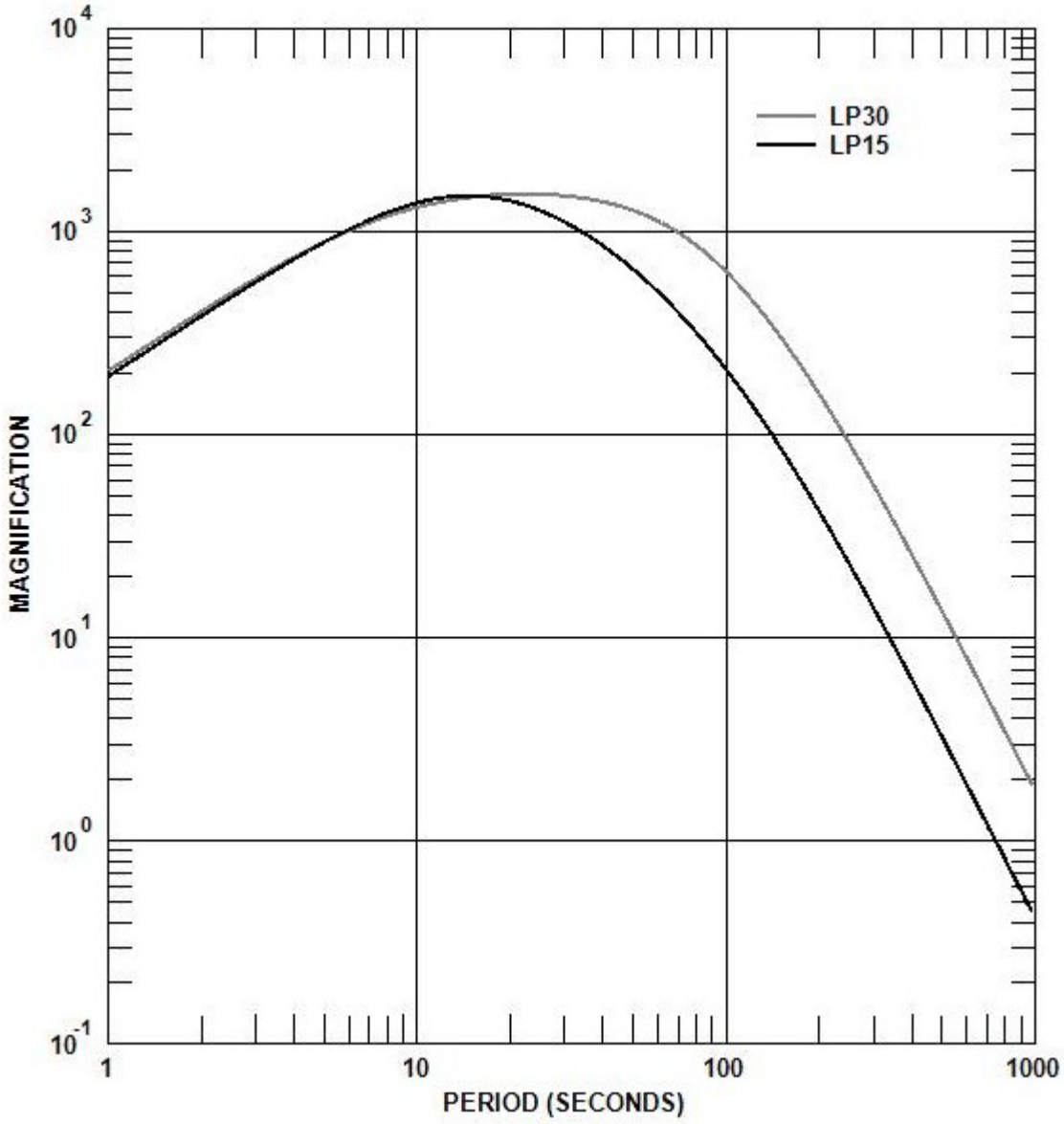

Figure 8.4 Amplitude responses computed from the *design* transfer functions of the two operating configurations of the World-Wide Standardized Seismograph Network long-period seismographs. Both are set to an operating magnification of 1,500 at the seismometer periods. LP30 designates the configuration using a 30 s galvanometer and LP15 designates the configuration using a 15 s galvanometer.

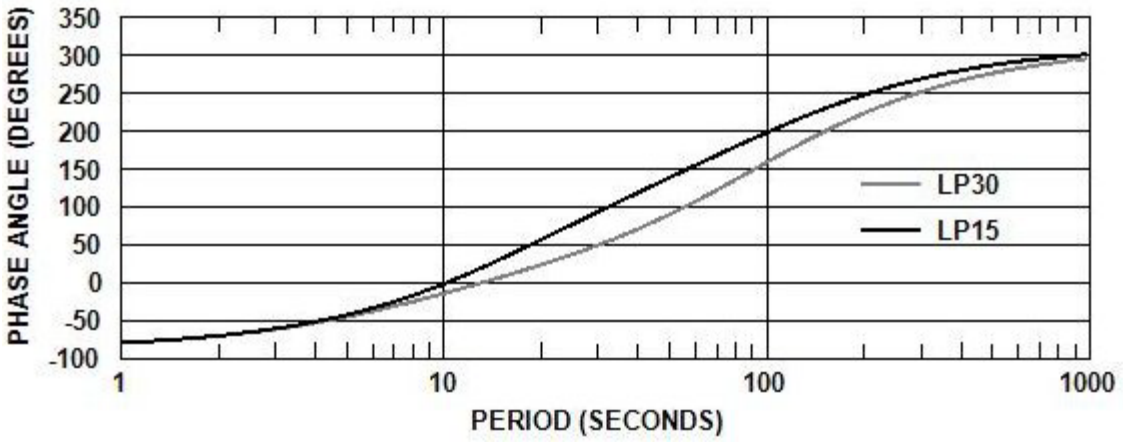

Figure 8.5 Phase responses computed from the *design* transfer functions of the two operating configurations of the World-Wide Standardized Seismograph Network long-period seismographs. LP30 designates the configuration using a 30 s galvanometer and LP15 designates the configuration using a 15 s galvanometer.

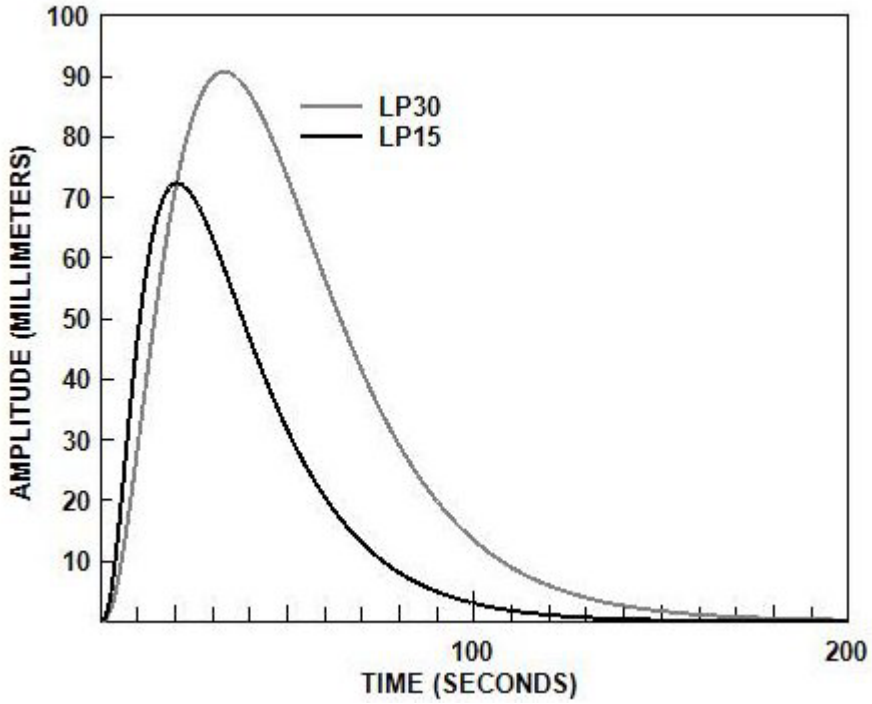

Figure 8.6 Step responses computed from the *design* transfer functions of the two operating configurations of the World-Wide Standardized Seismograph Network long-period seismographs. LP30 designates the configuration using a 30 s galvanometer and LP15 designates the configuration using a 15 s galvanometer.The LP30 step was generated using a calibration current of 0.08 milliamperes, and the LP15 step was generated using a calibration current of 0.2 milliamperes. The average value of 0.1036 was used for *G** in both cases.

8.3.2 WWSSN 30-100 Seismograph System *Typical* Transfer Function

Twenty-nine step responses were examined using the profiling method described in Appendix A2. The stations, components, and dates of the step responses used are shown in table 8.5. The step responses were taken from both vertical and horizontal component seismograms that were operating at magnifications of 1,500 or less. The step responses were chosen to avoid noise, both microseismic and thermal, in order to establish a more accurate and consistent data base for averaging profile times. Step response data from seismographs operating at higher magnification were not analyzed because of the greater effect of coupling on the transfer functions which would affect the step response profiles. The average values of T_s, T_g and G_g determined from the seismographs operating at 1,500 and lower are used to derive the transfer functions for the seismographs operating at higher magnifications.

Table 8.5. Stations, components, and dates of step responses used to generate the *typical* 30–100 second seismograph response.

Station	Component	Date	Station	Component	Date	Station	Component	Date
AAM	LPZ	10/19/63	GDH	LPN	10/19/63	KON	LPZ	04/28/65
BEC	LPZ	08/21/62	GDH	LPE	10/19/63	KON	LPN	04/28/65
BEC	LPE	08/21/62	GOL	LPZ	02/04/62	KON	LPE	04/28/65
CAR	LPZ	08/21/62	GOL	LPN	02/04/62	MDS	LPZ	02/14/62
CAR	LPN	08/21/62	GOL	LPZ	10/19/63	MDS	LPN	02/14/62
CAR	LPE	08/21/62	GOL	LPN	10/19/63	MDS	LPE	02/14/62
COP	LPZ	10/19/63	GOL	LPE	10/19/63	MUN	LPZ	04/03/63
COP	LPN	10/19/63	GSC	LPZ	10/19/63	TAU	LPZ	04/28/65
COP	LPE	10/19/63	KEV	LPZ	10/19/63	TAU	LPE	05/28/65
GDH	LPZ	10/19/63	KEV	LPE	10/19/63			

The average of profile times measured from the recorded steps are listed in table 8.6 together with times computed from the *typical* transfer function for the LPZ30 seismograph operating at a magnification of 1,500. A good fit resulted by setting the seismometer natural period, T_s, to 28.2 seconds and the galvanometer electrodynamic constant, G_g, to 0.002970 newton-meters per ampere. These two adjustable parameters have the greatest likelihood of adjustment and measurement errors in the LP30 seismograph.

Table 8.6. Comparison of step response profile times in seconds from average of 29 measured times and times computed from the LP30_1500 transfer function.

Profile	P.1L	P.25L	P.5L	P.75L	P1.0	P.75T	P.5T	P.25T	P.1T
Average Measured Time	5.22	8.42	13.23	18.51	32.24	48.93	63.45	79.76	99.85
Typical Computed Time	5.30	8.49	13.13	18.47	31.80	50.35	62.99	80.03	99.62

Typical transfer functions derived for the 30–100 long-period seismograph are listed in Table 8.7 together with adjusted values for T_g, G_g, κ_1 and computed values for λ_s, λ_g, σ^2 and S_c. Other parameters used to derive the transfer functions were taken from Table 8.3 including the average values for R_{11} and R_{22}.

Table 8.7. World-Wide Standardized Seismograph Network 30–100 long-period seismograph *typical* transfer functions.

	Computed Magnification			
	375	**750**	**1500**	**3000**
	Vertical Components			
Poles	–0.06239+j0.02103	–0.06540+j0.02476	–0.06782+j0.03570	–0.06349+j0.05634
Poles	–0.06239–j0.02103	–0.06540–j0.02476	–0.06782–j0.03570	–0.06349–j0.05634
Poles	–0.06380	–0.05645	–0.04667	–0.03714
Poles	–0.73637	–0.73769	–0.74283	–0.76102
Zeros	0.0	0.0	0.0	0.0
T_s	28.2	28.2	28.2	28.2
λ_s	1.803	1.803	1.803	1.803
T_g	98.1	98.1	98.1	98.1
G_g	0.002970	0.002970	0.002970	0.002970
λ_g	0.949	0.949	0.949	0.949
σ^2	0.00257	0.01025	0.04022	0.15072
κ_1	0.05743	0.11457	0.22717	0.43977
S_c	94.06	187.64	372.06	720.25
	Horizontal Components			
Poles	–0.06230+j0.02094	–0.06530+j0.02439	–0.06777+j0.03502	–0.06402+j0.05515
Poles	–0.06230–j0.02094	–0.06530–j0.02439	–0.06777–j0.03502	–0.06402–j0.05515
Poles	–0.06438	–0.05714	–0.04740	–0.03775
Poles	–0.73234	–0.73358	–0.73838	–0.75553
Zeros	0.0	0.0	0.0	0.0
T_s	28.2	28.2	28.2	28.2
λ_s	1.795	1.795	1.795	1.795
T_g	98.1	98.1	98.1	98.1
G_g	0.002970	0.002970	0.002970	0.002970
λ_g	0.949	0.949	0.949	0.949
σ^2	0.00240	0.00956	0.03753	0.14131
κ_1	0.05628	0.11235	0.22271	0.43192
S_c	87.35	174.37	345.66	670.36

The amplitude response curves derived from the transfer functions for the vertical components are shown in figure 8.7, and a phase response curve plotted for a magnification of 1,500 is shown in figure 8.8. When normalized to a standard magnification of 1,500 or less, the vertical and horizontal responses vary less than 1 percent in amplitude and 1° in phase over the period range from 1 to 1,000 s. The important differences between the vertical and horizontal transfer functions are the differences in the sensitivity constant, S_c, and this will be discussed in Section 9. Also, at magnifications of 1,500 and lower, the effect of coupling is small, with variations less than 1.5 percent in amplitude and 1° in phase over the 1,000-s period range. Hence, for magnifications of 1,500 or less, a single *typical* transfer function could be used for both vertical and horizontal components, so long as the appropriate sensitivity constant is used. Separate phase curves for the magnification settings are not warranted because of limited graphical resolution. When needed, the numerical amplitude, phase and group delay data can be computed using the transfer functions listed in table 8.6.

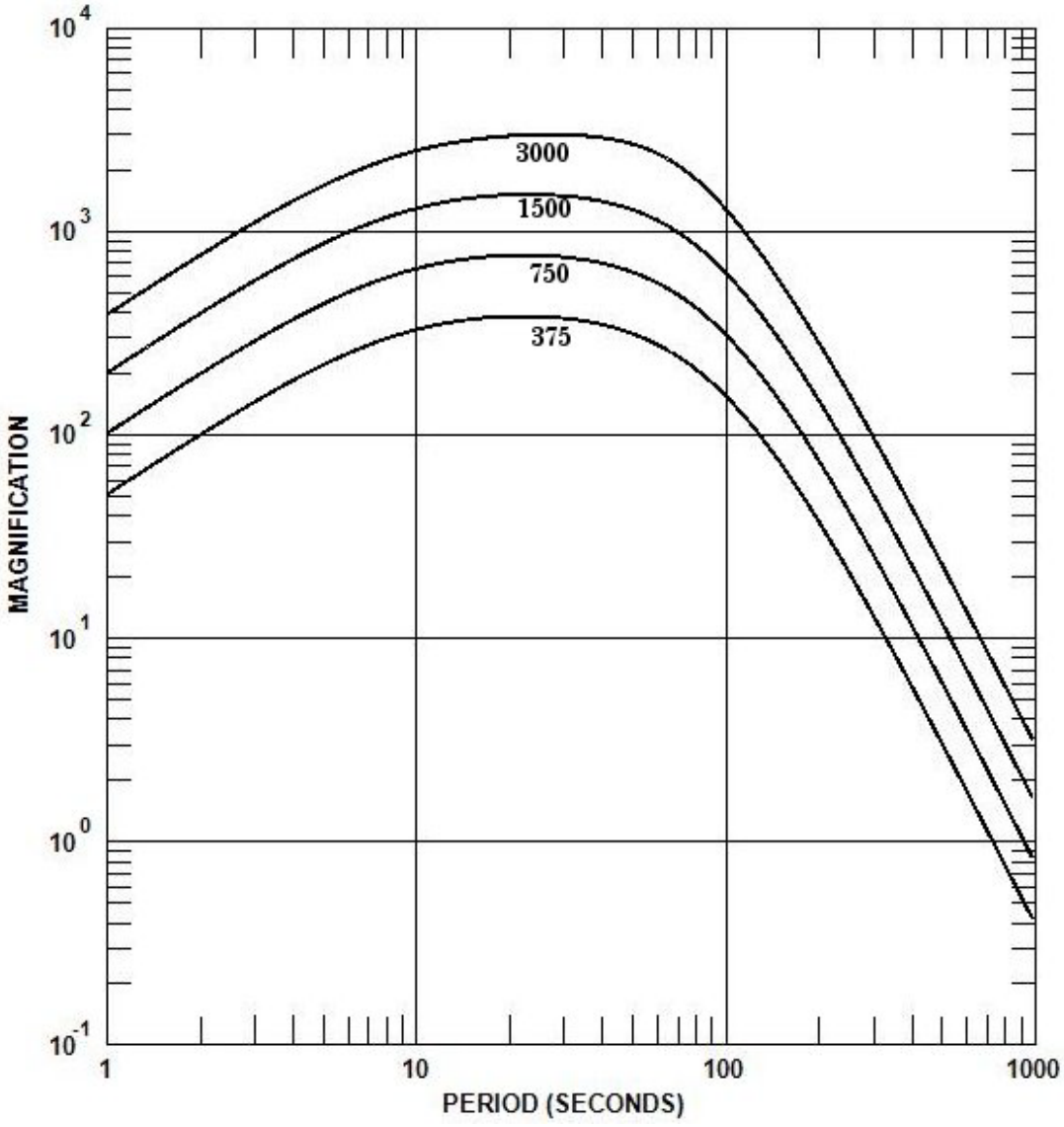

Figure 8.7 Computed magnification curves for World-Wide Standardized Seismograph Network LP30 *Typical* vertical seismograph.

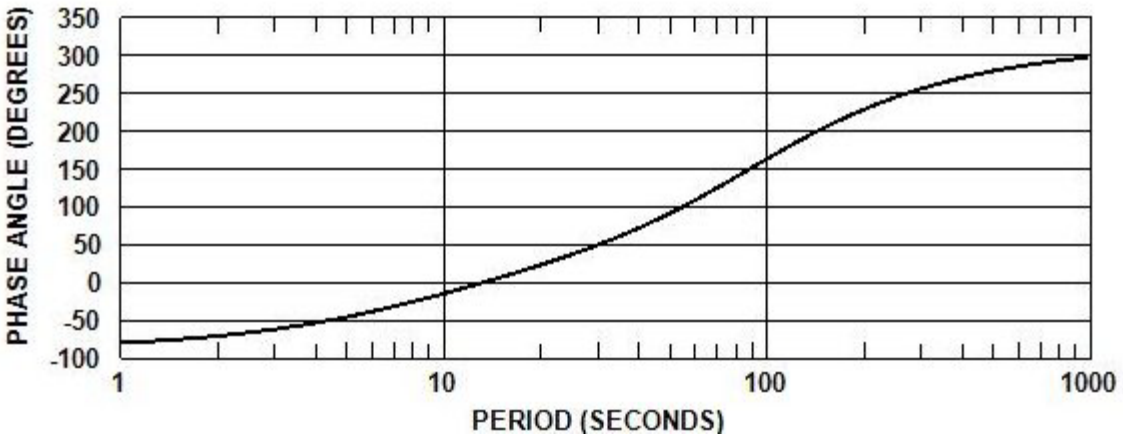

Figure 8.8 Computed phase curve for World-Wide Standardized Seismograph Network LP30 *Typical* vertical seismograph at a magnification of 1,500.

When set to the same magnification, the differences between the *typical* and the *design* amplitude responses are less than 2 percent in amplitude from a 1- to 100-s period, increasing to 13 percent at a 1,000-s period, and the differences cannot easily be resolved in a graphical plot of the curves. However, the difference between the sensitivities of the two transfer functions is significant, as demonstrated in figure 8.9, which shows the *typical* and *design* step responses with the same calibration inputs.

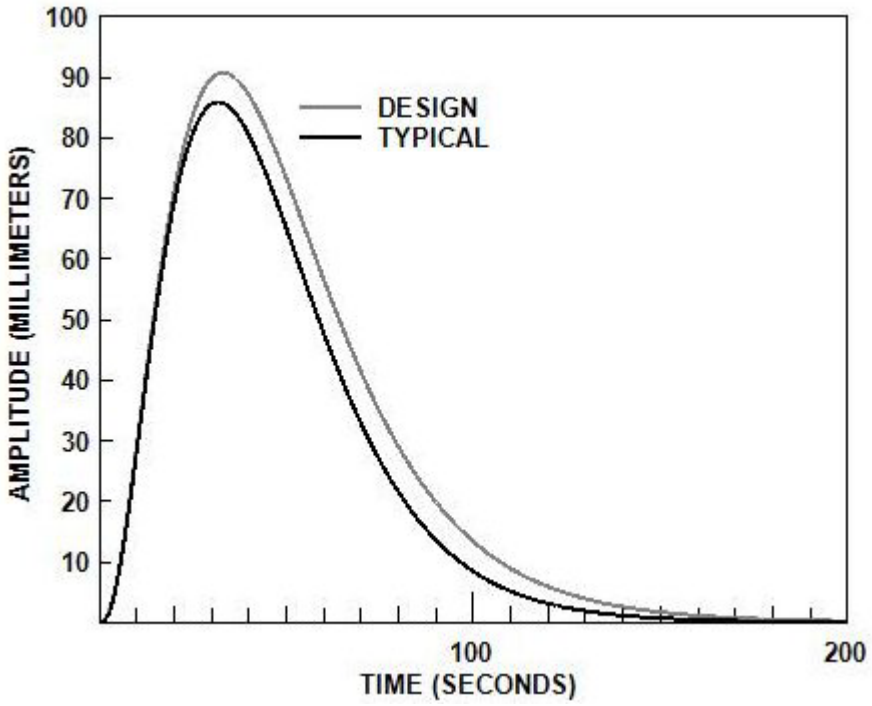

Figure 8.9 Step responses computed from LP30 *design* and *typical* transfer functions.

8.3.3 WWSSN 15-100 Seismograph System *Typical* Transfer Functions

The LP15 seismograph was operated over a much longer period of time than the LP30 seismograph and had much longer intervals between maintenance visits. Thirty step responses were analyzed using the method described in Appendix A2. The stations, components, and dates of the step responses used are shown in table 8.8. The average value for the adjustable galvanometer electrodynamic constant, G_g, was estimated to be 0.002968 newton-meters per ampere, and the galvanometer free period, T_g, was estimated to be 96.0 s. The seismometer period of 15 s was more stable than the earlier period of 30 s. The step responses analyzed were taken from vertical and horizontal component seismograms during quiet periods at stations operating with magnifications of 1,500 or less.

Table 8.8. Stations, components and dates of step responses used to generate the *typical* 15-100 s seismograph response.

Station	Component	Date	Station	Component	Date	Station	Component	Date
AAE	LPZ	12/31/66	BUL	LPZ	12/31/66	JCT	LPZ	12/31/66
AAE	LPN	12/31/66	COP	LPZ	12/31/66	JCT	LPN	12/31/66
AAE	LPE	12/31/66	COP	LPN	12/31/66	KEV	LPZ	12/31/66
AAM	LPZ	12/30/66	COP	LPE	12/31/66	KEV	LPN	12/31/66
ARE	LPZ	12/31/66	ESK	LPE	12/31/66	KEV	LPE	12/31/66
ARE	LPN	12/31/66	GDH	LPN	12/31/66	LEM	LPZ	12/31/66
ATH	LPZ	12/31/66	GDH	LPE	12/31/66	LPA	LPZ	12/31/66
BEC	LPZ	12/31/66	HKC	LPZ	12/31/66	LPS	LPZ	12/31/66
BHP	LPZ	12/31/66	HNR	LPZ	12/31/66	SJG	LPZ	07/01/69
BHP	LPN	12/31/66	HNR	LPE	12/31/66	SJG	LPE	07/01/69

The average of profile times measured from the recorded steps are listed in table 8.9 together with times computed from the *typical* transfer function for the LPZ15 seismograph operating at a magnification of 1,500.

Table 8.9. Comparison of step response profile times in seconds from average of 30 measured times and times computed from the LP15_1500 transfer function.

Profile	P.1L	P.25L	P.5L	P.75L	P1.0	P.75T	P.5T	P.25T	P.1T
Average Measured Time	3.45	5.36	8.03	11.32	20.63	34.98	45.18	59.04	74.88
Typical Computed Time	3.45	5.40	8.21	11.54	20.60	34.81	45.06	59.07	74.86

Typical transfer functions for the 15–100 long-period seismograph are listed in table 8.10 together with adjusted values for T_g, G_g, κ_1, and computed values for λ_s, λ_g, σ^2, and S_c. Other parameters used to derive the transfer functions were taken from table 8.3, including the average values for R_{11} and R_{22}.

Steady-state amplitude response curves computed for the *typical* WWSSN LP 15–100 seismograph are shown in figure 8.10, and a phase response curve computed for a magnification of 1,500 is shown in figure 8.11. Separate phase curves for the different magnification settings are not warranted because of limited graphical resolution. When needed, the numerical amplitude and phase data can be computed using the transfer functions listed in table 8.10.

Table 8.10. World-Wide Standardized Seismograph Network 15–100 long-period seismograph *typical* transfer functions.

	Computed Magnification				
	375	**750**	**1500**	**3000**	**6000**
	Vertical Components				
Poles	–0.06111+ j0.02365	–0.06146+j0.02334	–0.06294+j0.02195	–0.07027+j0.01104	–0.12664+j0.10170
Poles	–0.06111–j0.02365	–0.06146–j0.02334	–0.06294–j0.02195	–0.07027–j0.01104	–0.12664–j0.10170
Poles	–0.39927+ j0.12511	–0.39892+j0.12150	–0.39743+ j0.10572	–0.32972	–0.04583
Poles	–0.39927–j0.12511	–0.39892–j0.12150	–0.39743–j0.10572	–0.45049	–0.62165
Zeros	0.0	0.0	0.0	0.0	0.0
T_s	15.0	15.0	15.0	15.0	15.0
λ_s	0.953	0.953	0.953	0.953	0.953
T_g	96.0	96.0	96.0	96.0	96.0
G_g	0.002968	0.002968	0.002968	0.002968	0.002968
λ_g	0.932	0.932	0.932	0.932	0.932
σ^2	0.002283	0.009109	0.03631	0.1429	0.5465
κ_1	0.05405	0.10797	0.21556	0.4277	0 .8363
S_c	88.46	176.71	352.80	700.01	1368.76
	Horizontal Components				
Poles	–0.06110+ j0.02365	–0.06143+j0.02337	–0.06280+j0.02209	–0.06944+j0.01290	–0.13151+j0.09578
Poles	–0.06110–j0.02365	–0.06143-j0.02337	–0.06280-j0.02209	–0.06944-j0.01290	–0.13151-j0.09578
Poles	–0.39806+ j0.12903	–0.39773+ j0.12578	–0.39636+ j0.11177	–0.35505	–0.04665
Poles	–0.39806–j0.12903	–0.39773–j0.12578	–0.39636–j0.11177	–0.42439	–0.60863
Zeros	0.0	0.0	0.0	0.0	0.0
T_s	15.0	15.0	15.0	15.0	15.0
λ_s	0.951	0.951	0.951	0.951	0.951
T_g	96.0	96.0	96.0	96.0	96.0
G_g	0.002968	0.002968	0.002968	0.002968	0.002968
λ_g	0.932	0.932	0.932	0.932	0.932
σ^2	0.002129	0.008507	0.03390	0.1335	0.5112
κ_1	0.05303	0.1060	0.21161	0.41993	0.82173
S_c	82.25	164.41	328.21	651.31	1274.5

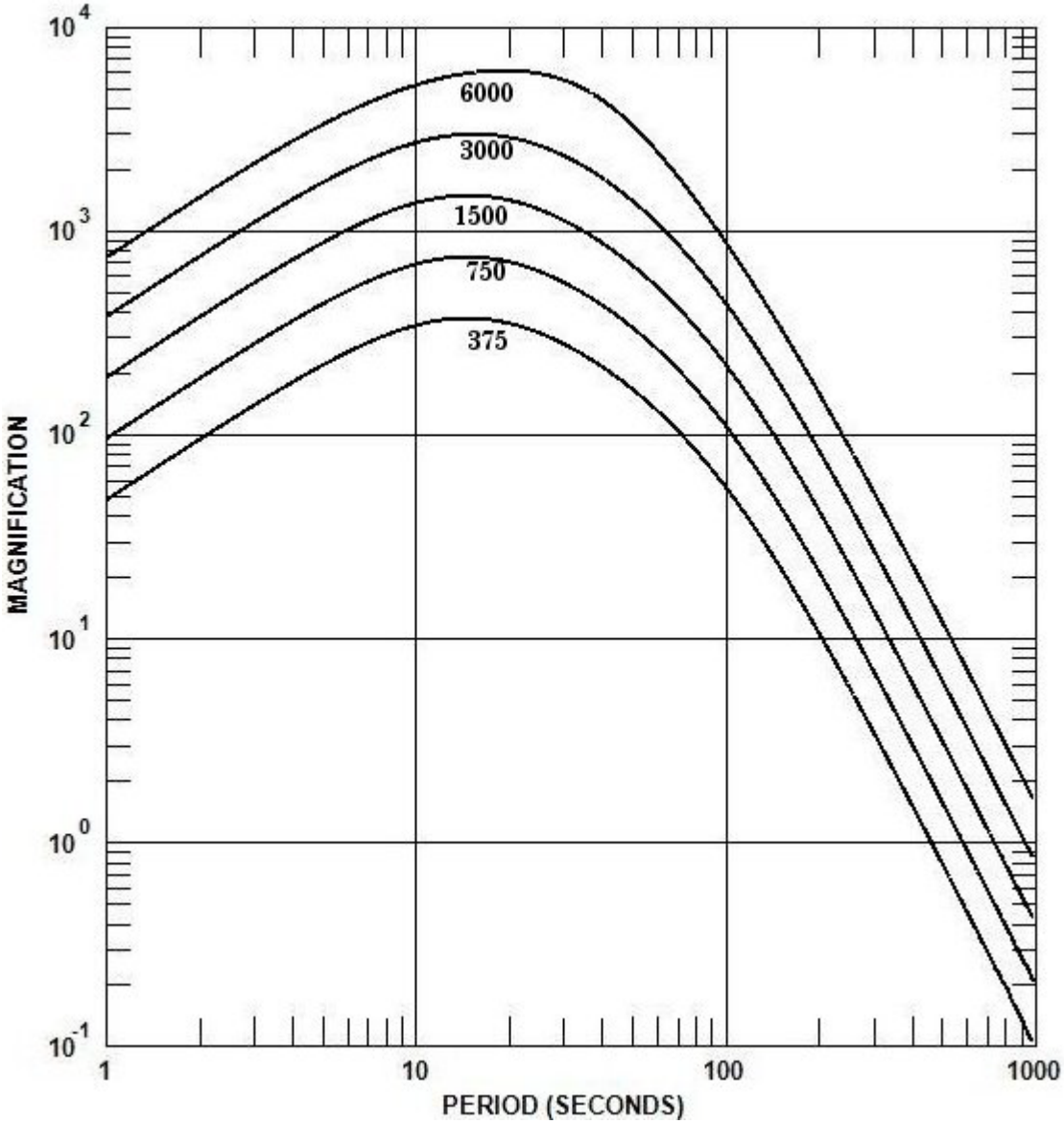

Figure 8.10 Computed magnification curves for World-Wide Standardized Seismograph Network LP15 *Typical* seismograph.

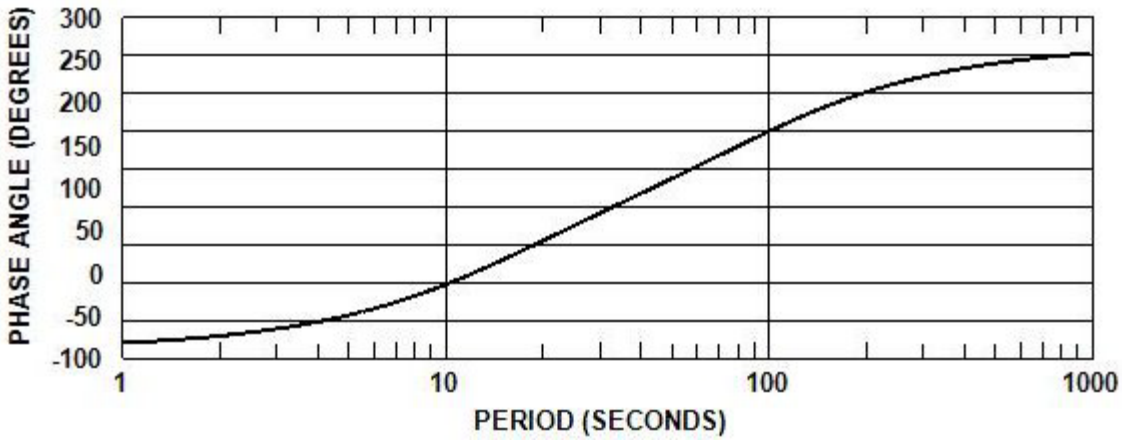

Figure 8.11 Computed phase response of World-Wide Standardized Seismograph Network 15–100 long-period seismograph.

As in the case of the LP30 seismograph, when normalized to a standard magnification of 1,500 or less, the LP15 vertical and horizontal frequency responses vary less than 1 percent in amplitude and 1° in phase in the period range from 1–1,000 s. The important difference between the vertical and horizontal transfer functions is the difference in the sensitivity constant, S_c, and this will be discussed in Section 9. Also, at magnification levels of 1,500 and lower, the effect of the coupling is small, with variations less than 1.5 percent in amplitude and 1° in phase over the 1,000-s period range. Hence, a single *typical* LP15 transfer function could be used in most cases for all vertical and horizontal components operated at 1,500 or less, so long as the appropriate sensitivity constant is applied.

9. WWSSN Calibration

9.1 WWSSN Calibration Procedures

Calibration of the WWSSN seismographs was based on several separate but dependent operations. The first step was the factory testing of a standard system to determine the absolute steady-state amplitude and phase response characteristics over the usable frequency band. The second step, also at the factory, was to determine the value of a calibration constant that relates the peak amplitude of a step response to the magnification of the seismograph at the seismometer operating period. The third step was the proper adjustment of the seismograph settings at the station during installation. The fourth step involved the application of a calibrating force, in the form of a rectangular step function, and use of the calibration constant to properly adjust the sensitivity of the seismograph. Thereafter, calibration step responses were recorded daily on the seismograms. Finally, during the first years of network operation, there were periodic tests and adjustments, to insure that the variable instrument parameters were kept within acceptable tolerances. Methods used for calibration are described in Appendix A and Appendix B of the *WWSSN Operation and Maintenance Manual*, Geotechnical Corp. (1962) and in an unpublished ASL report by Jerry Locke, entitled *Calibration of the WWSSN and ESN Seismograph Systems*.

The WWSSN seismometers were equipped with electromagnetic calibrators, which were coil-magnet devices mounted between the mass and frame of the instrument. When driven by a current, the calibrator imparted a force directly on the mass of the seismometer. This produced a measurable signal that was recorded on the seismogram. The calibrating force was equivalent to $G_c i_c$ newtons/ampere,

where G_c was the electrodynamic constant (assumed to be frequency-independent) of the calibrator and i_c was the applied current. The electrodynamic constant was determined by comparing the amplitude of a recorded pulse, a_i, that results from a step of current through the calibrator, to a recorded pulse, a_w, that was produced by removing a test weight, m, from the mass of the seismometer. For a WWSSN short-period seismometer,

$$G_c = \frac{a_i mg}{a_w i_c} \text{ newtons/ampere} \tag{9.1}$$

where

g is gravitational acceleration.

The "weight lift" was made from the horizontal seismometers by pulling up on a test weight that had been suspended on a thread attached between the seismometer mass and the frame. If the thread was properly adjusted to form an angle of 45° where it was attached to the mass, the force exerted by the test weight was equivalent to $mg/2$. For a WWSSN long-period pendulum-type seismometer,

$$G_c = \frac{a_i mgr_w}{a_w i_c r_c} \text{ newtons/ampere} \tag{9.2}$$

where

r_w is the distance from the hinge point to the point where the test weight is removed and
r_c is the distance from the hinge to the centerline of the coil.

The procedure used for the horizontal long-period seismometers is the same as described for short-period horizontal seismometers.

If the calibration input is a sine wave, the absolute steady-state response of a seismograph can be measured using the electrodynamic calibrator. The force exerted on the seismometer mass due to a steady-state, sinusoidal current through the calibrator is

$$f_i = G_c i_c \sin\omega t \text{ newtons} \tag{9.3}$$

where

ω is the angular frequency of the current.

The force acting on the mass due to a sinusoidal displacement of the earth is

$$f_e = Mx_m\omega^2 \sin\omega t \text{ newtons} \tag{9.4}$$

where

M is the inertial mass and
x_m is the displacement of the earth.

Then, when a sinusoidal current is flowing through the calibrator, the equivalent earth displacement is

$$x_m = \frac{G_c i_c \sin\omega t}{M\omega^2 \sin\omega t} \text{ meters} \tag{9.5}$$

The magnification of a seismograph can be defined as a_0/x_m, where a_0 is the amplitude of the recorded output. The magnification may be determined at any frequency, f, by applying a sinusoidal current through the calibrator, measuring the recorded output and using the expression

$$Magnification@f = \frac{Ma_o 4\pi^2 f^2}{G_c i_c} \tag{9.6}$$

or, in the case of a rotational seismometer,

$$Magnification@f = \frac{Ma_o 4\pi^2 f^2 r_{cm}}{G_c i_c r_c} \tag{9.7}$$

where

r_{cm} is the distance from the hinge point to the pendulum center of mass.

This was the most common method of calibrating seismographs at the time, and it was used to measure the steady-state response characteristics of the WWSSN seismographs during factory tests. The calibrator coil on the WWSSN short-period seismometer had an inductance of 600 millihenries, so it was important to measure the actual current through the coil at all frequencies rather than assume a constant current from a constant voltage source. Shake tables also were used but most had an inherent problem with tilt which made them all but unusable with pendulum-type seismometers.

Sine-wave generators were not furnished with the WWSSN systems for on-site steady-state calibration, so a different method was used to measure and adjust the magnifications at the stations. A relationship was established between the peak amplitude of a step response of the seismograph and its magnification at a reference period. In the laboratory, the seismograph was adjusted to the standard operating configuration and calibrated using a sine-wave generator, or a shake table in the case of the short-period seismograph. Then a measured current step was applied to the calibrator and the output was recorded. A calibration constant, K_c, was calculated from the relationship

$$K_c = \frac{G_c i_c magnification@T_s}{a_i} \text{ newtons/meter} \tag{9.8}$$

where

T_s is the reference period (normally, the seismometer period) and

a_i is the zero-to-peak amplitude of the pulse recorded on the seismogram when the current was removed. The calibration constant can also be computed from the transfer function.

At the stations, the magnification at the reference period was determined by applying a step of current through the calibrator and using the expression

$$Magnification@T_s = \frac{K_c a_i}{G_c i_c} \tag{9.9}$$

Magnifications at other periods were determined with the use of relative amplitude response curves derived from the test system during the laboratory testing.

There are some obvious disadvantages to this simple transient method of calibration. The calibration constant must be determined accurately, and the operating parameters of the seismograph at the station must be the same as those for the test system and maintained to close tolerances.

9.2 WWSSN Short-Period Seismograph Calibration

After the short-period seismometers and galvanometers were initially set up at the station (and again later during maintenance) they were tested to insure that the operating periods and damping were set correctly. During maintenance visits by ASL personnel the tests were recorded. The galvanometer period (nominally 0.75 s) and damping ratio (nominally critical) could not be adjusted but were checked to insure that they were within the specified tolerances (±5 percent in period). The seismometer period could be adjusted to 1.0 s and the damping was set during the calibration procedures. The electrodynamic constant of the calibrator on the short-period seismometer was adjustable. It was set during installation to a standard value of 2.0 N/A using a weight lift test and readjusted if necessary during maintenance.

During factory tests, the calibration constant, K_c, was determined to have a value of 7,300 N/m (newtons/meter) at a reference period of 1.0 s. In setting the magnification of the WWSSN short-period seismograph two adjustments were made: the peak amplitude of the step response to a standard input current was adjusted to a standard value of 44 mm using a trim attenuator on the control box, and the overshoot ratio of the step response was adjusted to a value of 1/17 using a seismometer damping trim resistor also on the control box. At the higher magnifications, these adjustments were interactive and somewhat difficult to make.

The magnifications of the WWSSN short-period seismographs (SPMag) were computed as follows:

$$SPMag\,@1\text{sec} = \frac{7300ca_i}{G_c i_c} \tag{9.10}$$

The values of G_c (normally 2.0) and i_c are listed on the seismograms. The parameter c is a correction factor for damping. Its value is unity if the overshoot ratio is 1/17. The values of c for overshoot ratios other than 1/17 were determined in laboratory tests and may be scaled from the chart in figure 9.1. The chart is in agreement with values computed from the transfer function for a SP seismograph operated at a magnification of 50,000.

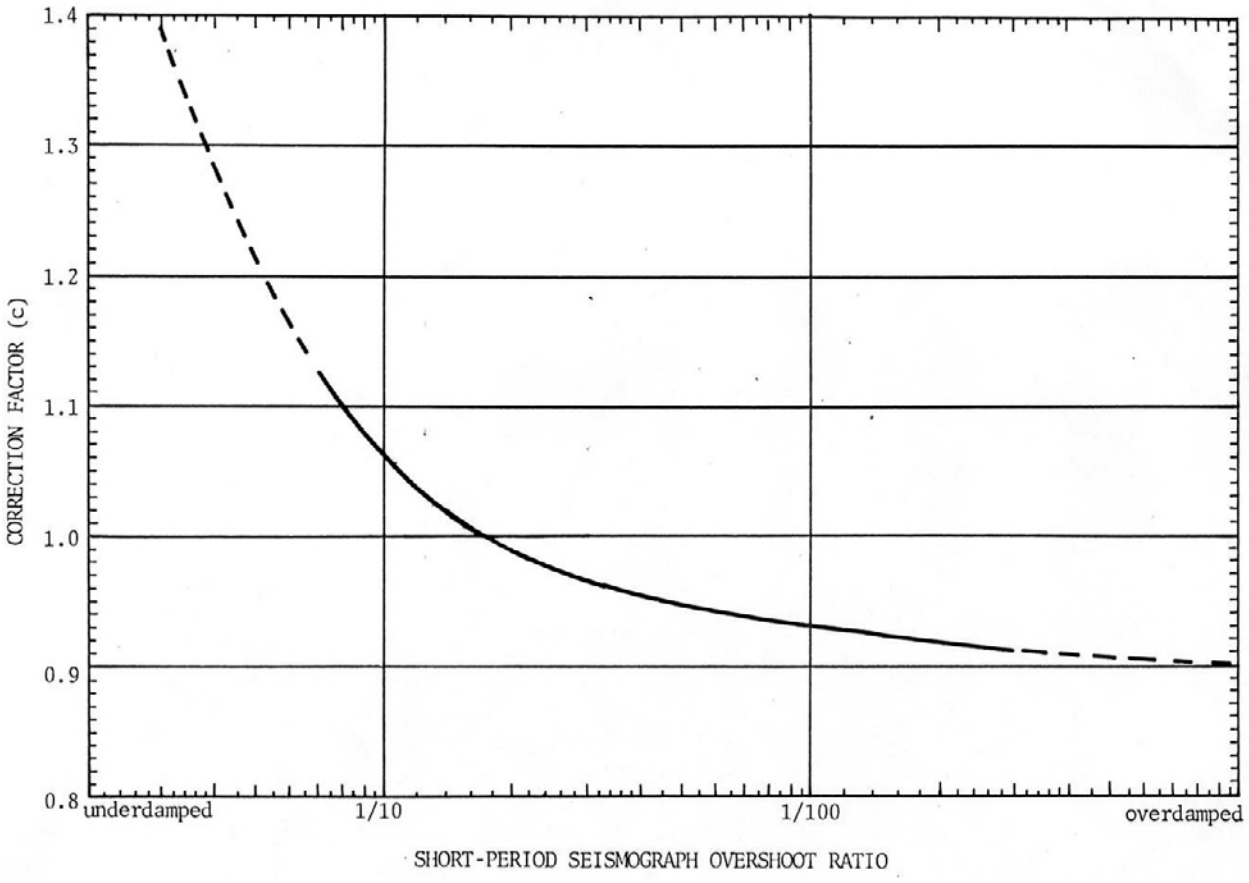

Figure 9.1 Correction factor for World-Wide Standardized Seismograph Network short-period magnification vs. overshoot ratio; taken from Geotechnical Corp. (1962).

Standard values of short-period magnification settings, calibration currents used, and corresponding standard step deflections are listed in table 9.1 below.

Table 9.1. World-Wide Standardized Seismograph Network short-period standard calibration currents and deflections.

Nominal Magnification at 1.0 second	Calibration Current (milliamperes)	Deflection (millimeters)
400,000	0.4	44
200,000	0.8	44
100,000	1.6	44
50,000	3.2	44
25,000	6.4	44
12,500	12.8	44
6,250	20.0	34

A comparison of magnifications obtained using standard procedures and those computed from the short-period transfer function is shown in table 9.2. The standard magnifications were derived from equation 9.10 using the values for the calibration currents and step response amplitudes listed in table 9.1. The computed magnifications were derived from the short-period transfer function with the forward current gain and damping adjusted to produce the prescribed step amplitude and overshoot ratio when convolved with a calibration current step having a value as listed in table 9.1. The computed calibration constants were derived from equation 9.8 using the computed magnifications shown in table 9.2.

Table 9.2. Comparison of magnifications and calibration constants obtained using standard procedures and those computed from the short-period transfer function.

	SP Magnification						
Nominal	6,250	12,500	25,000	50,000	100,000	200,000	400,000
Standard Magnification	6,205	12,547	25,094	50,188	100,375	200,750	401,500
Standard Prescribed Calibration Constant	7,300	7,300	7,300	7,300	7,300	7,300	7,300
Computed Magnification	6,002	12,141	24,286	48,582	97,492	19,6301	407,054
Computed Calibration Constant	7,061	7,064	7,065	7,066	7,090	7,138	7,401

The differences between the standard and computed magnifications at 50,000 and lower are consistently about 3.2 percent. The differences could be ascribed to measurement error during calibration tests or to a consistent error in parameter values used in the transfer function. In either case, this is good agreement considering that the measurement accuracies during setup and testing at the factory were not expected to be better than 5 percent, and it confirms reasonable accuracies for the instrument constants used to generate the transfer function.

The differences between the standard and computed magnifications above 50,000 are due partly to changes in coupling and inductive effects as κ_1 and R_{11} are adjusted. These factors were not taken into account in the simple calibration scheme used.

The magnification of a short-period seismograph component can be determined using the appropriate computed calibration constant from table 9.2 in place of the prescribed calibration constant (7300) in equation 9.10. The magnification can be determined using the calibration current noted on the seismogram, which is normally the same as that listed in table 9.1, and the step response amplitude measured from the seismogram. A scaling factor to determine the actual amplitude on the seismogram can be obtained by measuring the distance between the minute marks, which is set at 60 mm for the short-period seismograms. An average of measurements taken over several days is recommended if the background noise is moderate to high. A correction factor for overshoot ratio, shown in figure 9.1, should be used if necessary.

9.3 WWSSN Long-Period Seismograph Calibration

After the instruments were set up at the stations, the operating periods of the galvanometers and seismometers were set to their prescribed values. The air-damped period of the galvanometers were set to 100 s by tilting the base backward or forward using base leveling screws. Similarly, the long-period seismometer periods were adjusted by tilting the instruments backward or forward. All of the tests at a station involving the seismometers and galvanometers were recorded photographically and attached to the installation report.

The long-period seismometer had a calibrator consisting of a separate coil and magnet mounted adjacent to the signal coil and magnet. The electrodynamic constants of the calibrators were not adjustable. The values were determined at the station using a weight lift test and they are noted on the seismograms. In the WWSSN Operation and Maintenance Manual, Geotechnical Corp. (1962), the electrodynamic constant of the calibrator on a long-period seismometer was redefined as

$$G^* = \frac{G_c r_c}{r_{cm}} \tag{9.11}$$

The values listed on the long-period seismograms are given for G^*, and the equation used to compute G^* from the weight lift becomes

$$G^* = \frac{a_i mg}{a_w i_c} \tag{9.12}$$

for the vertical seismometer test, and

$$G^* = \frac{a_i mg}{2a_w i_c} \tag{9.13}$$

for the horizontal seismometer test.

The equation used for setting the long-period magnification (LPMag) using the calibration constant becomes

$$LPMag\,@\,T_s \text{ sec} = \frac{K_c a_i}{G^* i_c} \tag{9.14}$$

Because the value of G^* varied from seismometer to seismometer, the procedures for setting the magnification to the standard values were different than they were with the short-period instruments. The first step was to perform the weight lift test to determine G^*. Then, equation 9.14 was used to calculate the peak amplitude, a_i, needed to produce the desired magnification using a standard calibration current, i_c, and the calibration constant, K_c. Finally, step and trim attenuators on the galvanometer control box were used to adjust the peak amplitude of the output pulse to the calculated setting. The step attenuator on the control box could then be used to adjust the magnification up or down in 6 dB steps. Seasonal changes in magnification setting were needed at some stations to account for variations in microseism amplitudes.

9.3.1 WWSSN 30-100 Seismograph Calibration Constants

In a factory test, the value of the calibration constant, K_c, for 30–100 LP seismograph was determined to be 0.135 N/m at a reference period of 30 s. The standard magnification settings and calibration currents are given in table 9.3. A data user can verify or determine the magnification of the seismograph component from Eq. 9.14 by using measured values of peak amplitude of the calibration pulse, the prescribed value for K_c, and the values for G^* and i_c noted on the seismogram.

Table 9.3. World-Wide Standardized Seismograph Network 30-100 seismograph calibration currents

Nominal Magnification at 30 seconds	Control Box Setting (dB)	Calibration Current (milliamperes)
3,000	6	0.04
1,500	12	0.08
750	18	0.16
375	24	0.32

Peak pulse amplitudes and calibration constants for the 30–100 seismograph computed from the *design* transfer functions are listed in table 9.4. The amplitudes and constants were derived by setting the computed magnification to a standard setting by adjusting κ_1, then using a calibration current listed in table 9.3 to produce the simulated step response. The average G^* values listed in table 8.3 for the vertical and horizontal seismometers were used in the computations.

Table 9.4. Step pulse amplitudes and the resulting calibration constants computed from the *design* LP 30–100 seismograph transfer functions. (mm, millimeters)

	LP 30–100 *Design* Seismograph			
Standard Setting	375	750	1,500	3,000
	Vertical Component			
Peak Pulse Amplitude (mm))	90.8	90.8	90.8	91.1
Calibration Constant (0.135 nominal)	0.137	0.137	0.137	0.136
	Horizontal Component			
Peak Pulse Amplitude (mm)	87.5	87.5	87.5	87.8
Calibration Constant(0.135 nominal)	0.132	0.132	0.132	0.131

The increase in step pulse amplitude and resulting decrease in the calibration constant at the highest magnification are due to the galvanometer-seismometer coupling in equation A1.54, which is not taken into account in this calibration procedure, but the effects are relatively small for the 30–100 seismograph. There is about a 4.2 percent difference between the computed calibration constants for the vertical and horizontal components. This has greater significance and is due to the differences in the physical parameters of the two components, a fact also not taken into account in this calibration procedure. These errors were reported by Toybas and others (1977) in their analysis of the WWSSN 15–100 seismograph.

Overall, the differences for the 30–100 seismograph between the factory-determined calibration constant and the constants computed from the *design* transfer function using average values for G^* are well within a reasonable estimate of measurement errors during the factory tests. This suggests that the test system was closely configured to the vertical component described by the *design* transfer function and that the values given in table 8.3 for the non-adjustable seismograph parameters are reasonably accurate.

Calibration constants computed using the *typical* 30–100 transfer functions listed in table 8.7 are shown in table 9.5. Based on average values for G^*, magnifications set using the original calibration constant (0.135 N/m) were about 7 percent higher for the vertical components and about 3 percent higher for the horizontal components compared to magnifications determined using the *typical* transfer functions, reflecting the differences in the values used for G_g and T_s in fitting the average step response profile.

Table 9.5. Step pulse amplitudes and the resulting calibration constants computed from the LP 30–100 *typical* seismograph transfer functions based on average step response profiles. (mm, millimeters)

	LP 30–100 *Typical* Seismograph			
Nominal Magnification	375	750	1,500	3,000
	Vertical Component			
Peak Pulse Amplitude (mm))	85.9	85.9	85.9	86.2
Calibration Constant (0.135 nominal)	0.145	0.145	0.145	0.144
	Horizontal Component			
Peak Pulse Amplitude (mm)	83.3	83.3	83.3	83.5
Calibration Constant (0.135 nominal)	0.139	0.139	0.139	0.138

9.3.2 WWSSN 15–100 Seismograph Calibration Constants

The change in seismometer period was made at the existing stations over a period of time. With the lower seismometer period, a higher magnification setting of 6,000 was achievable at a few stations with low background noise.

A calibration constant for the 15–100 seismograph, having a value of 0.449 N/m, was provided in Appendix B of the *WWSSN Operation and Maintenance Manual* (Geotechnical Corp., 1962). This was used to set the magnifications at the stations and to determine the magnification of an operating system. The standard magnification settings and calibration currents used to generate the step inputs are given in table 9.6.

Table 9.6. World-Wide Standardized Seismograph Network 15–100 seismograph calibration currents.

Nominal Magnification at 15 seconds	Control Box Setting (dB)	Calibration Current (milliamperes)
6,000	0	0.05
3,000	6	0.1
1,500	12	0.2
750	18	0.4
375	24	0.8

Peak pulse amplitudes and calibration constants for the 15–100 seismograph computed from the *typical* transfer functions given in table 8.10 are listed in table 9.7. The amplitudes and constants were derived by adjusting the computed magnification to a standard setting, then using a calibration current listed in table 9.6 to produce the simulated step response. The average G^* values listed in table 8.3 for the vertical and horizontal seismometers were used in the computations.

Table 9.7. Step response amplitudes and the resulting calibration constants computed from the LP 15–100 seismograph transfer functions based on average step response profiles. (mm, millimeters)

	LP 15–100 *Typical* Seismograph				
Nominal Magnification	375	750	1,500	3,000	6,000
	Vertical Component				
Peak Pulse Amplitude (mm)	74.0	74.0	74.2	75.0	79.6
Calibration Constant (0.449 nominal)	0.420	0.420	0.419	0.414	0.390
	Horizontal Component				
Peak Pulse Amplitude (mm)	71.7	71.8	71.9	72.7	76.7
Calibration Constant (0.449 nominal)	0.402	0.402	0.401	0.397	0.376

The changes in the calibration constants at higher magnification settings are caused by galvanometer-seismometer coupling. They are more significant in this case than in the case of the LP30 seismograph. The effects of coupling were not taken into account in the setting and determination of magnification at the stations. Nor was the difference in vertical and horizontal sensitivity taken into account, as pointed out by Toybas and others (1977). Magnifications were set at the stations by adjusting the peak amplitudes of the recorded step responses to equal the peak amplitudes computed from equation 9.14 for the desired magnification, after first measuring the G^* values. Assuming average values for G^*, a magnification of 1,500 set at a station using the original calibration constant (0.449) will be about 7.0 percent lower for the vertical component and about 10.7 percent lower for the horizontal component than magnifications determined using the *typical* calibration constants, and the differences will be greater at higher magnification settings. Stated another way, the average magnifications based on the *typical* calibration constants for the LP15 seismographs at the 1,500 setting was about 1,395 for the vertical components and about 1,340 for the horizontal components.

9.3.3 Determination of Seismogram Magnification

We recommend using the calibration constants derived from the *typical* transfer functions for determining long-period seismogram magnification. Based on the averaging of step response profiles, these are likely to be more accurate than the prescribed calibration constants; they also take into account the differences in sensitivity between the vertical and horizontal components and the effects of coupling at the higher magnifications.

To determine the magnification of a long-period seismogram using a *typical* calibration constant listed in table 9.5 or 9.7, the first step is to measure the peak amplitude of the step response. This should be an average of measurements taken over several days of calibration to minimize interference from noise. Then the magnification at the seismometer period can be derived from equation 9.14 using the appropriate calibration constant, the peak step response amplitude in meters, the calibration current in amperes as listed on the seismogram, and the value for G^* listed on the seismogram. The computed magnification should continue to be valid unless there is a change in the parameter values listed on the seismogram or an obvious change in the shape or amplitude of the step response.

A user-generated transfer function will provide more accurate calibration for a specific long-period component. The procedures used to generate a user transfer function described in Appendix A2 will produce a transfer function for one of the standard magnification settings of the seismograph and an associated step response. Consider starting with the parameters listed in table 8.7 or 8.10 for the *typical* transfer function, then adjust the parameters G_g, T_g, and T_s until there is a good fit between the recorded pulse and a trial computed pulse. The galvanometer electrodynamic constant, G_g, is the most important

variable in the group. As an alternate, a close profile match might be found by checking the profiles listed in tables A1.1 or A1.2. The peak amplitude of the computed step response can be used in equation 9.14, together with the value of G^* listed on the seismogram, to calculate a calibration constant for the magnification setting chosen. This can then be used in the same equation together with the peak amplitude of the recorded step response to determine the operating magnification of the seismograph at the seismometer period. The computed calibration constant for the 1,500 setting will be valid for all magnifications set at 1,500 or lower.

In this section on calibration, some issues have been raised regarding the accuracy of the WWSSN long-period seismograph calibration. The step response data recorded on the seismograms can be used to resolve these issues. We hope that the information provided in this report will serve that purpose.

References Cited

Bogart, B.P, 1961, The transfer function of a short-period vertical seismograph: Bulletin of the Seismological Society of America, v. 51, p. 503–513.

Bolt, B.A., 1976, Nuclear explosions and earthquakes, the parted veil: San Francisco, Calif., Freeman, 309 p.

Bormann, P., ed., 2012, New manual of seismological observatory practice (NMSOP-2), IASPEI: Potsdam, Germany, GFZ German Research Centre for Geosciences, accessed August 12, 2014, at http://nmsop.gfz-potsdam.de, DOI: 10.2312/GFZ.NMSOP-2; urn:nbn:de:kobv:b103-NMSOP-2.

Eaton, J.P., 1957, Theory of the electromagnetic seismograph: Bulletin of the Seismological Society of America, v. 47, p. 37–76.

Espinosa, A.F., G.H. Hutton, and H.J. Miller, S.J., 1962, A transient technique for seismograph calibration: Bulletin of the Seismological Society of America, v. 52, p. 767–779.

Espinosa, A.F., G.H. Hutton, and H.J. Miller, 1965, A transient technique for seismograph calibration—Manual and standard set of theoretical transient responses: Ann Arbor, Mich., University of Michigan, Institute of Science and Technology, Vesiac Special Report No. 4410-106 X.

Geotechnical Corp., 1962, Operation and maintenance manual—Worldwide seismograph system, model 10700: Garland, Texas, Teledyne-Geotech Inc.

Hagiwara, T., 1958, A note on the theory of the electromagnetic seismograph: Bulletin of the Earthquake Research Institute, v. 36, v. 139–164.

Johnson, B.P., and Matheson H., 1962, An analysis of inertial seismometer-galvanometer combinations: National Bureau of Standards, NBS Report 7554.

Kisslinger, C., and Howell, B.F., 2003, Seismology and physics of the Earth's interior in the US (1900–1960), *in* International Handbook of Earthquake and Engineering Seismology, Part B, edited by Lee, W.H.K., Kanamori, H., Jennings, P.C., and Kisslinger, C., eds.: Amsterdam, Academic Press, 1,453 p.

Lee, W.H.K., and Benson, R.B., 2008, Making non-digital-recorded seismograms accessible online for studying earthquakes, *in* Historical seismology, Frechet, J., Meghraoui, M., and Stucchi, M., eds.: Berlin, Springer, p. 403–427.

Mitchell, B.J., and Landisman, M., 1969, Electromagnetic constants by least-squares inversion: Bulletin of the Seismological Society of America, v. 59, p. 1,335–1,348.

Nuttli, O., and McEvilly T.V., 1961, The response characteristics of the long-period seismographs of the Saint Louis University network: Earthquake Notes, v. 32, p. 27–36.

Oliver, J., and Murphy, L.M., 1971, WWNSS—Seismology's global network of observing stations: Science, v. 174, p. 254–261.

Romney, C., 2009, Detecting the bomb: Washington, D.C., New Academia, 307 p.

Savill, R.A., Carpenter, E.W., and Wright, J.K., 1962, The derivation and solution of indicator equations for seismometer-galvanometer combinations including the effect of seismometer inductance: Geophysical Journal of the Royal Astronomical Society, v. 6, p. 409–424.

Sorrels, G.G., 1971, A preliminary investigation into the relationship between long-period seismic noise and local fluctuations in the atmospheric pressure field: Geophysical Journal of the Royal Astronomical Society, v. 26, p. 71–82.

Stearns, S.D., and David, R.A., 1988, Signal processing algorithms: Englewood Cliffs, N.J., Prentice-Hall, Inc., 349 p.

Stearns, S.D., and Hush, D.R., 1990, Digital signal analysis: Englewood Cliffs, N.J., Prentice-Hall, Inc, 440 p.

Toybas, V., Teikari, P., and Vesanen, E., 1977, Magnification of WWSS long-period seismographs: Geophysica, v. 14, p. 251–276.

Appendix A1. Derivation of a Generalized World-Wide Standardized Seismograph Network Transfer Function

A1.1 Introduction

The following introductory paragraphs are intended for defining the parameters and processes used in the derivation and use of the World-Wide Standardized Seismograph Network (WWSSN) system transfer functions. For a more general review of modern seismic sensors, we recommend the New Manual on Seismological Observatory Practice, Chapter 5 by Prof. Erhard Wielandt (see Borman [2012]).

A1.1.1 Fundamentals of a Simple Mechanical Seismometer

Both the seismometer and galvanometer used in an electromagnetic seismograph can be modeled as damped harmonic oscillators. A very simple model of a mechanical seismometer, such as the one shown in figure A1.1, comprises an inertial mass, a spring, and an oil-filled dashpot. By summing the forces acting on the mass, such an oscillator in its rest position can be described by the following equation of motion

$$m\frac{d^2z}{dt^2} + d\frac{dz}{dt} + uz = 0 \qquad \text{(A1.1)}$$

or

$$\frac{d^2z}{dt^2} + \frac{d}{m}\frac{dz}{dt} + \frac{u}{m}z = 0 \qquad \text{(A1.2)}$$

where

m is inertial mass,
d is viscous damping coefficient,
u is spring constant,
z is relative mass-frame displacement and
t is time.

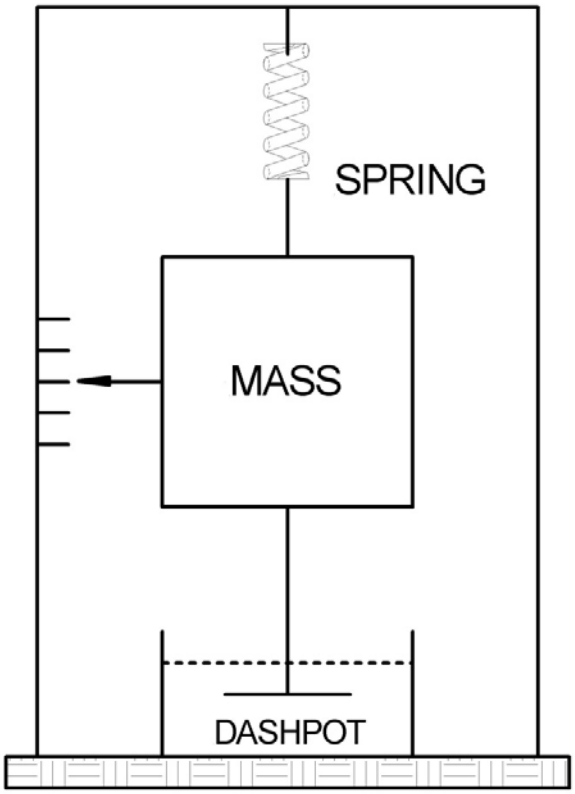

Figure A1.1 Simple seismometer.

(Note: A vertically suspended mass will be subjected to a gravitational force as well, but this will normally be offset by a spring force of equal and opposite direction such that only the initial position of the mass relative to the frame is affected.)

At this point, we will define two important instrument parameters to replace the coefficients in equation A1.2 by letting

$$\omega_o = \sqrt{\frac{u}{m}} \tag{A1.3}$$

$$\lambda = \frac{d}{2\omega_o m} \tag{A1.4}$$

As will become apparent in the next several steps, ω_o is the natural angular frequency of the seismometer and λ is defined as the damping ratio. Using the new coefficients, equation A1.2 can be rewritten as

$$\frac{d^2 z}{dt^2} + 2\lambda\omega_o \frac{dz}{dt} + \omega_o^2 z = 0 \tag{A1.5}$$

The general solution for this quadratic differential equation, as given in most textbooks on differential equations, is

$$z(t) = A_0 e^{r_1 t} + B_0 e^{r_2 t} \tag{A1.6}$$

where

A_0 and B_0 are constants related to initial conditions and r_1 and r_2 are the roots of the quadratic equation.

These may be written as

$$r_1 = -\lambda\omega_o + \omega_o\sqrt{\lambda^2 - 1} \tag{A1.7}$$

$$r_2 = -\lambda\omega_o - \omega_o\sqrt{\lambda^2 - 1} \tag{A1.8}$$

If the damping ratio, λ, is greater than one, the roots are real, and the mass, when displaced, will return to its rest position without crossing it. This is described as an *overdamped* condition.

If the damping ratio equals one, the roots are real and the mass will return to its rest position in the shortest time without overshooting. This is described as a *critically damped* condition.

If the damping ratio is less than one, the roots will be imaginary and take the form

$$-\lambda\omega_o \pm j\omega_o\sqrt{1 - \lambda^2} \qquad \text{where } j = \sqrt{-1} \tag{A1.9}$$

In this case, the solution to equation A1.5 will contain trigonometric functions causing the mass to oscillate with decaying amplitude about its rest position. This is described as an *underdamped* condition. The solution, in this case, can be written as

$$z(t) = e^{-\lambda\omega_o t}\left(C_1 \sin\omega_o\sqrt{1-\lambda^2}\ t + C_2 \cos\omega_o\sqrt{1-\lambda^2}\ t\right) \tag{A1.10}$$

or as

$$z(t) = C_3 e^{-\lambda\omega_o t}\ \sin\left(\omega_o\sqrt{1-\lambda^2}\,t + \phi\right) \tag{A1.11}$$

where C_1 and C_2 are constants and

$$C_3 = \sqrt{C_1^2 + C_2^2}\ \text{ and the phase angle } \phi = \tan^{-1}\frac{C_2}{C_1} \tag{A1.12}$$

In the underdamped condition, the damped angular frequency is

$$\omega_d = \omega_o\sqrt{1-\lambda^2} \tag{A1.13}$$

In the special case where the damping ratio is equal to zero, equation A1.11 can be rewritten as

$$z(t) = C_3 e^{-\lambda\omega_o t}\ \sin\left(\omega_o t + \alpha\right) \tag{A1.14}$$

The seismometer will oscillate with amplitude C_3 and at a natural angular frequency of ω_o radians per second, or a natural frequency, f_o, of $\omega_o/2\pi$ hertz and a natural period, T_o, of $2\pi/\omega_o$ seconds.

In practice, the natural period cannot be measured directly for most instruments, including the WWSSN instruments, because of viscous air damping. However, it is possible to measure the air damped period directly from a record of the oscillations. Then the natural period can be calculated from the following equation.

$$T_o = T_d\sqrt{1-\lambda^2} \tag{A1.15}$$

where

T_d is the measured damped period.

But first the damping coefficient must be determined from the same record of oscillations. Given the successive positive peak amplitudes, $x_1, x_2, \ldots x_n$, of the decaying oscillations, the logarithmic decrement, δ, is defined as

$$\delta = \frac{1}{n} \ln \left[\frac{x_1}{x_{n+1}} \right] \tag{A1.16}$$

Then the damping ratio can be computed from the following relationship

$$\lambda = \frac{\delta}{\sqrt{4\pi^2 + \delta^2}} \tag{A1.17}$$

With the two important physical parameters of our mechanical oscillator, the next step might be to determine its transfer function and to determine from that the response to various inputs, such as earth displacement and calibration forces. For a simple mechanical seismometer, as described above, this information can be obtained by adding forcing functions to the equation of motion and solving the quadratic differential equation. For electromagnetic and electronic seismographs, with their higher-order system equations, the solutions are easier to obtain using the tools and methods described in the next section.

A1.1.2 Basic Use of Fourier and Laplace Transformations

The Laplace transform is useful as an operator in solving the differential equations, and the Fourier transform is used to determine the frequency response characteristics of the instruments; they are both used in convolution processes to determine the time-domain responses to various forcing functions. The following definitions and operations were condensed from an earlier edition of Stearns and Hush (1990). Many of the programs used in the analysis of the instrumentation and data were also based on algorithms found in Stearns and Hush (1990) and its companion text, Stearns and David (1988). Derivations of the equations are not provided as these are thoroughly covered in available texts, including the one listed above.

The Fourier transform of $f(t)$ is defined as

$$F(j\omega) = \int_{-\infty}^{\infty} f(t) e^{-j\omega t}\, dt \tag{A1.18}$$

where

$F(j\omega)$ is the frequency spectrum of the function $f(t)$.

If the function is multiplied by a decaying exponential, $e^{-\sigma t}$, where σ is greater than zero, then

$$F(\sigma + j\omega) = \int_{0}^{\infty} f(t) e^{-(\sigma + j\omega)t}\, dt \tag{A1.19}$$

where we assume $f(t) = 0$ for $t < 0$. If we define a complex number $s = \sigma + j\omega$, then

$$F(s) = \int_{0}^{\infty} f(t) e^{-st}\, dt \tag{A1.20}$$

This is the familiar equation for the one-sided Laplace transform. Tables of Laplace transforms are widely available. In the following discussions, only a few transform pairs will be used and these are summarized below.

Function		Laplace Transform
Impulse	$\delta(t)$	1
Unit Step	$u(t)$	$1/s$
Derivative	$df(t)/dt$	$sF(s) - f(0)$

It will be generally assumed that initial conditions are zero when transforming the derivative.

A general expression for a seismograph in the Laplace domain is

$$R(s) = F(s)H(s) \tag{A1.21}$$

where

$R(s)$ is the recorded output
$F(s)$ is the force acting on the inertial mass and
$H(s)$ is the system transfer function.

If the forcing function is earth motion, then

$$F_e(s) = -MX(s)s^2 = -MV(s)s = -MA(s) \tag{A1.22}$$

where $X(s)$, $V(s)$, and $A(s)$ are earth displacement, velocity, and acceleration, respectively, and M is the inertial mass. In the case of a pendulum-type instrument, earth motion generates a torque acting about the hinge point. For a calibrating force applied through an electromagnetic calibrator attached to the mass

$$F_c(s) = G_c I_c(s) \tag{A1.23}$$

where

$I_c(s)$ is the current through the calibrator and
G_c is the electrodynamic constant of the calibrator.

A transfer function of any linear time-invariant system (for example, damped harmonic oscillator) can be represented by a ratio of polynomials in the Laplace domain as

$$H(s) = \frac{s^m + a_{m-1}s^{m-1} + \ldots + a_2 s^2 + a_1 s + a_0}{s^n + b_{n-1}s^{n-1} + \ldots + b_2 s^2 + b_1 s + b_0} \tag{A1.24}$$

or, after factoring, as

$$H(s) = K_l \frac{(s - z_m)(s - z_{m-1})\ldots(s - z_2)(s - z_1)}{(s - p_n)(s - p_{n-1})\ldots(s - p_2)(s - p_1)} \tag{A1.25}$$

where

K_l is a lumped constant related to sensitivity.

Typically, transfer functions are tabulated by listing the roots of the denominator (poles), the roots of the numerator (zeros), and any sensitivity constants that are needed to determine the absolute magnitudes at a given frequency or period, which allows one to recover K_l.

Transfer functions are evaluated by converting the factors, in the Laplace domain, to the frequency domain by letting $s = j\omega$. This is equivalent to setting σ (the real part of the complex function s) equal to zero and evaluating the Laplace function along the imaginary axis of the s plane. A Fourier transfer function then becomes

$$H(j\omega) = K_l \frac{(j\omega - z_m)(j\omega - z_{m-1})\ldots(j\omega - z_2)(j\omega - z_1)}{(j\omega - p_n)(j\omega - p_{n-1})\ldots(j\omega - p_2)(j\omega - p_1)} \tag{A1.26}$$

The poles and zeros may be real or complex. Each factor of the polynomial can be individually evaluated for a given ω. If we let α_i equal the real part and β_i equal the imaginary part of a pole (or zero), then the magnitude of the factor is

$$|j\omega - p_i| = \sqrt{\alpha_i^2 + (j\omega - \beta_i)^2} \tag{A1.27}$$

and the phase angle contribution of each factor has the form

$$\theta_i = \tan^{-1}\left[\frac{(j\omega - \beta_i)}{\alpha_i}\right] \tag{A1.28}$$

Letting $Z(\omega)$ represent the product of the absolute amplitudes of the zeros and $P(\omega)$ represent the product of the absolute amplitudes of the poles, the amplitude response of the transfer function at any given ω is

$$|H(j\omega)| = K_l \frac{|Z(\omega)|}{|P(\omega)|} \tag{A1.29}$$

and the phase angle is determined by subtracting the sum of the phase angles computed from the individual poles, $\theta_p(\omega)$, from the sum of the phase angles computed from the individual zeros, $\theta_z(\omega)$.

$$\theta(j\omega) = \theta_z(\omega) - \theta_p(\omega) \tag{A1.30}$$

A1.1.3 Example Use of a Transfer Function

As an example, we will write the following subsidiary equation of motion in the s domain for the seismometer described earlier in this section.

$$Z(s)\left(s^2 + 2\lambda\omega s + \omega^2\right) = \frac{F(s)}{m} \tag{A1.31}$$

where

$F(s)$ is an arbitrary force given in the Laplace domain.

Note that the inertial mass now appears on the right hand side of this equation. If the forcing function is an impulse, with a Laplace transform equal to 1, then

$$Z(s) = H(s) = \frac{1}{m\left(s^2 + 2\lambda\omega s + \omega^2\right)} \tag{A1.32}$$

which is the transfer function for the instrument.

If the forcing function is earth displacement, then

$$Z(s) = H(s)\, mX(s)\, s^2 = \frac{-X(s)\, s^2}{s^2 + 2\,\lambda\,\omega\, s + \omega^2} \qquad \text{(A1.33)}$$

The negative sign is placed to show that the mass-frame displacement is of opposite direction from earth displacement. For a seismometer, one would also expect to find a sensitivity constant, call it *K,* on the right hand side of this equation. Let the natural period, *T*, equal 1.0 second (s) and the damping ratio, λ, equal 0.8, then

$$\frac{Z(s)}{X(s)} = \frac{-K\, s^2}{(s - 6.283 - j.0437)(s - 6.283 + j.0437)} \qquad \text{(A1.34)}$$

and we have the Laplace equation of mass-frame displacement with respect to earth displacement for a simple mechanical seismometer. It has two imaginary poles and two zeros at zero. The frequency response of this instrument is determined by converting the equation A1.34 to the Fourier domain by replacing *s* with $j\omega$ as follows.

$$\frac{Z(j\omega)}{X(j\omega)} = \frac{-K(j\omega)^2}{(j\omega - 6.283 - j.0437)\,(j\omega - 6.283 + j.0437)} \qquad \text{(A1.35)}$$

Letting *K* equal 1.0 (no mechanical or optical magnification), the amplitude and phase-response functions of this example instrument for an input of earth displacement can be computed as a function of the period, *T*, in seconds. The results are shown in figure A1.2. There is a bit of arbitrariness over phase lag or lead, but in this case, we know intuitively that at very short periods, the inertial mass will be nearly stationary as the frame vibrates, the magnification will be nearly 1, and the mass-frame displacement will be lagging earth displacement by nearly 180°.

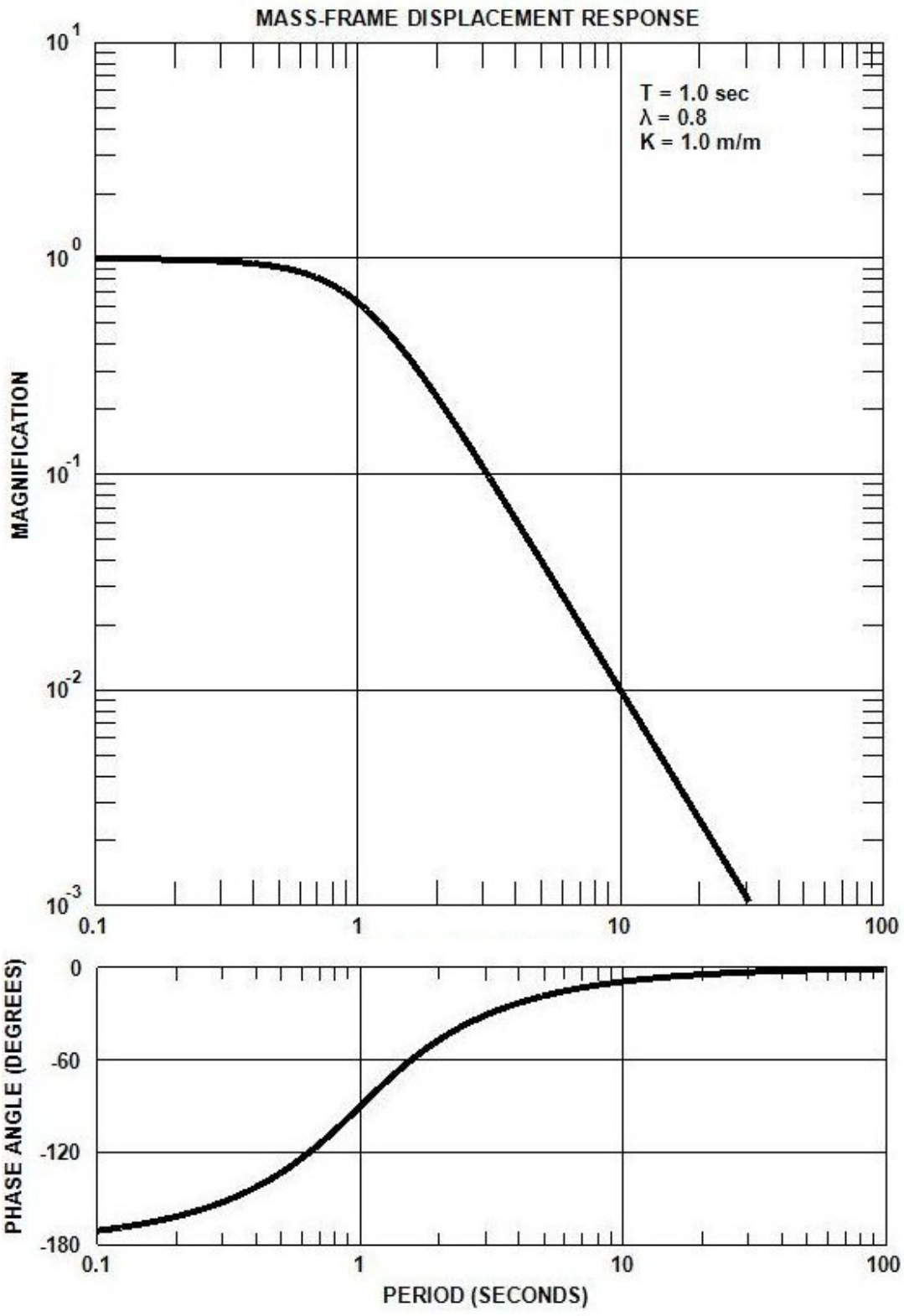

Figure A1.2 Example seismometer amplitude and phase response as a function of period. (sec, seconds; m/m, meters per meter)

Because calibration step functions were such an integral part of the WWSSN calibration routine, and because simulations of calibration output signals are used in the next section during the derivation of the transfer functions, it is appropriate to examine how simulated calibration responses are computed. The time history of the output, *r(t)*, of a seismometer caused by a force, *f(t)*, acting on the mass can be written as the convolution of the time history of the forcing function and the impulse response, *h(t),* of the instrument.

$$r(t) = f(t) * h(t) \text{ (* denotes convolution)} \tag{A1.36}$$

This can be expressed in the frequency domain as

$$R(j\omega) = F(j\omega)\, H(j\omega) \tag{A1.37}$$

And, if initial conditions are ignored, in the *s* domain as

$$R(s) = F(s)\, H(s) \tag{A1.38}$$

The impulse response, when needed, can be computed directly from the instrument transfer function using an inverse fast Fourier transform (FFT). For the example seismometer, it will appear as shown in figure A1.3.

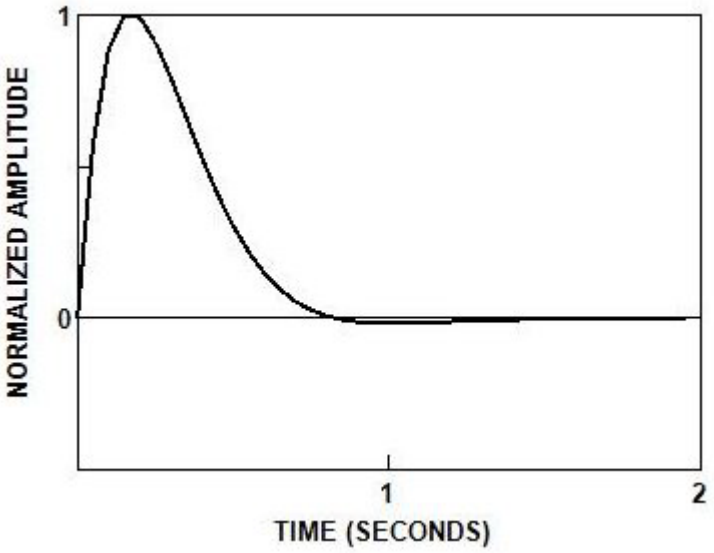

Figure A1.3 Example seismometer impulse response.

Computing the response to a force other than an impulse following the method used in this report involves a sequence of steps. A time history of the forcing function is prepared as a digital file of real numbers. The FFT used requires a file of 2^k samples, where *k* is an integer. Typically, for short-period instruments, a file length of 8,192 samples and a sample interval of 0.05 s would be appropriate. This file is passed through a forward FFT, which transforms the file to a series of complex numbers in the frequency domain. The transfer function is also transformed to the frequency domain by replacing *s* with $j\omega$. The Fourier transfer function is then reduced, using magnitude and phase angle calculations (see eqs. A1.27–A1.30), to a series of complex numbers of the same length as the input signal. The product of these two files is passed through an inverse FFT to produce a time history of the instrument response to the calibration input.

As an example, we will simulate a calibration signal using a 0.1 kilogram test mass (a force of 0.981N, assuming a 1-*g* gravitational field) applied to the example seismometer mass at a time of 5 s and removed after 5 s. The output signal that results is shown in figure A1.4. A "weight lift" of this type was used in the WWSSN to calibrate the electromagnetic calibrators. Instead of the rectangular form shown in figure A1.4, the output of the WWSSN seismometers from the application of a weight lift would have been two pulses of opposite polarity occurring at 5 and 10 s, because the electromagnetic seismometers produce an output proportional to the mass-frame velocity rather than displacement. In practice, the first pulse caused by the application of the weight was not used because of the difficulty in smoothly applying the weight to the seismometer mass.

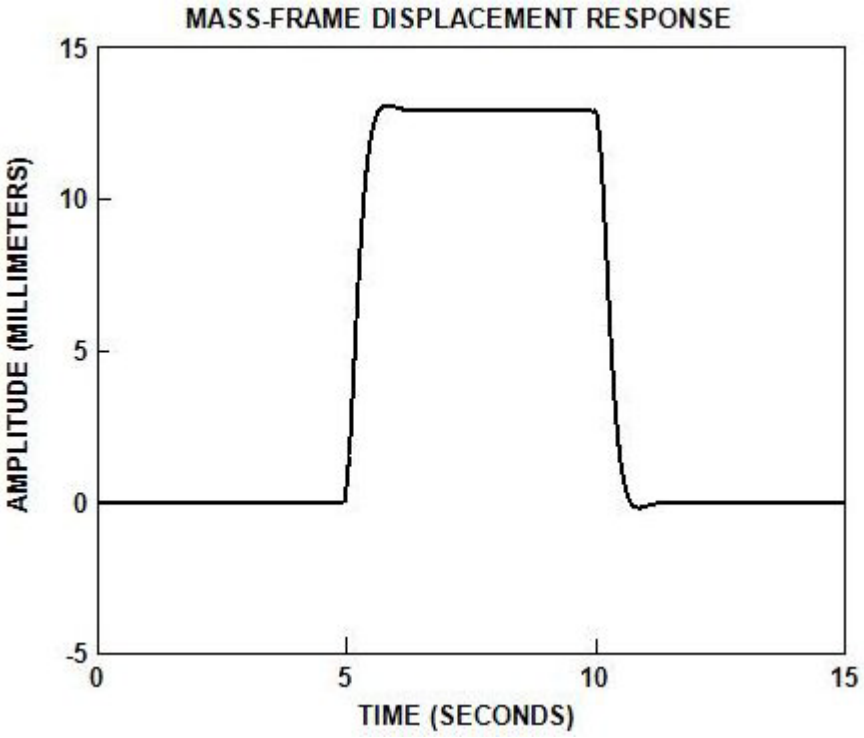

Figure A1.4 Example response to a weight being applied to and removed from a mechanical seismometer mass.

The complexity of electromagnetic and electronic seismographs is much greater than the simple instrument described above. However, the procedures used to analyze and calibrate more advanced seismographs are essentially the same.

A1.2 Generalized System Equation for an Electromagnetic Seismograph

The term "electromagnetic seismograph" has been generally used in the past and will be used here to refer to seismometer-galvanometer combinations in which the signal current is generated by a moving coil in a magnetic field and the recorded output is produced by a moving coil in a magnetic field attached to a galvanometer suspension. There have been a number of excellent papers published that describe the derivation of a generalized theoretical seismograph transfer functions. See, for example, Eaton (1957), Hagiwara (1958), Bogart (1961), Johnson and Matheson (1962) and Savill and others (1962). The derivation that follows is intended to focus more on a parametric description of the

seismograph and less on the basic theory which is well covered in earlier publications. It will establish the definitions and terminology needed to describe the WWSSN transfer functions.

A generalized circuit diagram for an electromagnetic seismograph is depicted in figure A1.5. In the circuit shown

e_s	is voltage generated in seismometer signal coil
R_s	is resistance in seismometer signal coil
L_s	is inductance in seismometer signal coil
e_g	is voltage generated in galvanometer signal coil
R_g	is resistance in galvanometer signal coil
R_1, R_2, R_3	are equivalent T-network resistances

Let

$$R_{11} = \frac{(R_1 + R_s)(R_2 + R_g) + (R_2 + R_g)R_3 + (R_1 + R_s)R_3}{R_2 + R_g + R_3} \tag{A1.39}$$

$$R_{22} = \frac{(R_1 + R_s)(R_2 + R_g) + (R_2 + R_g)R_3 + (R_1 + R_s)R_3}{R_2 + R_s + R_3} \tag{A1.40}$$

$$\kappa_1 = \frac{R_3}{R_2 + R_g + R_3} \tag{A1.41}$$

$$\kappa_2 = \frac{R_3}{R_1 + R_s + R_3} \tag{A1.42}$$

$$\alpha = \frac{L_s}{R_{11}} \tag{A1.43}$$

where

R_{11}	is total resistance in the seismometer circuit
R_{22}	is total resistance in the galvanometer circuit
κ_1	is forward current gain of the coupling circuit
κ_2	is back current gain of the coupling circuit
α	is ratio of inductance to total resistance in seismometer circuit

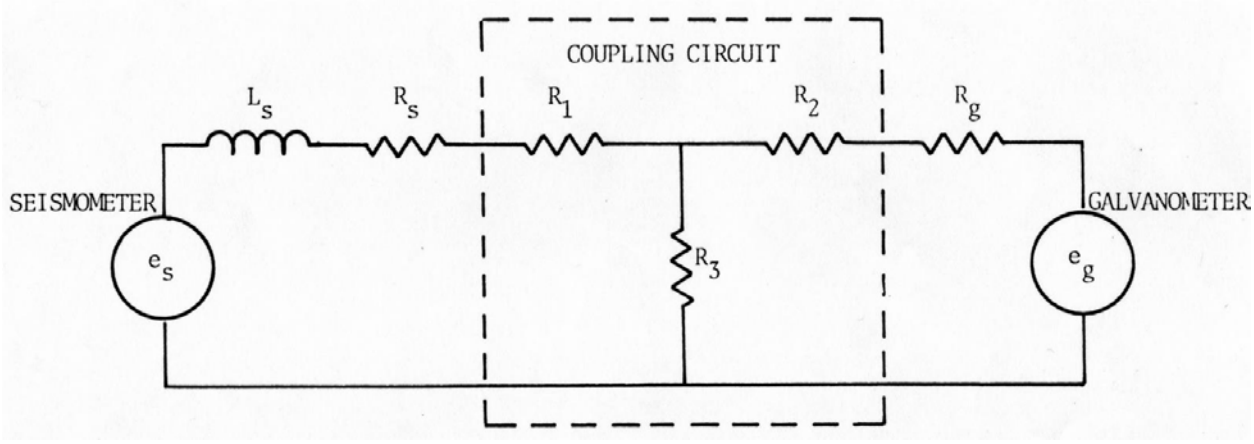

Figure A1.5 Equivalent circuit for an electromagnetic seismograph.

In practice, the coupling circuit may have been more complex than shown in figure A1.5. However, any two-terminal resistive network can be reduced to the equivalent circuit shown in the figure. The coupling circuit is completely defined by the three measurable parameters κ_1, R_{11}, and R_{22}. Values for the equivalent T-network resistances, should they be needed, can be computed from the following relationships

$$\kappa_2 = \kappa_1 \frac{R_{22}}{R_{11}} \tag{A1.44}$$

$$R_1 = \frac{R_{11} - R_s - \kappa_1\left(R_{22} - \kappa_2 R_s\right)}{1 - \kappa_1\kappa_2} \tag{A1.45}$$

$$R_2 = \frac{R_{22} - R_g - \kappa_2\left(R_{11} - \kappa_1 R_g\right)}{1 - \kappa_1\kappa_2} \tag{A1.46}$$

$$R_3 = \frac{\kappa_1\left(R_2 + R_g\right)}{1 - \kappa_1} \tag{A1.47}$$

and L_s can be measured.

Currents flowing in the circuit can be defined as follows:

i_{ss}	is current through the seismometer due to e_s
i_{sg}	is current through the galvanometer due to e_s
i_{gg}	is current through the galvanometer due to e_g
i_{gs}	is current through the seismometer due to e_g

Summation of the voltage drops in the two-loop network leads to the following Laplace subsidiary equations:

$$I_{ss}(s) = \frac{E_s(s)}{R_{11}(\alpha s + 1)} \tag{A1.48}$$

$$I_{sg}(s) = I_{ss}(s)\frac{R_3}{R_2 + R_g + R_3} = \kappa_1 I_{ss}(s) \tag{A1.49}$$

$$I_{gg}(s) = \frac{\alpha s E_g(s)}{(\alpha s + 1)(R_2 + R_g + R_3)} + \frac{E_g(s)}{R_{22}(\alpha s + 1)} \tag{A1.50}$$

$$I_{gs}(s) = \frac{\kappa_2 E_g(s)}{R_{22}(\alpha s + 1)} = \frac{\kappa_1 E_g(s)}{R_{11}(\alpha s + 1)} \tag{A1.51}$$

For purposes of analysis, the block diagram shown in figure A1.6 is a useful representation of a galvanometric seismograph. The input to the seismograph, F(s), is a force acting on the mass. The output, *R(s)*, is a recorded deflection that results from an angular displacement, φ(s), of the galvanometer mirror. Parameters of the seismograph are defined as follows:

M	is inertial mass (kilograms)
λ_{so}	is seismometer air damping ratio
ω_s	is seismometer natural angular frequency (radians/second)
G_s	is electrodynamic constant of seismometer coil (volt-seconds/meter for the short-period seismometer and volt-seconds/radian for the long-period seismometer.)
K_g	is moment of inertia about galvanometer suspension (kilogram-meter^2)
λ_g	is galvanometer air damping ratio
ω_g	is galvanometer natural angular frequency (radians/second)
G_g	is electrodynamic constant of galvanometer coil (newton-meters/ampere)
r_o	is distance from galvanometer mirror to recorder (1 meter for WWSSN)

The inputs to the first summing junction are forces acting on the inertial mass of the seismometer:

F(s)	is force due to earth or mass displacement (newtons)
F_d(s)	is force due to electromagnetic damping (newtons)
F_r(s)	is force due to galvanometer reaction (newtons)
R(s)	is optical record

It is worth noting that the galvanometer in figure A1.6 serves both as a motor with an output proportional to newton-meters/ampere and as a generator with an output proportional to volt-seconds/radian. When reduced to fundamental dimensions (mass, length, time, and electric charge), these units are equivalent, so the single electrodynamic constant, G_g, can be used in both cases.

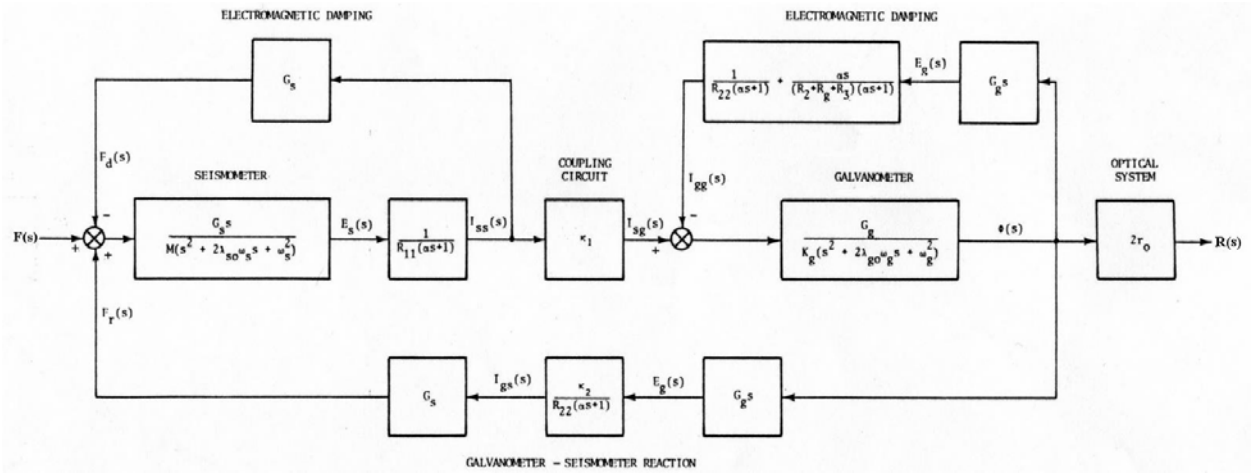

Figure A1.6 Block diagram of an electromagnetic seismograph transfer function.

If the seismometer is rotational (a term used here when the mass is suspended as a pendulum) rather than translational, then the inputs to the first summing junction would be torques acting about the hinge point. In this case, the seismometer subsidiary equation becomes

$$\frac{G_s s}{K_s\left(s^2 + 2\lambda_{so}\omega_s s + \omega_s^{\,2}\right)} \tag{A1.52}$$

where

K_S is the pendulum moment of inertia.

Transfer functions for elements other than the seismometer and galvanometer in figure A1.6 are derived from the circuit equations given above.

The transformation of the block diagram in figure A1.6, using block diagram algebra, yields the following equations:

$$\frac{R(s)}{F(s)} = \frac{\dfrac{-2r_o\kappa_1 G_s G_g s}{MR_{11}K_g}}{\left(\left(s^2 + 2\lambda_{so}\omega_s s + \omega_s^2\right)(\alpha s+1) + \dfrac{G_s^2 s}{MR_{11}}\right)\left(s^2 + 2\lambda_{go}\omega_g s + \omega_g^2 + \dfrac{G_g^2 s}{K_g R_{22}(\alpha s+1)} + \dfrac{\alpha G_g^2 s^2}{K_g\left(R_2+R_g+R_3\right)(\alpha s+1)}\right) - \dfrac{G_s^2 G_g^2 \kappa_1^{\,2} s^2}{MK_g R_{11}^2(\alpha s+1)}} \tag{A1.53}$$

for a translational electromagnetic seismograph, and

$$\frac{R(s)}{F(s)} = \frac{\dfrac{-2r_o\kappa_1 G_s G_g s}{K_s R_{11}K_g}}{\left(\left(s^2 + 2\lambda_{so}\omega_s s + \omega_s^2\right)(\alpha s+1) + \dfrac{G_s^2 s}{K_s R_{11}}\right)\left(s^2 + 2\lambda_{go}\omega_g s + \omega_g^2 + \dfrac{G_g^2 s}{K_g R_{22}(\alpha s+1)} + \dfrac{\alpha G_g^2 s^2}{K_g\left(R_2+R_g+R_3\right)(\alpha s+1)}\right) - \dfrac{G_s^2 G_g^2 \kappa_1^{\,2} s^2}{K_s K_g R_{11}^2(\alpha s+1)}} \tag{A1.54}$$

for a rotational electromagnetic seismograph, where we have simply replaced M in equation A1.53 with K_s.

The coefficients of s in the numerators are the seismograph sensitivities, designated S_c in this report. Standard magnifications were set by adjusting the forward current gain, κ_1. In the case of the

short-period seismographs, R_{11} was also adjustable and was used to set the seismometer damping. The negative term in the denominator of each equation is the reaction of the seismometer to the galvanometer current, i_g. It represents a positive feedback that, at high magnifications, causes a low-Q resonant effect.

When expanded, the denominators of the transfer functions become fifth-order polynomials (after the cancellation of a pole and zero at $1/\alpha$), or fourth-order polynomials (if seismometer inductance is negligible). All of the instrument parameters were measurable directly or indirectly, and equivalent T-network resistances were computed from equations provided earlier in this section.

Letting the seismograph transfer function be designated $H(s)$, then for an input of earth displacement

$$R(s) = MX(s)s^2H(s) \text{ (translational)} \tag{A1.55}$$

$$R(s) = Mr_{cm}X(s)s^2H(s) \text{ (rotational)} \tag{A1.56}$$

where

r_{cm} is the distance from the hinge to the center of mass. For a step input of force from a calibration current

$$R(s) = G_c i_c H(s) \text{ (translational)} \tag{A1.57}$$

$$R(s) = G_c i_c r_c H(s) \text{ (rotational)} \tag{A1.58}$$

where

G_c is the electrodynamic constant of the calibrator,
i_c is the current through the calibrator and
r_c is the distance from the hinge to the centerline of the calibrator coil.

If seismometer coil inductance can be neglected, as is the case for the WWSSN long-period (LP) seismographs, the transfer function becomes less complex. In this case, the subsidiary equation for the long-period transfer function is reduced to

$$H(s) = \frac{R(s)}{F(s)} = \frac{\dfrac{-2r_0\kappa_1 G_s G_g s}{K_s R_{11} K_g}}{\left(s^2 + 2\lambda_{so}\omega_s s + \omega_s^2 + \dfrac{G_s^2 s}{K_s R_{11}}\right)\left(s^2 + 2\lambda_{go}\omega_g s + \omega_g^2 + \dfrac{G_g^2 s}{K_g R_{22}}\right) - \dfrac{G_s^2 G_g^2 \kappa_1^2 s^2}{K_s K_g R_{11}^2}} \tag{A1.59}$$

The damping coefficient for the seismometer can be written as

$$2\lambda_s\omega_s = 2\lambda_{so}\omega_s + \frac{G_s^2}{K_s R_{11}} \tag{A1.60}$$

where

λ_s is the combined air and electromagnetic damping

$$\lambda_s = \lambda_{so} + \frac{G_s^2}{2\omega_s K_s R_{11}} \tag{A1.61}$$

Likewise, for the galvanometer

$$2\lambda_g\omega_g = 2\lambda_{go}\omega_g + \frac{G_g^2}{K_g R_{22}} \tag{A1.62}$$

and

$$\lambda_g = \lambda_{go} + \frac{G_g^2}{2\omega_g K_g R_{22}} \tag{A1.63}$$

The positive feedback produced by back currents generated within the galvanometer coil is expressed by the negative second-order coefficient in equation A1.58, and this may be rewritten as follows:

$$\frac{G_s^2 G_g^2 \kappa_1^2}{K_s K_g R_{11}^2} = 4\omega_s \omega_g (\lambda_s - \lambda_{so})(\lambda_g - \lambda_{go})\, \kappa_1 \kappa_2 \tag{A1.64}$$

This shows that the magnitude of the galvanometer feedback depends on electromagnetic damping and the current gain in the coupling circuit. Galvanometer feedback often is referred to as coupling in descriptions of electromagnetic seismographs. Hagiwara (1958) defined a coupling factor, σ^2, as follows (using our notation)

$$\sigma^2 = \frac{(\lambda_s - \lambda_{so})(\lambda_g - \lambda_{go})\, \kappa_1 \kappa_2}{\lambda_s \lambda_g} \tag{A1.65}$$

Using the expressions given just above and letting the sensitivity

$$S_c = \frac{2 r_o \kappa_1 G_s G_g}{K_s R_{11} K_g} \tag{A1.66}$$

we can rewrite the WWSSN LP transfer function as follows

$$H(s) = \frac{R(s)}{F(s)} = \frac{-S_c s}{\left(s^2 + 2\lambda_s \omega_s s + \omega_s^2\right)\left(s^2 + 2\lambda_g \omega_g s + \omega_g^2\right) - 4\lambda_s \omega_s \lambda_g \omega_g \sigma^2 s^2} \tag{A1.67}$$

And by expanding the denominator,

$$H(s) = \frac{-S_c s}{s^4 + (2\lambda_s \omega_s + 2\lambda_g \omega_g) s^3 + (\omega_s^2 + \omega_g^2 + 4\lambda_s \omega_s \lambda_g \omega_g (1 - \sigma^2)) s^2 + (2\lambda_s \omega_s \omega_g^2 + 2\lambda_g \omega_g \omega_s^2) s + \omega_s^2 \omega_g^2} \tag{A1.68}$$

Written in this form, the dynamic response of the long-period seismograph is expressed as the function of the five parameters ω_s, λ_s, ω_g, λ_g, and σ^2. This is an especially useful form in curve-fitting and other applications where the period and damping of the instruments can be determined or estimated without knowledge of the complete set of physical parameters.

Appendix A2. Method used to Profile a WWSSN Long-Period Step Response

There were several reports with topics relevant to long-period seismograph calibration during the early years of the World-Wide Standardized Seismograph Network (WWSSN). These included papers by Espinosa and others (1962, 1965) and a paper by Mitchell and Landisman (1969). Espinosa and others (1962) described methods of calibrating long-period seismographs using transient techniques and later published a manual with a large set of transient responses that could be used as overlays to estimate instrument period and damping. Mitchell and Landisman (1969) described a method of fitting a synthetic step response to a digitized recorded step response using least squares inversion. They demonstrated the technique using step response data recorded at a WWSSN station.

The long-period step response profiling described here is intended to provide a relatively easy method of estimating values for the three adjustable instrument parameters: T_s, T_g, and G_g. This method is based on the structure of the step response but does not require full digitization of the calibration segment. It was used to derive the *typical* long-period transfer functions from profile averages and can be used to derive transfer functions for individual seismograph components.

The archive contains film copies of the WWSSN seismograms. These are scanned at 3,200 pixels per inch and the scanned images are placed in files formatted as tagged image files (TIF). A photo processor can be used to crop an image of the step response and print the cropped image on an 8 × 10 inch sheet at about twice the magnification of the original seismogram, roughly 130–150 millimeters (mm) for the peak of the step response. It is important that the seismogram edge be included in the saved image. Either the 'on' or 'off' pulse can be used.

The procedure involves profiling a step response using nine data points as shown in figure A2.1. As a first step, a baseline is drawn through the center of the trace where first motion is detected from the onset of the pulse. The baseline must be parallel to the edge of the seismogram. This is important because the galvanometer trace is perpendicular to the edge of the seismogram, not the record trace, which follows a helical path around the recorder drum at an angle determined by the translation rate.

A starting point is chosen for the step onset. A point is found where the first motion of the pulse is detected, then the point is scaled back the equivalent of about 0.5 second (s) to account for visually undetectable motion of less than 0.1 mm on the seismogram. Using this point, a start line is drawn perpendicular to the baseline and extended just beyond the peak of the pulse. A second vertical line is drawn perpendicular to the baseline through the peak of the pulse.

The amplitude of the peak is measured in millimeters. Points are then marked off on the vertical line through the peak corresponding to 0.1, 0.25, 0.5, and 0.75 parts of the peak amplitude. Through these points, lines perpendicular to the vertical line are drawn to intersect the start line and the leading and trailing edges of the pulse. A small drafting triangle with its center marked on the base is helpful in keeping these horizontal lines perpendicular to the vertical line.

The minute marks are spaced at either 15 or 30 mm on the original seismogram depending on the drum translation rate. By measuring between the leading edges of the minute marks, a conversion factor from millimeters to seconds can be obtained. The magnification between the printed image and the original seismogram can also be obtained. Slight variations in the scaled length of the minute marks, usually less than 0.5 mm, can be expected in different places on the record due to differential shrinkage during the processing of the original records.

Measurements are taken between the start line and the points shown in figure A2.1. The measurements are converted to seconds and define the profile of the step response. The profile of the leading edge of the pulse, from the onset to the peak, is determined primarily by the period and damping of the seismometer; the profile of the trailing edge is determined primarily by the period and damping of the galvanometer.

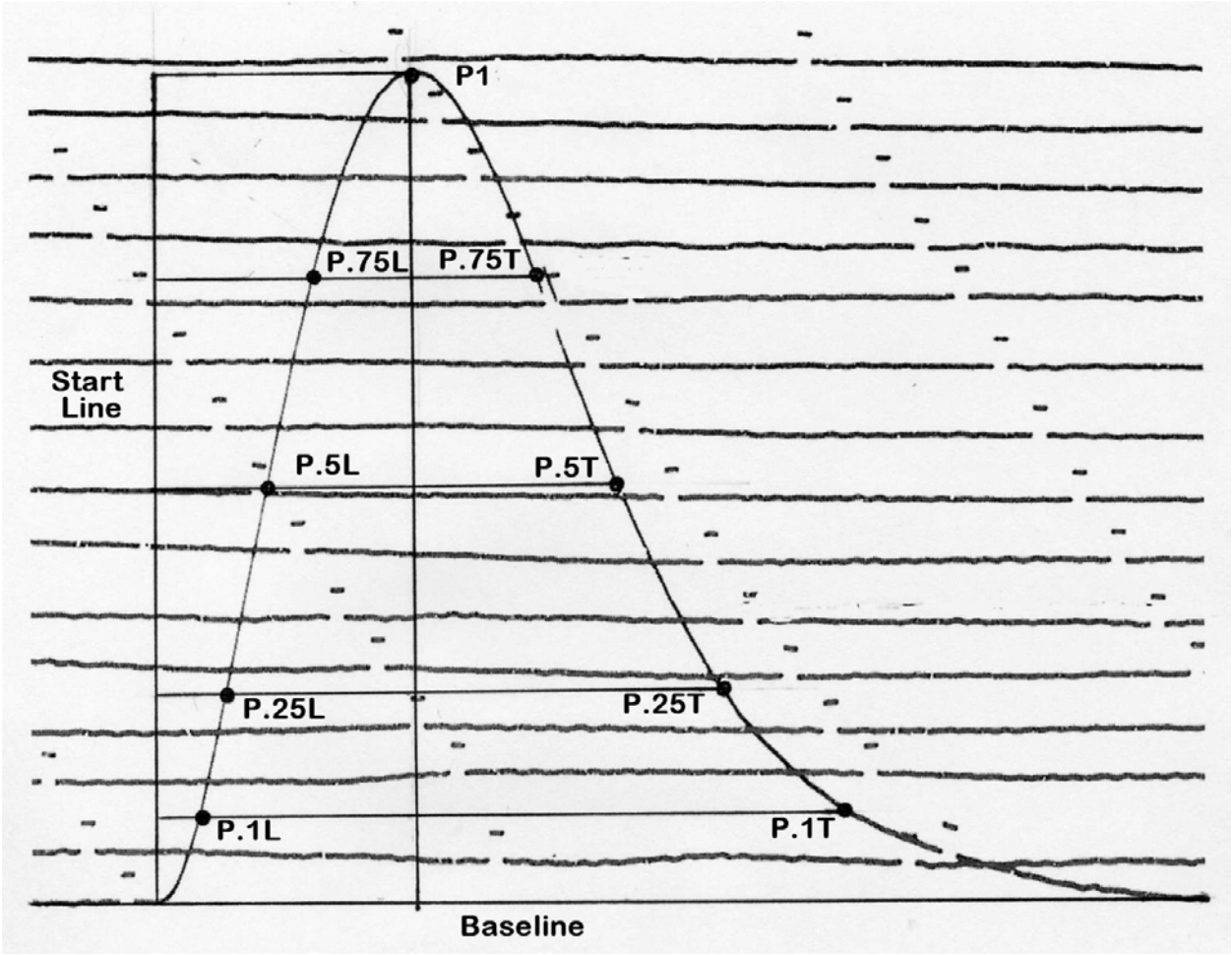

Figure A2.1 Setup for measuring profile of a long-period step response. The labels on the measured points denote the amplitude on the step response relative to the peak amplitude and if the point is leading (L) or trailing (T) the peak.

Step response profiles can be computed from a transfer function to simulate the recorded steps. A trial transfer function derived from any set of instrument parameters using equation A1.59 or A1.68 is convolved with an input of current applied to the calibration coil to simulate the recorded on and off pulses. (See Section A1.1.3 for a note on the computational steps used.) For the long-period seismograph, an input file length of 8,192 samples with a sampling interval of 0.1 s would be appropriate. The input calibration forcing function will be a torque equal to $G^* i_c r_{cm}$, where G^* is the calibration constant listed on the seismogram label if the computed profile is to model a recorded profile, i_c is the calibration current, and r_{cm} is the seismometer center of mass. (To see why r_{cm} is used

instead of r_c, refer to equation 9.11.) The simulated calibration should be applied for several minutes so that the 'off' pulse does not affect the measurements. The input file is passed through a forward fast Fourier transform (FFT) transforming it to a series of complex numbers in the frequency domain. Next, the trial transfer function is transformed to the frequency domain by replacing s with $j\omega$. Using equations 8.21 through 8.30, the Fourier transfer function is reduced to a file of complex numbers of the same length as the input file. The product of the input file and the transfer function is then passed through an inverse FFT to produce the time history of the instrument response to the calibration input. To produce an output in units of millimeters, the sensitivity constant must be increased by a factor of 1,000.

This computational procedure was used to generate the listing of profiles shown in Table A2.1 for the LP30 seismograph and in table A2.2 for the LP15 seismograph. The profiles in the tables show the effects of variation in the seismograph parameters T_s, T_g, and G_g. There are at least eight additional parameters that contribute to the response characteristics of the seismograph. For the most part, these are mechanical or electrical constants whose values were fixed during manufacture and generally held to within acceptable tolerances. The profiles were derived using vertical-component parameters and a magnification setting of 1,500. Results from using the parameters for a horizontal component are the same to within 0.1 s. However, the sensitivity constant, S_c, will be different. The horizontal-component value of S_c will be the product of the vertical-component value and the ratio of K_s(vertical)/K_s(horizontal).

The data presented in the tables are useful as a guide in estimating the values of critical parameters when compared with profiles obtained from recorded step responses. Trial transfer functions can be computed and used to test parameter values until a good fit is made with the measured profile. The *typical* LP15 and LP30 transfer functions, which are based on an average of measured profile values, were derived in this way. A curve-fitting routine could be used but was found not to be necessary for determining the *typical* transfer functions because only a few trial runs were needed.

Table A2.1 Profiles computed for step responses derived from vertical component World-Wide Standardized Seismograph Network (WWSSN) LP30 seismograph operating at a magnification of 1,500 showing effects of changes in important seismograph parameters. (%, percent)

	Gg	T_s	λ_s	T_g	λ_g	σ^2	S_c	P.1L	P.25L	P.5L	P.75L	P1.0	P.75T	P.5T	P.25T	P.1T
Gg - 0%	0.0030880	30.0	1.916	98.1	1.010	0.0392	378.55	5.41	8.69	13.49	19.06	33.10	53.16	67.15	86.53	109.53
Gg - 1%	0.0030571	30.0	1.916	98.1	0.994	0.0394	376.50	5.43	8.72	13.53	19.10	33.10	52.97	66.76	85.73	108.12
Gg - 2%	0.0030262	30.0	1.916	98.1	0.978	0.0397	374.70	5.45	8.75	13.57	19.14	33.10	52.80	66.37	84.95	106.73
Gg - 3%	0.0029954	30.0	1.916	98.1	0.962	0.0400	373.11	5.47	8.78	13.61	19.18	33.10	52.62	66.00	84.18	105.35
Gg - 4%	0.0029645	30.0	1.916	98.1	0.946	0.0403	371.31	5.49	8.81	13.65	19.23	33.10	52.46	65.63	83.43	103.99
Gg - 5%	0.0029336	30.0	1.916	98.1	0.931	0.0406	369.60	5.51	8.84	13.69	19.27	33.10	52.29	65.27	82.70	102.66
Gg - 6%	0.0029027	30.0	1.916	98.1	0.915	0.0409	368.00	5.53	8.87	13.73	19.31	33.10	52.13	64.92	81.96	101.32
Gg - 7%	0.0028718	30.0	1.916	98.1	0.900	0.0412	366.23	5.55	8.90	13.78	19.36	33.10	51.97	64.57	81.24	100.00
Gg - 8%	0.0028410	30.0	1.916	98.1	0.885	0.0416	364.81	5.57	8.94	13.82	19.40	33.20	51.82	64.22	80.53	98.69
Gg - 9%	0.0028101	30.0	1.916	98.1	0.870	0.0419	363.22	5.60	8.97	13.86	19.45	33.20	51.67	63.90	79.84	97.41
Gg - 10%	0.0027792	30.0	1.916	98.1	0.855	0.0423	361.71	5.62	9.00	13.90	19.49	33.20	51.53	63.57	79.17	96.15
Tg - 1%	0.003088	30.0	1.916	97.1	1.002	0.0390	378.05	5.39	8.65	13.43	18.96	32.90	52.72	66.52	85.57	108.12
Tg - 2%	0.003088	30.0	1.916	96.1	0.994	0.0389	377.73	5.37	8.61	13.36	18.86	32.70	52.28	65.88	84.61	106.71
Tg - 3%	0.003088	30.0	1.916	95.2	0.986	0.0388	377.42	5.35	8.58	13.30	18.76	32.50	51.88	65.31	83.75	105.45
Tg - 4%	0.003088	30.0	1.916	94.2	0.978	0.0386	377.17	5.33	8.54	13.24	18.66	32.30	51.45	64.68	82.80	104.07
Tg - 5%	0.003088	30.0	1.916	93.1	0.969	0.0384	376.64	5.30	8.50	13.17	18.55	32.00	50.97	64.00	81.79	102.60
Tg - 6%	0.003088	30.0	1.916	92.2	0.961	0.0383	376.33	5.28	8.47	13.11	18.45	31.80	50.56	63.42	80.92	101.34
Ts -1%	0.003088	29.7	1.897	98.1	1.010	0.0392	378.44	5.38	8.64	13.41	18.93	32.90	52.79	66.68	85.90	108.72
Ts - 2%	0.003088	29.4	1.878	98.1	1.010	0.0392	378.44	5.35	8.58	13.32	18.81	32.70	52.40	66.20	85.27	107.91
Ts - 3%	0.003088	29.1	1.859	98.1	1.010	0.0392	378.44	5.32	8.53	13.23	18.68	32.50	65.72	65.72	84.66	107.12
Ts - 4%	0.003088	28.8	1.841	98.1	1.010	0.0392	378.63	5.29	8.48	13.15	18.56	32.30	51.66	65.24	84.03	106.33
Ts - 5%	0.003088	28.5	1.822	98.1	1.010	0.0392	378.65	5.26	8.42	13.06	18.43	32.00	51.29	64.77	83.43	105.57
Ts - 6%	0.003088	28.2	1.803	98.1	1.010	0.0392	378.75	5.22	8.37	12.97	18.30	31.80	50.92	64.30	82.82	104.80
Ts - 7%	0.003088	27.9	1.784	98.1	1.010	0.0392	378.87	5.19	8.32	12.88	18.17	31.50	50.55	63.83	82.22	104.05
Ts - 8%	0.003088	27.6	1.765	98.1	1.010	0.0392	379.06	5.16	8.26	12.79	18.04	31.30	50.17	63.37	81.63	103.32
Ts - 9%	0.003088	27.3	1.746	98.1	1.010	0.0393	379.16	5.13	8.21	12.70	17.91	31.10	49.80	62.90	81.04	102.59
Ts - 10%	0.003088	27.0	1.727	98.1	1.010	0.0393	379.38	5.09	8.15	12.61	17.78	30.80	49.43	62.44	80.46	101.88

Table A2.2 Profiles computed for step responses derived from vertical component WWSSN LP15 seismograph operating at a magnification of 1,500 showing the effects of changes in important seismograph parameters. (%, percent)

	G_g	T_s	λ_s	T_g	λ_g	σ^2	S_c	P.1L	P.25L	P.5L	P.75L	P1.0	P.75T	P.5T	P.25T	P.1T
Gg - 0%	0.0030880	15.00	0.953	98.1	1.010	0.0346	354.80	3.42	5.34	8.13	11.45	20.60	35.47	46.69	62.80	82.14
Gg - 1%	0.0030571	15.00	0.953	98.1	0.994	0.0351	354.50	3.43	5.36	8.17	11.50	20.70	35.46	46.52	62.25	80.91
Gg - 2%	0.0030262	15.00	0.953	98.1	0.978	0.0356	354.00	3.45	5.39	8.20	11.55	20.70	35.46	46.37	61.72	79.72
Gg - 3%	0.0029954	15.00	0.953	98.1	0.962	0.0360	353.40	3.46	5.41	8.24	11.60	20.80	35.46	46.21	61.20	78.55
Gg - 4%	0.0029645	15.00	0.953	98.1	0.946	0.0366	353.01	3.48	5.43	8.27	11.65	20.90	35.46	46.06	60.70	77.41
Gg - 5%	0.0029336	15.00	0.953	98.1	0.931	0.0371	352.50	3.49	5.46	8.31	11.70	21.00	35.46	45.92	60.21	76.30
Gg - 6%	0.0029027	15.00	0.953	98.1	0.915	0.0376	352.10	3.50	5.48	8.35	11.75	21.00	35.47	45.78	59.74	75.22
Gg - 7%	0.0028718	15.00	0.953	98.1	0.900	0.0375	348.36	3.52	5.50	8.38	11.81	21.10	35.48	45.65	59.29	74.18
Gg - 8%	0.0028410	15.00	0.953	98.1	0.885	0.0373	344.61	3.53	5.52	8.42	11.86	21.20	35.49	45.53	58.86	73.18
Gg - 9%	0.0028101	15.00	0.953	98.1	0.870	0.0371	340.87	3.55	5.55	8.46	11.91	21.30	35.50	45.42	58.43	72.20
Gg - 10%	0.0027792	15.00	0.953	98.1	0.855	0.0369	337.12	3.56	5.57	8.50	11.97	21.30	35.52	45.31	58.03	71.27
Tg - 1%	0.0030880	15.00	0.953	97.1	1.002	0.0345	354.81	3.41	5.33	8.11	11.41	20.50	35.17	46.20	61.95	80.76
Tg - 2%	0.0030880	15.00	0.953	96.1	0.994	0.0345	354.68	3.40	5.32	8.08	11.36	20.40	34.87	45.71	61.12	79.41
Tg - 3%	0.0030880	15.00	0.953	95.2	0.986	0.0344	354.62	3.40	5.30	8.06	11.32	20.30	34.58	45.23	60.29	78.07
Tg - 4%	0.0030880	15.00	0.953	94.2	0.978	0.0343	354.54	3.39	5.29	8.04	11.28	20.20	34.28	44.74	59.47	76.74
Tg - 5%	0.0030880	15.00	0.953	93.1	0.969	0.0342	354.37	3.38	5.28	8.01	11.24	20.00	33.98	44.26	58.66	75.43
Tg - 6%	0.0030880	15.00	0.953	92.2	0.961	0.0341	354.40	3.37	5.26	7.99	11.20	19.90	33.69	43.78	57.85	74.14
Ts - 1%	0.003088	14.85	0.944	98.1	1.010	0.0346	354.93	3.39	5.30	8.06	11.36	20.50	35.33	46.56	62.67	82.00
Ts - 2%	0.003088	14.70	0.935	98.1	1.010	0.0347	355.05	3.37	5.26	8.00	11.27	20.30	35.21	46.44	62.54	81.88
Ts - 3%	0.003088	14.55	0.925	98.1	1.010	0.0347	355.15	3.34	5.21	7.93	11.17	20.20	35.07	46.31	62.41	81.74
Ts - 4%	0.003088	14.40	0.916	98.1	1.010	0.0347	355.25	3.32	5.17	7.87	11.08	20.10	34.95	46.18	62.29	81.61
Ts - 5%	0.003088	14.25	0.906	98.1	1.010	0.0347	355.56	3.29	5.13	7.80	10.99	20.00	34.82	46.06	62.17	81.48
Ts - 6%	0.003088	14.10	0.897	98.1	1.010	0.0348	355.76	3.26	5.09	7.73	10.90	19.90	34.70	45.94	62.05	81.36
Ts - 7%	0.003088	13.95	0.887	98.1	1.010	0.0348	356.00	3.24	5.04	7.67	10.81	19.70	34.59	45.83	61.64	81.25
Ts - 8%	0.003088	13.80	0.878	98.1	1.010	0.0349	356.56	3.21	5.00	7.60	10.72	19.60	34.47	45.71	61.82	81.13
Ts - 9%	0.003088	13.65	0.869	98.1	1.010	0.0350	356.95	3.18	4.96	7.53	10.63	19.50	34.35	45.60	61.71	81.02
Ts - 10%	0.003088	13.50	0.859	98.1	1.010	0.0311	357.57	3.16	4.91	7.46	10.53	19.40	34.24	45.49	61.60	80.91

Glossary of Symbols and Abbreviations

Symbols

The location given is the equation (e), figure (f), page (p), or table (t) in which the symbol is first introduced. Units are given where appropriate.

Symbol	Definition	Units	Location
A	Ampere (unit of electrical current)	ampere	f6.1
A_0	A constant of amplitude related to initial conditions	meters	eA1.6
a_i	Amplitude of recorded pulse on seismogram produced by a calibrator current	meters	e9.1
$a_{m-1}...$	Coefficients of an m^{th} degree polynomial		eA1.24
a_o	Amplitude of recorded sine wave on seismogram due to a calibration input	meters	e9.6
a_w	Amplitude of recorded pulse on seismogram produced by a weight lift	meters	e9.1
B_0	A constant of amplitude related to initial conditions	meters	eA1.6
$b_n...$	Coefficients of an n^{th} degree polynomial		eA1.24
c	Correction factor for damping of short-period seismometer		e9.10
C_1	Amplitude constant	meters	eA1.10
C_2	Amplitude constant	meters	eA1.10
C_3	Amplitude constant	meters	eA1.11
d	Viscous damping coefficient	newton-seconds-meter^{-1}	eA1.1
e_g	Voltage generated in galvanometer signal coil	volts	fA1.5
e_s	Voltage generated in seismometer signal coil	volts	fA1.5
$E_s(s)$	The Laplace transform of the voltage generated in seismometer signal coil	volt-seconds	eA1.48
f	Frequency of oscillation	hertz	e9.6
$F(j\omega)$	The Fourier transform of a general function, *f(t)*, with input unspecified	unspecified	eA1.18
$F(s)$	The Laplace transform of a general function, *f(t)*, with input unspecified	unspecified	eA1.20
$F(s)$	The Laplace transform of a force due to earth motion or calibration	newton-seconds	e8.1
$f(t)$	The time history of a general function, *f(t)*, with input unspecified.	unspecified	eA1.18
$f(t)$	Time history of force acting on an inertial mass	newtons	eA1.36
$F_c(s)$	Laplace transform of force due to current through a calibrator	newton-seconds	eA1.23
f_e	Force acting on an inertial mass due to a sinusoidal displacement of the earth	newtons	e9.4

$F_e(s)$	Laplace transform of force due to earth motion	newton-seconds	eA1.22
f_i	Force acting on an inertial mass due to a current flowing through a calibrator	newtons	e9.3
f_o	Instrumental natural (undamped) frequency of oscillation	hertz	p61
g	Acceleration of gravity	meters-second^{-2}	e9.1
G	Electrodynamic constant of a short-period calibrator	newtons-ampere^{-1}	f6.1
G^*	Electrodynamic constant of a long-period calibrator	newtons-ampere^{-1}	e9.11
G_c	Electrodynamic constant of a calibrator	newtons-ampere^{-1}	e9.1 e9.2
G_g	Electrodynamic constant of a galvanometer coil	newton-meters-ampere^{-1}	e8.1
G_s	Electrodynamic constant of a long-period seismometer coil	volt-seconds-radian^{-1}	e8.1
G_s	Electrodynamic constant of a short-period seismometer coil	volt-seconds-meter^{-1}	e8.1
$H(j\omega)$	Frequency response (amplitude and phase) of a seismograph to input of earth motion	unspecified	eA1.26
$\lvert H(j\omega) \rvert$	Amplitude response of a seismograph to input of earth motion	unspecified	eA1.29
$H(s)$	A seismograph system transfer function; Laplace transform of impulse response	unspecified	eA1.21
$h(t)$	Time history of an impulse response	unspecified	eA1.36
i_c	Current flowing through a calibrator	amperes	e9.1
$I_c(s)$	Laplace transform of current flowing through a calibrator	ampere-seconds	eA1.23
i_{gg}	Current through the galvanometer due to e_g	amperes	p71
$I_{gg}(s)$	Laplace transform of current through the galvanometer due to e_g	ampere-seconds	eA1.50
i_{gs}	Current through the seismometer due to e_g	amperes	p71
$I_{gs}(s)$	Laplace transform of current through the seismometer due to e_g.	ampere-seconds	eA1.50
i_{sg}	Current through the galvanometer due to e_s	amperes	p71
$I_{sg}(s)$	Laplace transform of current through the galvanometer due to e_g	ampere-seconds	eA1.49
i_{ss}	Current through the seismometer due to e_s	amperes	p71
$I_{ss}(s)$	Laplace transform of current through the seismometer due to e_s	ampere-seconds	eA1.46
j	Square root of negative one; denotes an imaginary number		t8.2a
k	A variable integer		p68
K	A sensitivity constant	unspecified	eA1.34
K_c	Calibration constant used to set or determine magnification of a seismograph	newtons-meter^{-1}	e9.8
K_g	Moment of inertia of galvanometer coil about the suspension	kilogram-meter^2	e8.1

K_I	A constant related to sensitivity	unspecified	eA1.25
K_s	Moment of inertia of seismometer pendulum about the hinge	kilogram-meter^2	p23
L_s	Seismometer signal coil inductance	henrys	fA1.5
M	Seismometer inertial mass	kilograms	e8.1
m	Example seismometer inertial mass	kilograms	eA1.1
m	A variable integer		eA1.24
n	A variable integer		eA1.16
N	Newton (unit of force)	newton	f6.1
$P(\omega)$	Product of the absolute amplitudes of the poles in the polynomial		eA1.29
$P.1L, P.25L, ...$	Measurements of time from step onset to the leading edge of a long-period step response taken at several amplitudes relative to the peak amplitude (see figure A2.1)	seconds	t8.6
$P.1T, P.25T,...$	Measurements of time from step onset to the trailing edge of a long-period step response taken at several amplitudes relative to the peak amplitude (see figure A2.1)	seconds	t8.6
$p_n...$	Roots (poles) of an n^{th} degree polynomial		eA1.25
$R(j\omega)$	Fourier transform of the time history, r(t), of a seismograph record	meter-seconds	eA1.37
$R(s)$	Laplace transform of the time history, r(t), of a seismograph record	meter-seconds	eA1.21
$r(t)$	Time history of a seismograph recording	meters	eA1.36
r_1	Root of a quadratic equation		eA1.7
R_1	Equivalent T-network resistance	ohms	fA1.5
R_{11}	Total resistance in the seismometer circuit	ohms	e8.1
R_2	Equivalent T-network resistance	ohms	e8.1
r_2	Root of a quadratic equation		eA1.8
R_{22}	Total resistance in the galvanometer circuit	ohms	e8.1
R_3	Equivalent T-network resistance	ohms	e8.1
R_c	Calibrator coil resistance	ohms	t8.1
r_c	Distance from pendulum hinge to centerline of calibrator coil	meters	e9.2
r_{cm}	Distance from hinge to the pendulum center of mass	meters	e9.7
r_{co}	Distance from pendulum hinge to the center of oscillation	meters	t8.3
R_g	Galvanometer coil resistance	ohms	e8.1
r_o	Distance from the galvanometer mirror to the recorder (1.0 m for the WWSSN)	meters	e8.1
R_s	Seismometer signal coil resistance	ohms	fA1.5
r_w	Distance from seismometer hinge to point of weight lift	meters	e9.2
s	Laplace transform frequency variable	seconds^{-1}	e8.1
S_c	Long-period seismograph sensitivity constant	kilogram^{-1}-meter^{-1}-seconds^{-1}	e8.3

S_c	Short-period seismograph sensitivity constant	kilogram^{-1}-seconds^{-1}	e8.2
t	Time	seconds	eA1.1
T_d	Damped oscillation period of instrument	seconds	eA1.15
T_g	Natural (undamped) period of galvanometer	seconds	t8.4
T_o	Natural (undamped) oscillation period of instrument	seconds	eA1.15
T_s	Natural (undamped) oscillation period of seismometer	seconds	t8.4
u	Spring constant	newtons-meter^{-1}	eA1.1
$X(j\omega)$	Earth displacement in the Fourier domain	meter-seconds	eA1.35
$X(s)$	Earth displacement in the Laplace domain	meter-seconds	eA1.22
$x_1, x_2, \ldots x_n$	Successive peak amplitudes	meters	p61
x_m	Sinusoidal earth displacement	meters	e9.4
z	Relative seismometer mass-frame displacement	meters	A1.1
$Z(j\omega)$	Fourier transform of seismometer relative mass-frame displacement	meter-seconds	eA1.31 eA1.35
$Z(s)$	Laplace transform of seismometer relative mass-frame displacement	meter-seconds	eA1.31
$Z(\omega)$	Product of the absolute amplitudes of the zeros in the polynomial		eA1.29
$z_m \ldots$	Roots (zeros) of an mth degree polynomial		A1.25
α	Ratio of inductance to total resistance in the seismometer circuit	henrys-ohms^{-1}	e8.1
α_i	Real part of a complex number		eA1.27
β_i	Imaginary part of a complex number		eA1.27
δ	Logarithmic decrement		eA1.16
$\theta(j\omega)$	Phase response of a transfer function for any given ω	radians	eA1.30
θ_i	Phase angle of a factor in a polynomial	radians	eA1.28
θ_p	Sum of phase angles computed from individual poles	radians	eA1.30
θ_z	Sum of phase angles computed from individual zeros	radians	eA1.30
κ_1	Forward current gain of the coupling circuit	ampere-ampere^{-1}	e8.1
κ_2	Back current gain of the coupling circuit	ampere-ampere^{-1}	eA1.42
λ	Damping ratio (ratio of actual damping to critical damping)		eA1.4
λ_g	Galvanometer damping ratio with combined air and electromagnetic damping		t8.4
λ_{go}	Galvanometer damping ratio with air damping only		e8.1
λ_s	Seismometer damping ratio with combined air and electromagnetic damping		t8.4
λ_{so}	Seismometer damping ratio with air damping only		e8.1
π	Ratio of circumference of circle to its diameter: 3.14159265……..		eA1.17
σ	Real part of a complex number		eA1.19
σ^2	Galvanometer-seismometer coupling factor		eA1.65
φ	Phase angle	radians	eA1.10 eA1.12

ω_d	Damped angular frequency of oscillation	radians-second^{-1}	eA1.13
ω_g	Galvanometer natural (undamped) frequency of oscillation	radians-second^{-1}	e8.1
ω_o	Natural angular frequency of oscillation	radians-second^{-1}	eA1.3
ω_s	Seismometer natural (undamped) frequency of oscillation	radians-second^{-1}	e8.1

Abbreviations

15-100	Seismograph with 15s seismometer and 100s galvanometer
30-100	Seismograph with 30s seismometer and 100s galvanometer
ASL	Albuquerque Seismological Laboratory
Cal Cur	Calibration current
C&GS	United States Coast and Geodetic Survey
Comp	Seismograph component (vertical, north or east)
Corr	Timing correction
DARPA	Defense Advanced Research Projects Agency
dB	Decibels
DMC	Data management center
ESSA	Environmental Science Services Administration
FFT	Fast Fourier transform
GMT	Greenwich Mean Time
Hz	Hertz; frequency of oscillation in cycles/second
IRIS	Incorporated Research Institutions for Seismology
jpeg	Joint Photographic Experts Group; a compressed digital image format
km	Kilometer
LP	Long period
LP15	Long-period seismograph with fifteen-second seismometer period
LP30	Long-period seismograph with thirty-second seismometer period
LPE	Long-period east-component seismograph
LPMag	Long-period magnification
LPN	Long-period north-component seismograph
LPZ	Long-period vertical-component seismograph
LPZ30	Long-period vertical-component seismograph with thirty-second seismometer period
Mag	Magnification
m	Meter
min	Minute
mm	Millimeter
ms	Millisecond
NOAA	National Oceanic and Atmospheric Administration

NSF	National Science Foundation
P	Seismic primary body wave
Q	Quality (sharpness) of a resonant peak
s	Second
S	Seismic secondary body wave
SP	Short period
SP 50K	Short-period seismograph operating at magnification of 50,000
SPE	Short-period east-component seismograph
SPMag	Short-period magnification
SPN	Short-period north-component seismograph
SPZ	Short-period vertical-component seismograph
SPZ 50K	Short-period vertical -component seismograph operating at magnification of 50,000
TIF or tif	Tagged image file; an uncompressed digital image format
US	United States
USGS	U.S. Geological Survey
USSR	Union of Soviet Socialist Republics
WWSSN	World-Wide Standardized Seismograph Network
WWV	Code of radio station broadcasting time signals

ISSN 2331-1258 (online)
http://dx.doi.org/10.3133/ofr20141218